UNIVERSITÀ DEGLI STUDI DI FIRENZE

Dipartimento di Fisica – Scuola di Dottorato in Scienze

DOTTORATO DI RICERCA IN FISICA

XXII ciclo

AMS RADIOCARBON MEASUREMENTS FOR CARBONACEOUS AEROSOL SOURCE APPORTIONMENT AT LABEC, FLORENCE

Giulia Calzolai

Supervisore: Prof. Franco Lucarelli

Coordinatore di Dottorato: Prof. Alessandro Cuccoli

Settore disciplinare FIS/07

Dicembre 2009

Index

Introduction

The atmospheric aerosols, despite their tiny concentration in the air, have a relevant impact on a wide range of issues, spanning from the local to the global scale.

Many epidemiologic studies on human exposures to ambient particulate matter have clearly established a statistically significant correlation between fine particles concentration in the air and health effects, even very serious such as cancers.

Moreover, increasing concerns originate by the role of aerosols in climate change, and in particular in global warming and changes in hydrological cycles, which appear to be among the major environmental issues of the 21st century. Although the level of scientific understanding of the involved mechanisms is still low, the aerosol effects are estimated to give a relevant contribution in these issues, and the uncertainties on both their effects and their sources constitute one of the dominant uncertainties in climate change models.

Aerosol effects are strictly depending on particle size, chemical composition and, obviously, on the concentrations in the air.

Carbonaceous aerosols consist of soot (elemental carbon, EC) and of a wide variety of organic compounds (organic carbon, OC); all together, they account for a large part of the (fine) particulate matter and sometimes they exceed 50% of the particulate mass. Carbonaceous aerosols are thought to play a major role in both the health and the climatic effects of aerosols; in any case, due to their complexity, the level of understanding and the knowledge of the sources for this aerosol fraction are very low.

The determination of the particulate matter sources and the estimation of their impact is very important not only to enhance the scientific understanding of aerosols but also to develop possible policies aimed at the reduction of atmospheric pollution. In this

perspective, the possibility of distinguishing between anthropogenic and natural sources is highly desirable.

To this aim, radiocarbon measurements are a powerful tool, because of their unique capability of assessing the contribution due to fossil fuel combustion. Radiocarbon is instable: it is produced in the stratosphere and in the troposphere by nuclear reaction of thermalized neutrons (produced as secondary cosmic rays) on atmospheric nitrogen and it decays with a half-life of about 5700 years. As far as they live, organisms are in equilibrium with the atmosphere and have the same radiocarbon concentration. When they die, they behave as a close system and therefore their radiocarbon content is more and more depleted due to the radiocarbon decay. Thanks to this mechanism, fossil fuels are radiocarbon-free, while biogenic and biomass burning sources are characterised by about the same radiocarbon concentration of the present-day atmosphere.

Radiocarbon measurements on the EC and OC fractions of the aerosol improve the carbonaceous aerosol source apportionment since they allow full and unambiguous distinction and quantification of the contributions to the aerosol load in atmosphere coming from natural and anthropogenic sources: this information is fundamental for models on climate change. Due to the tiny carbon quantities involved and to the experimental difficulties involved in the OC/EC separation, these radiocarbon applications often appear to be a real experimental challenge. Due to the poor quantities of carbon, these measurements would not be possible without AMS (*Accelerator Mass Spectrometry*), which is based on the use of a tandem accelerator as an ultra-sensitive mass spectrometer. This technique has incredibly enhanced the sensitivity of the radiocarbon analysis with respect to the radiometric method.

In order to be analysed by AMS radiocarbon measurements, aerosol samples have to be properly prepared, as they have to be inserted into the ion source of the accelerator as graphite beads. At the INFN LABEC laboratory (Florence) a sample preparation laboratory was already set up for medium-size samples (~600 μg of carbon) and it is mainly used for radiocarbon dating purposes. However, a new preparation line was needed to fulfil specific requirements for aerosol samples: in particular, it was necessary to produce a system allowing the separation of EC and OC during the preparation of the graphite beads and optimised for lower mass samples (~100 μg of carbon).

The aim of this PhD work was the design and the implementation of a new sample preparation line fulfilling the above quoted requirements, as well as its full testing and characterization by AMS measurements on sets of produced samples. Due to the long

time necessary for the sample preparation, we set as a first objective the test of the line for TC analysis, on both medium and small size samples (down to ~100 μg). However, the sample preparation line and also all the test measurements were projected since the beginning keeping in mind the final purpose of measuring the radiocarbon content on the separate EC and OC fractions. In this manner, only the different thermal separation protocols will need to be tested in order to obtain reliable measurements on the two carbon fractions.

Thesis overview

In the first Chapter, the topic of aerosol studies is introduced and aerosol basic properties are reported; a detailed description is reserved to the aerosol carbonaceous fraction, which is one of the most important for both its abundance and its effects, and to the reference analysis methods of carbonaceous aerosols. In the latter part of the Chapter, an in-depth discussion on the carbonaceous aerosol source apportionment by radiocarbon measurements, which is the final aim of this thesis, is given.

In the second Chapter, a brief description of the 3MV Tandetron accelerator installed at LABEC and of the related beam lines is given; basics on AMS measurements are also reported.

In the third Chapter, the new sample preparation laboratory for the aerosol samples, especially developed, installed and tested during this PhD activity, is comprehensively described.

In the fourth Chapter, results are reported from the first tests performed on the new sample preparation line, aimed at fully characterising the line itself, at controlling the suitability of the produced samples for AMS measurements and, finally, at checking the reliability of the AMS results obtained for these samples. A first step towards the reduction of the sample size was made since these first tests, as they were performed on samples slightly smaller (~75%) than the samples routinely prepared for radiocarbon dating measurements.

In the fifth Chapter, first results from tests and measurements performed on aerosol samples are reported. Moreover, some preliminary tests about sample-size reduction opportunities at LABEC were performed, and results are shown in the latter part of this Chapter. In fact, the reduction of the sample size, with respect to the one commonly

measured for radiocarbon dating, is a key point for radiocarbon measurements on the separate carbonaceous fractions (EC and OC).

In the Appendix, some excerpts from the IBA (*Ion Beam Analysis*) activities I carried out during these three years are reported. In fact, although the main project developed during this PhD work has been focused on the AMS radiocarbon measurements for carbonaceous aerosol source apportionment, I also continued some IBA activities I had approached during my degree project, which concerned the implementation of PIXE (*Particle Induced X-ray Emission*) and PIGE (*Particle Induced γ-ray Emission*) analyses on atmospheric aerosol samples. Methodological results on the combined use of PIXE and PIGE for accurate geochemical characterization and quantitative analysis of the fine dust are shown. Moreover, a comparison of PIXE and XRF (*X-ray Fluorescence*) techniques is presented. An optimisation of combined PIXE-XRF measurements may reduce the accelerator beam time necessary for our analysis with an improvement in the detection efficiency for the elements of interest. As far as PIXE-PIGE measurements are concerned, results from the analysis of the fine dust trapped in ice cores from Antarctica are presented and briefly contextualised in the frame of the specific paleoclimatic study.

Chapter 1

Carbonaceous aerosol

Nowadays, great interest in atmospheric aerosols is due to their large impact on human health and on the environment, despite their tiny concentrations in air.

In this Chapter, basic properties of aerosol are reported, with a focus on the aerosol carbonaceous fraction, one of the most important both for its abundance and its effects, as well as the carbonaceous aerosol reference analysis methods. In the final part of the Chapter, a detailed discussion on the carbonaceous aerosol source apportionment by radiocarbon measurements, which is the final aim of this thesis, is given.

§ 1.1 Aerosol properties and effects

As is well known, atmosphere is not only composed of gases: it also contains suspended particles both solid and liquid, characterised by sizes spanning over about 5 orders of magnitude, from ~1nm up to ~100μm. The suspended particles are called *atmospheric aerosols* (or *airborne particulate matter*) and may be directly introduced into the air by natural or anthropogenic sources (*primary* aerosol), or produced in air by chemical-physical reactions of gases, vapours or suspended particles (*secondary* aerosol). Their concentrations in air may range from hundreds of ng/m^3 in remote areas up to hundreds of $\mu g/m^3$ in the most polluted industrial or urban areas, depending on a quantity of parameters (e.g. emission sources and meteorological conditions) [Hind99].

The increasing interest in atmospheric aerosol is due to its impact on human health (respiratory and cardio-respiratory problems linked to air pollution [Pope02]) and on the environment (visibility, atmospheric radiative transfer [IPCC07]).

The role of atmospheric aerosol in producing the aforementioned effects on both health and environment is determined by aerosol basic (and often interdependent) properties such as chemical composition, water solubility, atmospheric residence time, optical properties, and size distribution (in mass, volume, number or surface). Particles are generally more conveniently classified on the basis of "effective diameters" in place of their linear dimensions. Among the defined effective diameters (e.g., optical diameter, electrical mobility diameter) the aerodynamic one is the most used, as both aerosol atmospheric dynamics (i.e. transport and removal from the air) and deposition within the human respiratory system are governed by particle aerodynamic properties. The *aerodynamic diameter* (D_{ae}) is defined as the size of a unit-density sphere with the same aerodynamic characteristics [Marp76].

Ambient aerosols display multi-modal distributions of particle number, surface area and volume by particle size; such distributions may vary depending on location, atmospheric conditions and aerosol sources. As shown in Figure 1.1, the smallest particles (below 0.1 μm) are typically the most abundant, while most of the particle volume, and therefore most of the mass, is usually found in particles with diameters larger than 0.1 μm. Most of the surface area is between 0.1 and 1.0 μm.

In the mass distribution by particle size, aerosols tend to form a characteristic bimodal distribution (Figure 1.1, panel "c"). Most of the mass is confined in two separate fractions, called the *coarse mode* and the *accumulation mode*, with particles of the coarse mode having a larger diameter with respect to the accumulation mode ones.

Particles with diameter up to 2.5 μm[1] are called *fine particles,* while particles with diameter below 0.1 μm are called *ultrafine particles*. Ultrafine particles are apparent as the largest peak in the number distribution (Figure 1.1, panel "a"), and can be subcategorized into two smaller modes, called the *Aitken mode* and the *nucleation mode*.

The coarse mode contains particles that are generally produced by geochemical sources such as wind-blown dust, sea spray particles, pollen grains and mould spores. In urban sites, the coarse mode also contains road dust re-suspended by traffic and particles generated by the wearing of moving parts (catalysers, breaks, tires, railways).

The chemical composition of the coarse fraction reflects the chemical composition of the sources. Coarse particles contain soil related elements (Al, Si, Ca, Fe, Mg, Sr, Ti,

[1] The fine particles are also called $PM_{2.5}$ (Particulate Matter with diameter below 2.5 μm) and include all the accumulation mode particles.

etc.) such as oxides, sea spray elements (Na, Cl, Mg, S, etc.) and organic compounds from plant debris. In urban sites, the coarse fraction can also contain elements due to the wearing of vehicles (Zn, Sb, Cu, Fe, Cr). Coarse particles removal generally occurs by settling and, since the process is quite efficient, the residence time in the atmosphere is short, typically of the order of hours.

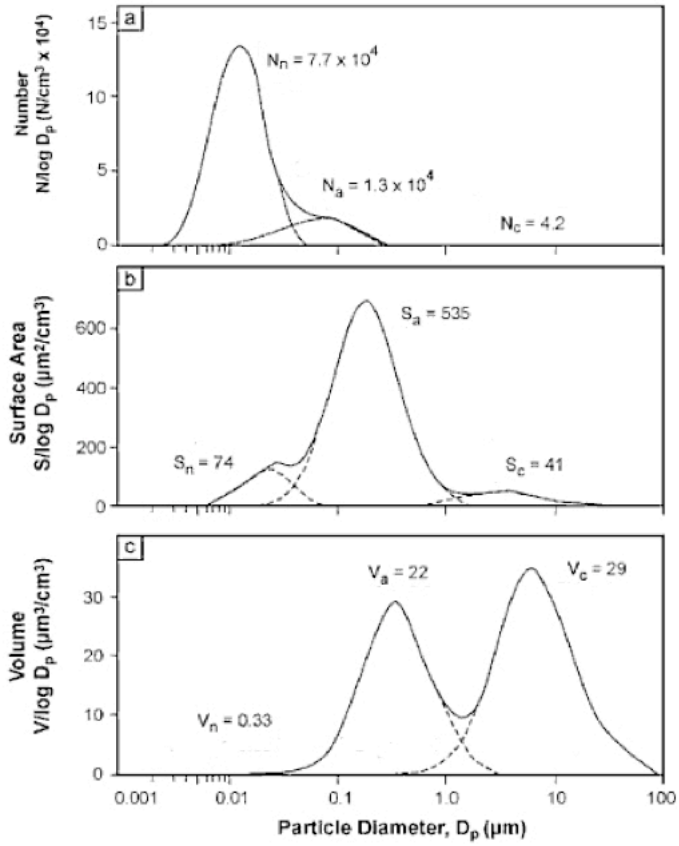

Figure 1.1: Size distributions by number of particles (a), surface area (b) and volume (c). Adapted from [EPA05].

The fine and ultrafine aerosols include particles formed by *nucleation* (i.e. condensation of low vapour-pressure substances formed by high-temperature vaporization or by chemical reactions in the atmosphere to form new particles called nuclei), by *coagulation* (i.e. the combination of two or more particles to form a larger particle) or by *condensation* (i.e. condensation of gas or vapour molecules on the surface of existing particles).

The chemical composition of the fine and ultrafine aerosols mainly reflects the chemical composition of the condensed gases: organic compounds, ammonium sulphates and ammonium nitrates constitute the major components of particles in such

mode. The components that are very important for health effects, although present only in minor or even trace quantity, are soot, heavy and transition metals (Cd, Pb, Hg and Cr, Mn, Co, Ni, V) and viruses.

Ambient atmospheric aerosols are typically present in the air in concentrations between a few $\mu g/m^3$ and a few hundred $\mu g/m^3$, corresponding to less than 0.1 ppm by mass; despite their tiny concentrations, atmospheric aerosols have a relevant impact on both human health and environment.

Health effects are clearly connected to the different penetration of the particles into the breathing apparatus, with smaller particles more easily reaching the deeper levels and therefore being potentially more dangerous. Only particles with $D_{ae} < 10$ μm (called PM_{10}) enter into the respiratory apparatus, while larger ones are stopped in the uppermost respiratory system and quickly expunged. Early evidences of health effects from human exposure to ambient particles date back to the early 1990s [Dock93]. Nowadays, a statistically relevant correlation between particulate matter levels and adverse impacts on human health has been clearly established, and reduced lung function, lung cancer, cardiopulmonary mortalities and elevated rates of premature mortality have been associated to short-term and/or long-term exposures to fine particulate matter [Liu09, Pope02].

Among the environmental effects, the reduction of visibility [Char67, IMPRep], due to the scattering and absorption of sunlight by atmospheric particles, is the most commonly experienced effect. Moreover, as aerosols carry most of the toxic metals, acids and nitrates of the atmosphere, dry or wet aerosol deposition may produce soil and water contamination and damages to vegetation and buildings [Sabb95].

Nowadays, great concern is aroused by the interaction of aerosols with the Earth's climate: in fact, aerosols contribute to the Earth's radiation budget by both direct and indirect mechanisms (see Figure 1.2). As direct effects, aerosols scatter and absorb both sunlight and thermal radiation, which is also emitted by the same aerosols. As an indirect effect, aerosols act as cloud condensation nuclei (CCN) and ice nuclei (IN), inducing cloud and fog formation and modifying microphysical cloud properties. As far as the indirect effects are concerned, it is worth stressing that clouds have a large role in the Earth's radiation budget, as they cover about 60% of the surface of our planet. There is evidence that small changes in macrophysical (coverage, structure, altitude) and microphysical properties (droplet size, phase) have significant effects on climate. The enhancement of the reflection of solar radiation due to the more abundant but smaller

cloud droplets in a cloud (*cloud albedo* or *Twomey effect*) and the increase of cloud lifetime (and thus of its reflectivity) due to the reduced precipitation efficiency in clouds having smaller droplets (*cloud lifetime* or *second indirect effect*) are among the indirect effects having larger impact on the Earth's radiation budget [Hayw00, Lohm05].

The evaluation of reliable estimates of the direct and indirect global annual mean *radiative forcing*[2] (RF) due to present-day concentrations of anthropogenic aerosols is one of the major environmental issues of the 21st century.

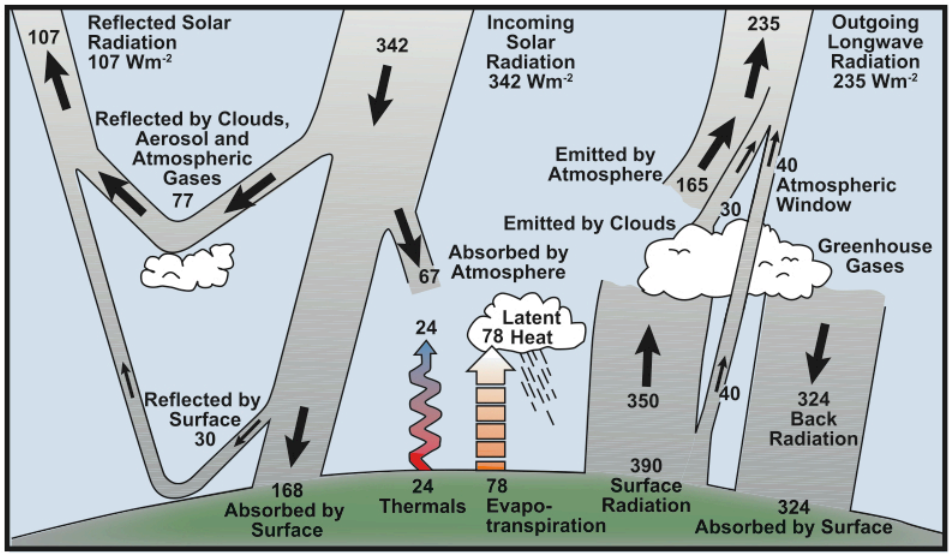

Figure 1.2: Estimate of the Earth's annual global mean energy balance. The Earth's surface and the atmosphere absorb respectively about one half and one fifth of the incoming solar radiation, while the remaining part is reflected back to space. The Earth's surface transfers its absorbed energy to the atmosphere by warming the air in contact with the surface (thermals), by evapo-transpiration and by longwave radiation that is absorbed by clouds and greenhouse gases. The atmosphere in turn radiates longwave energy back to Earth as well as out to space. Over the long term, the amount of incoming solar radiation absorbed by the Earth and atmosphere is balanced by the Earth and atmosphere releasing the same amount of outgoing longwave radiation [IPCC07, Kieh97].

Concerning the direct interaction (scattering and absorption) of aerosols with both the incoming solar radiation and the outgoing infrared radiation emitted by the Earth's surface, the produced radiative forcing (RF) may be both negative and positive. The net direct radiative forcing is evaluated to be negative, as well as the one caused by the indirect interaction (change in cloud properties, and especially in their *albedo*, i.e. in their reflectivity). The report of 2007 of the IPCC (*Intergovernmental Panel on Climate Change*) gave the evaluations of the principal components of the radiative forcing of

[2] Radiative forcing is a measure of how the energy balance of the Earth-atmosphere system is influenced when factors that affect climate are altered. The term forcing is used to indicate that Earth's radiative balance is being pushed away from its normal state [ICCP07].

climate change as evaluated in 2005 relative to 1750 (beginning of the industrial era) as summarised in Figure 1.3. The radiative anthropogenic forcing terms taken into account are due to the greenhouse gases (strongly positive), the ozone (with the stratospheric one negative and the tropospheric one positive), the stratospheric water vapour (positive), the surface albedo (depending on human land use), the aerosols and the contrails (i.e. persistent cirrus clouds reflecting solar radiation and trapping outgoing longwave radiation, formed because of aviation activities; contrails cloud properties can also be changed due to aviation aerosols). The only considerable natural radiative forcing between 1750 and 2005 is solar irradiance; volcanic eruptions can originate short-lived (2÷3 y) cooling effects. Since no important eruption has been experienced since 1991 (Mt. Pinatubo eruption), these effects have been neglected.

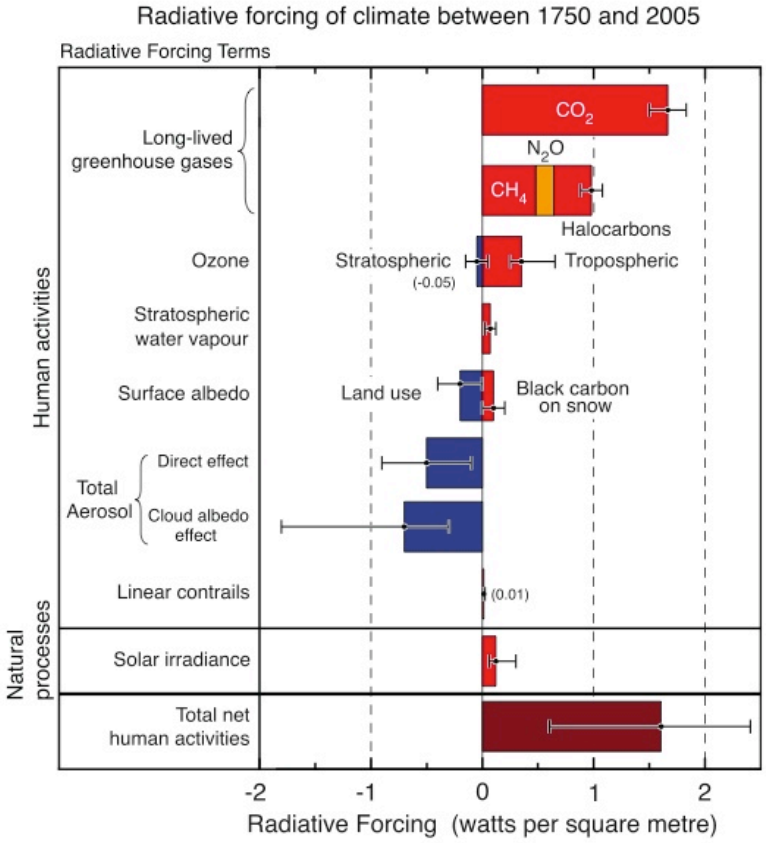

Figure 1.3: Global average radiative forcing (RF) estimates in 2005.

Nowadays, the uncertainty on the aerosol component constitutes the dominant uncertainty on the whole anthropogenic radiative forcing estimate, as the level of scientific understanding of the mechanisms leading to the aerosol effects on climate is

still low. Moreover, the uncertainty on how much the atmospheric aerosols counteract the warming effects of anthropogenic greenhouse gases leads to large uncertainties in the sensitivity of climate to human perturbations and, therefore, on projections of climate change: in the future aerosol cooling is expected to decline because of the pursuit of a cleaner atmosphere, thus possibly enhancing the predicted global warming [Andr05].

Finally, aerosols play a role in climate change not only as far as global warming is concerned: in fact because of aerosols clouds not only are brighter, but also less efficient at releasing precipitation. These two aerosol effects on clouds, together, result in changes in atmospheric thermal structure, surface cooling, disruption of regional circulation systems such as monsoons and suppression of rainfall. Therefore, they can lead to a weaker hydrogeological cycle and to a dryness of the planet, worsening the already alarming scenario concerning the availability of fresh water [Rama09].

§ 1.2 The aerosol carbonaceous fraction

Carbon is typically the largest elemental fraction of atmospheric aerosol particles, present in many different chemical and physical forms. This extreme diversity is at the origin of the recently increased interest in carbonaceous aerosols as it leads to important effects on both human health and climate modification [Gele04]. Carbonaceous particles can constitute about 40% of urban aerosol, and can be also more abundant depending on the location and on the particle size fraction [Pösc05]; in Europe, carbon appears to be a major, if not the main, aerosol constituent [tenB04].

The total carbon (TC) present as aerosol in the atmosphere can be expressed as the sum of *organic carbon* (OC), *elemental carbon* (EC) and *carbonate carbon* (CC). CC originates from resuspension of crustal material containing carbonate species, thus from specific sources such as street abrasion, construction sites and desert dust [Jank08]. Its contribution to the TC in atmospheric aerosols is mostly negligible, as it is usually less than 5% [Spur99, tenB04]. Therefore, sometimes, the TC is also defined as the sum of all carbon contained in the particles, except in the form of carbonates.

EC has a graphitic microstructure, and is emitted as primary particles (soot) from incomplete combustion processes possibly occurring when either fossil fuel or biomass are burnt (therefore, EC is mainly anthropogenic). Primary OC particles can be emitted from combustion sources, together with EC, or from natural sources such as debris,

pollen, spores and algae. OC can also be formed in the atmosphere as secondary aerosol (SOA: *secondary organic aerosol*) through gas-phase photochemical processes.

EC, the main constituent of soot, is almost exclusively responsible for the light absorption of the aerosols, which is continuous and covers the whole visible spectral range with only a slight dependence on wavelength [Horv93]. Because of this property, EC is often referred to as *black carbon* (BC). Although the terms EC and BC are often used interchangeably, it is worth keeping in mind that both EC and BC are operationally defined by the measurement method applied (thermal or thermal-optic for EC, and only optic for BC), i.e. they refer to different chemical-physical properties [Wats05].

OC is formed by hundreds of different organic compounds; concerning its optical properties, OC is mainly light-scattering, since only two classes of organic compounds (polycyclic aromatics hydrocarbons and humic-like substances) are slightly light-absorbing. OC can also enhance the EC absorption efficiency when it is mixed with EC, as it may occur in combustion soot, that is often "contaminated" with organic compounds [Spur99, Wats05, Pösc06].

Due to these different optical properties, EC and OC alter the radiative properties of the atmosphere in opposite ways, and thus play an opposite role in the aerosol radiative forcing. In fact, OC is estimated by the IPCC07 to exert a negative direct radiative forcing, evaluated to be -0.19±0.20 W/m^2 (from anthropogenic sources; 90% confidence range), while a large positive component of the radiative forcing from aerosols is ascribed to EC. The direct RF of EC is estimated to be 0.34±0.25 W/m^2. Moreover, EC is also responsible for a further warming effect, as the presence of soot particles in snow could cause a decrease in the albedo of snow and affect snowmelt: the RF for this effect is estimated to be 0.10±0.10 W/m^2 [IPCC07]. In Figure 1.4, the RFs for carbonaceous particles (OC and BC, i.e. EC) are reported together with the RFs evaluated for the direct scattering effect of sulphates (which are highly scattering) and mineral dust. Due to rather large uncertainties, no apportionment of the indirect cloud albedo effect to each aerosol type was made.

By the comparison of Figure 1.3 and Figure 1.4 it turns out that the contribution of EC to the overall radiative forcing is comparable with the one estimated[3] for methane (CH_4), the second greenhouse gas for relevance of RF, after carbon dioxide (CO_2). There is great uncertainty on the EC RF, and some studies (e.g. [Jaco01]) give larger

[3] Methane RF is estimated to be 0.48 W/m^2 with a ~10% uncertainty (90% confidence range).

estimates of its value, suggesting that the magnitude of the direct radiative forcing from the EC itself might exceed that due to methane, thus implying that EC might be the second most important component of global warming after carbon dioxide.

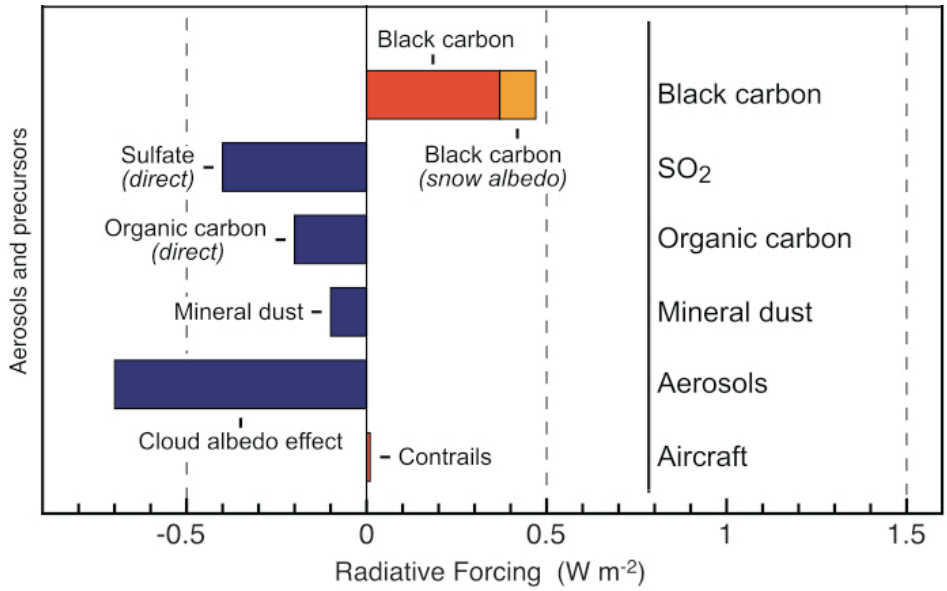

Figure 1.4: Radiative forcing evaluations for anthropogenic aerosols and aerosol precursors; RFs in 2005 due to emissions and changes since 1750 (adapted from [IPCC07]).

As far as aerosol effects on human health are concerned, OC contains several types of highly toxic compounds. Among them, it is worthwhile to recall the polycyclic aromatic hydrocarbons (PAHs), which are produced industrially and in biomass burning. PAHs are known as some of the most toxic and carcinogenic compounds, even at extremely low concentrations [Jaco00]. Moreover, both organic compounds in ultrafine particles and EC itself play an important role in the process of generation of reactive oxygen species within cells, which is likely to be the starting point for the occurrence of respiratory problems and the exacerbation of underlying cardiovascular diseases [Kenn07].

§ 1.3 Basics on aerosol sampling

Without claiming to be exhaustive, a very short introduction on aerosol sampling is reported in this paragraph.

An aerosol sampler can be schematically described as follows. Air is pumped through the sampler and particles are collected by *impaction* and/or *filtration*. In the

impaction process the air stream is forced to make an abrupt change in direction: the heavier particles, due to their higher inertia, cannot follow the air stream and impact onto a surface (impaction foil). In the filtration process, the air stream is forced (by a pressure gap application) to pass through a filter (or membrane) whose fibres intercept the particles.

In order to collect by filtration all the aerosol particles with dimensions lower than a fixed aerodynamic diameter (for example, PM_{10} or $PM_{2.5}$ or PM_1), a pre-impaction stage is installed upstream of the filter to eliminate the larger particles: these devices are classified as *single-mode* samplers. Conversely, samplers that separate and collect the aerosol in different size classes are called *fractionated* or *multi-mode* samplers. Multi-mode inertial impactors accomplish size fractionating by arranging several impaction stages in series.

The sampling time sequence can be discrete or continuous. *Cumulative* samplers carry out the sampling in discrete periods by repeated changes of filters (or impaction plates); when the filter changing is automatic the sampler is usually referred to as a *sequential* sampler. *Continuous* samplers continuously collect the aerosol and deposit it on a spot that is continuously moved along the collecting substrate, thus producing a "strip" or "streak" of pollution. Since the characteristic aerosol temporal variations occur on several scales, from diurnal patterns (hours) through synoptic behaviour (days) to seasonal trends (months), the sampling *time resolution* can vary from hours to months. The collection of size-fractionated (or "size-segregated") samples with a high time resolution (of the order of hours) is the best solution to get a detailed aerosol characterization. However, this would produce huge amounts of samples to be analysed and aerosol deposits collected by multi-mode samplers with good time resolution may be too small also for very sensitive analysis methods. As a consequence, when studying long-term behaviours it is convenient to sample with daily resolution. Sampling strategies (i.e. size and time resolution) have to be accurately chosen on the basis of the specific problem investigated (air quality monitoring, pollution source identification, climate studies, etc.).

Among the most common used instruments for the PM_X collection on a daily basis, there are the *Low Volume* (LV, air flux < 3 m^3/h) single-mode sequential samplers. These devices, which can be equipped with PM_{10}, $PM_{2.5}$ and PM_1 inlets, collect the aerosol on 47 mm diameter circular filters. Sampler models properly designed to meet

the European regulation standards on PM_{10} and $PM_{2.5}$ concentration measurements work at a flux of 2.3 m^3/h and are commercially available.

In order to study minor aerosol components, like for example Polycyclic Aromatic Hydrocarbons, *High Volume* (HV, air flux > 3 m^3/h) samplers are also commonly used. To avoid filter clogging, these devices usually collect the aerosol on filters with larger surface with respect to the ones used with LV samplers. As a consequence, the collected mass is larger but the aerosol deposit thickness may be of the same order of that of LV samplers, depending on the specific device features. For example, the Digitel DHA-80 HV sequential sampler (Figure 1.5) may collect PM_{10} on 150 mm diameter circular filters, working with an air flux of 30 m^3/h. In this case the sampled volume for time unit (and thus the collected mass) is ~ 13 times larger with respect to a standard LV sampler (working at 2.3 m^3/h with 47 mm diameter filters), but the deposit thickness is only ~1.2 times higher. The Digitel DHA-80 HV sequential sampler was used to collect some samples analysed in this work (see § 5.1).

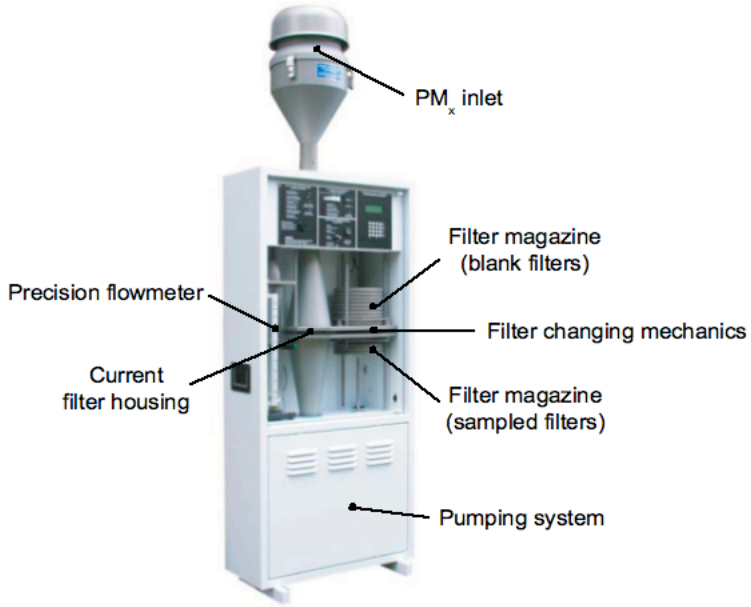

Figure 1.5: The Digitel DHA-80 HV sequential sampler.

For both LV and HV samplers, the particulate matter concentration can be obtained by weighting the filters before and after the sampling, in both the cases after a storage period (24-48 hours) in a temperature and humidity controlled room (ambient temperature = (20 ± 1) °C, relative humidity = (50 ± 5)%). Measurements can be

performed by means of an analytical balance (sensitivity 1 μg); electrostatic effects may be avoided by the use of a de-ionising gun.

Typical values of the aerosol masses that can be collected by LV and HV samplers during one day are reported in Table 1.1. These values were evaluated assuming a PM_{10} concentration of 30 $\mu g/m^3$, which is quite common for an urban environment.

	Volume (m^3)	Collecting area (cm^2)	PM_{10} mass (μg)	PM_{10} deposit thickness ($\mu g/cm^2$)
LV (2.3 m^3/h)	55	13	1650	125
HV (30 m^3/h)	720	150	21600	140
HV/LV	13	12	13	1.1

Table 1.1: Typical values of the aerosol masses that can be collected by LV and HV samplers during one day, assuming a PM_{10} concentration of 30 $\mu g/m^3$.

As concerns the collecting substrates, the most commonly used ones are the quartz fibre filters, the PTFE-Teflon $(CF_2)_n$ membranes, cellulose and polycarbonate membranes. Among them, only quartz filters are suited for thermal analysis.

§ 1.4 EC and OC analysis

§ 1.4.1 EC and OC determination

Thermal methods have a long history in the OC and EC determination in aerosol. These methods are based on the measurement of the quantity of carbon that leaves the filter as the temperature increases, following a specific thermal evolution in different analysis atmospheres (oxidising or inert). As previously mentioned, thermal methods may be applied only to aerosol samples accumulated on quartz fibre filters, since quartz is the only aerosol collecting support that can sustain high temperatures.

The most widely used method is based on a two-step combustion procedure: organic compounds are volatilized during a first step in oxygen-free helium atmosphere, while EC is evolved during the second step in oxidising atmosphere.

Nevertheless, the separation between OC and EC is ambiguous because some of the OC may turn into EC due to pyrolysis in an oxygen-deficient atmosphere (this phenomenon is called *charring*). The method may be optimised to minimise charring of organic compounds by performing a *flash heating*, i.e. a very fast increase of initial

temperature (~200°C/min), in order to favour desorption of organic compounds at the expense of charring [Cach89].

Thermo-optical methods couple the traditional thermal methods with the monitoring of optical properties of the sample, such as reflectance and transmittance, during the thermal evolution, in order to correct for charring. In fact, both reflectance and transmittance are dominated by EC and therefore decrease as a result of charring during pyrolysis and increase as light-absorbing carbon is burned (see Figure 1.6). The optical correction for charring is based on the assumption that the light extinction per mass unit of pyrolytically produced carbon is the same as the light extinction per mass unit of carbon removed until the monitored optical property regains the initial value. Since this condition is not fully verified, a slight bias in either direction in the demarcation between the OC and the EC might occur. However, this effect is estimated to be largely less important than if no optical correction is performed [Gele04].

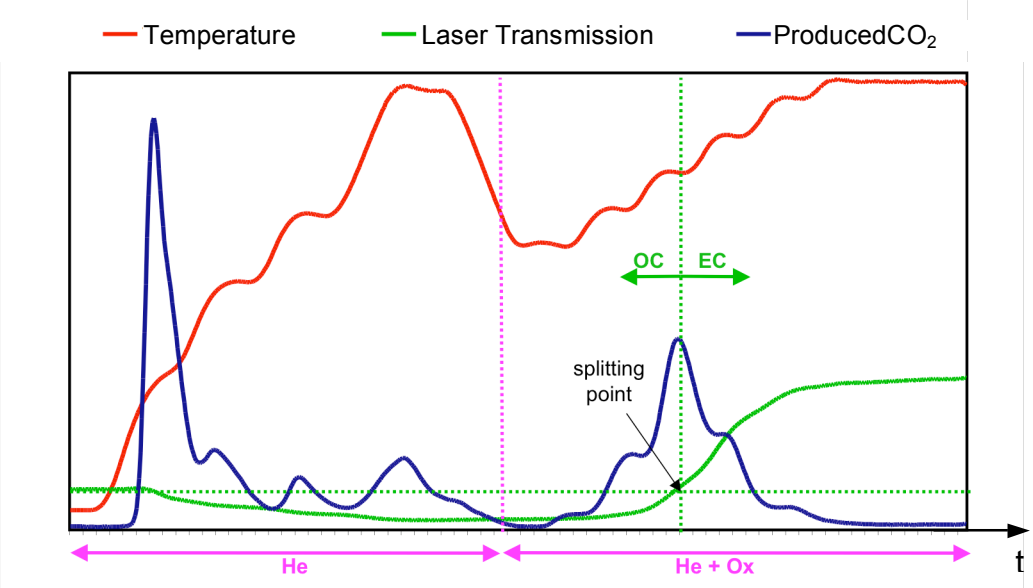

Figure 1.6: Thermogram for a Thermo-Optical Transmittance (TOT) analysis. The temperature is increased, by steps, up to ~870°C in He atmosphere; then the temperature is decreased, the sample is put in a oxidising atmosphere and is heated again, by steps, up to ~900°C. As far as OC pyrolyses (first part of the thermogram), the laser transmission decreases. When an amount of carbon equal to the one pyrolysed is burnt, the laser transmission regains its initial value: at this point, all the OC is really burnt (splitting point between EC and OC).

The thermo-optical transmission method (TOT, [Turp90]) is likely to produce more correct results, when the two methods, based on the monitoring of either the reflectance of the transmittance, possibly disagree. In fact the monitoring of the reflectance can be

biased if only the sample surface regains the initial optical properties, thus possibly hiding some remaining pyrolytic carbon beneath it.

The TOT method has been developed by Sunset Laboratories Inc. into a commercial carbon analyser, which has become the reference instrument for EC and OC determination in aerosol; one of these instruments is also available at LABEC.

In TOT analysers by Sunset Lab. Inc., one punch (typically 1 or 1.5 cm^2) of the sample is introduced inside the oven and undergoes a two-step combustion. During the first phase, in helium, the oven temperature is raised, by steps, up to 870°C. The volatilised organic compounds are oxidised to CO_2 by means of a MnO_2 catalyser and then pass through a methanator to reduce the CO_2 to methane, which is finally quantified by a flame ionization detector (FID). During the second phase, the sample is heated (by steps) up to 900°C in a 2% oxygen/helium mixture; the produced CO_2 is again converted to methane and detected by the FID (see Figure 1.7). The charring correction is made by continuously monitoring the filter transmittance by means of a He-Ne laser at a wave-length of 632.8 nm (red) and of a photodetector. At the end of the analysis, the calibration is achieved through injection of a known volume of methane into the sample oven [Bae04].

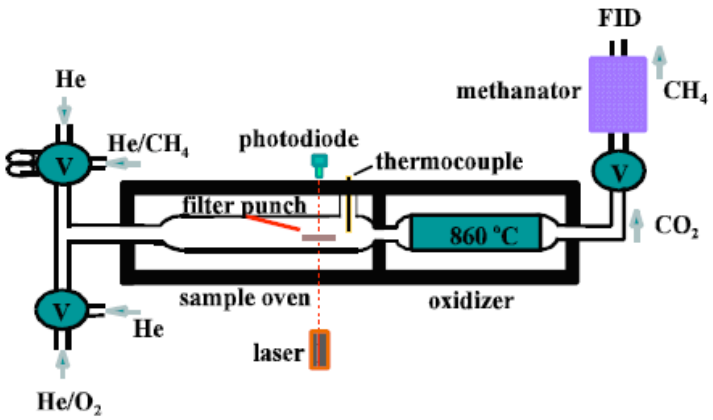

Figure 1.7: Scheme of the TOT EC/OC analyser by Sunset Lab. Inc.

With this instrument, the heating program may be selected by the analyst: the reference protocol is the NIOSH (*National Institute for Occupational Safety and Health*) method 5040 [Elle96].

Any CC that could be present can be removed prior to the carbon analysis by acidification (exposure of the filters to HCl fumes). Without this initial step, CC may be

detected as either OC or EC, since CC could evolve in almost any segment of the thermogram [Chow93].

§ 1.4.2 EC and OC separation

Charring constitutes a critical issue for analysis of specific properties of the single aerosol carbonaceous fractions, i.e. when EC and OC have not only to be quantified but also effectively separated in order to allow their specific study (e.g. for the determination of their isotopic or molecular composition).

In particular, the thermal elimination of OC for isolation of EC may incur in charring, thus producing a positive artefact. Therefore, the suppression of charring is particularly important for correct EC analysis, especially when properties quite different for the two carbonaceous fractions, EC and OC, are investigated (e.g., radiocarbon content, see § 1.4). Charring suppression may be optimised by water extraction and oxidative treatment of the filters [Szid09].

Water extraction does not affect EC, which is supposed to be completely insoluble in water, but effectively removes water soluble OC (WSOC), which appears to be the main fraction undergoing pyrolysis [Szid04b].

§ 1.5 Radiocarbon aerosol source apportionment

Among the three natural isotopes of carbon, only ^{14}C is instable and it is thus called "radiocarbon": it decays via beta emission to ^{14}N with a half-life of (5730 ± 40) years. Only a minimum part of the carbon on the earth is radiocarbon: the two stable isotopes of carbon, ^{12}C and ^{13}C, are respectively the 98.9% and the 1.1% of the total carbon, while the $^{14}C/^{12}C$ ratio in atmosphere is about $1.2*10^{-12}$.

Radiocarbon is mainly produced in the stratosphere and in the troposphere by nuclear reaction of thermalised neutrons (produced as secondary cosmic rays) on atmospheric ^{14}N, according to the reaction $^{14}N(n,p)^{14}C$ (occurring with a cross section of about 1.8 barn [Korf80]). After production, ^{14}C is rapidly oxidised to form first ^{14}CO and then $^{14}CO_2$. The $^{14}CO_2$, as well as the more common CO_2 formed by carbon stable isotopes, circulates in the atmosphere, dissolves into the oceans and is involved in plant photosynthesis, so that radiocarbon enters also in the biosphere where it spreads because of food chain (see Figure 1.8).

Due to its "proper" half-life, radiocarbon is the most employed radionuclide for

dating [Bowm90]: the formulation of main principles of this dating technique dates back to the late 1940's, at the hands of W. Libby and his colleagues [Libb49].

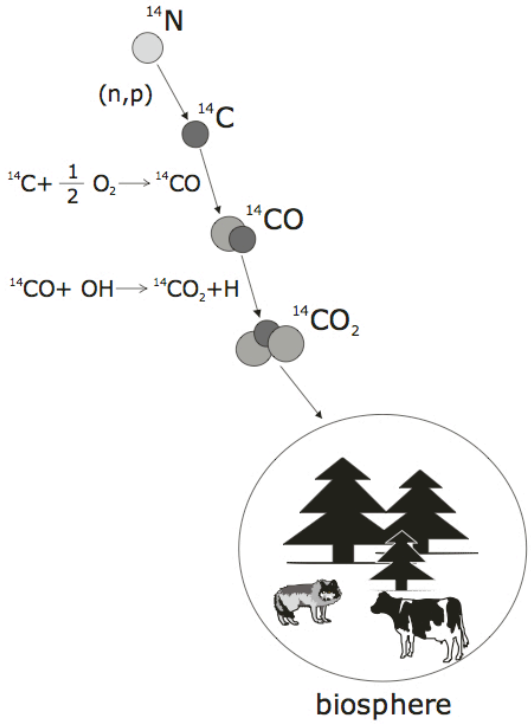

Figure 1.8: Schematic representation of the mechanisms of production and diffusion of radiocarbon.

Just a few years later, the applicability of atmospheric radiocarbon as a tracer for anthropogenic emissions from fossil fuel was seen in atmospheric CO_2 as the "Suess effect" [Sues55]. In the early part of the 20th century up until the 1950's, the atmospheric radiocarbon concentration was lowered because of dilution by large amounts of fossil-fuel derived CO_2 (the Suess effect is also called "industrial effect").

The first application to aerosol source apportionment dates back to 1955 [Clay55]: a really massive atmospheric sampling (nearly one week of continuous sampling) was needed to provide ~8.5 g of carbon for conventional liquid scintillation counting.

Since then, the progress in radiocarbon measurements sensitivity has been enormous, especially with the introduction of the Accelerator Mass Spectrometry (AMS), with a mg level capability. Nevertheless, sensitivity has always been a critical issue, as AMS development has been paralleled by evermore increasing concern about the origins and the effects of carbonaceous aerosols on health, visibility and climate. This concern has led to the necessity of performing radiocarbon measurements on a large number of carbonaceous aerosol fractions or even on individual compounds, with the highest

sampling resolution possible both in temporal scale and size-segregation. In this manner, the progress in radiocarbon measurements sensitivity has been paralleled by evermore decreasing sample quantities (sizes).

Nowadays, "radiocarbon speciation", i.e. the determination of the spatial and temporal distribution of ^{14}C in individual compounds and chemical fractions, represents one of the challenges of modern AMS [Curr00].

§ 1.5.1 Basic principles of radiocarbon source apportionment

The atmosphere serves as a reservoir and a conducting medium for many carbon compounds, ranging from the simplest gaseous form (CO_2) to complex structures comprising the carbonaceous particles. On the basis of this consideration, Libby assumed as one of the principle for the radiocarbon dating technique that all living organisms were characterised by the same carbonaceous isotopic ratios as the atmosphere[4]. He also assumed that, after death, they would behave as a close system, i.e. they would maintain the same ^{12}C and ^{13}C content while losing ^{14}C due to its radioactive decay. On these bases, radiocarbon is a reliable chronometer for dating and furthermore, a powerful tool for distinguishing aerosol sources, due to its unique power to discriminate fossil (i.e. ^{14}C-free) from contemporary carbon, i.e. to discriminate between carbon from anthropogenic fossil fuel combustion and biomass components.

The aim of a radiocarbon measurement, whatever its application is (dating, aerosol source apportionment or anything else), is to determine the concentration of the 14 mass isotopes among all the carbon atoms. By international convention, this concentration is usually expressed relative to the one present in the reference year 1950, as *percent of Modern Carbon* (pMC) or *fraction of Modern Carbon* (f_m). Although more precise definitions of these terms will be given in § 2.3.1 (together with details on how to measure them), in the meanwhile, for clarity purposes, we can define them as follows:

$$f_m = \frac{(^{14}C/^{12}C)_{sample}}{(^{14}C/^{12}C)_{AD1950}} \qquad (1.1)$$

$$pMC = 100 \cdot f_m$$

Therefore, fossil materials are characterised by a null f_m term:

[4] This assumption is not fully realistic because of isotopic fractionation occurring during natural biochemical processes and a correction is needed. A detailed discussion about this issue will be given in § 2.3.

$f_{m,fossil} = 0$

Materials from the last 50 years show values >1 as a consequence of the enhancement of the atmospheric ^{14}C due to nuclear tests (the "nuclear bomb excess" approximately doubled the atmospheric $^{14}C/^{12}C$ ratio during the mid-1960s!). Since the atmospheric nuclear test ban, biogeochemical relaxation has been manifest: Figure 1.9 shows the "biomass ^{14}C decay curve", i.e. the time record of ^{14}C in the living biosphere, as resulting from time series of atmospheric $^{14}CO_2$ [Levi97]. It appears clear that the f_m characterising biomass samples ($f_{m,bio}$) is necessarily a function of time, precisely of the years of biomass growth (and somehow of the space, because of a minor effect of fossil dilution due to fossil-fuel derived CO_2, more evident in anthropised regions). An exhaustive review of tropospheric bomb ^{14}C data is reported in [Hua04b].

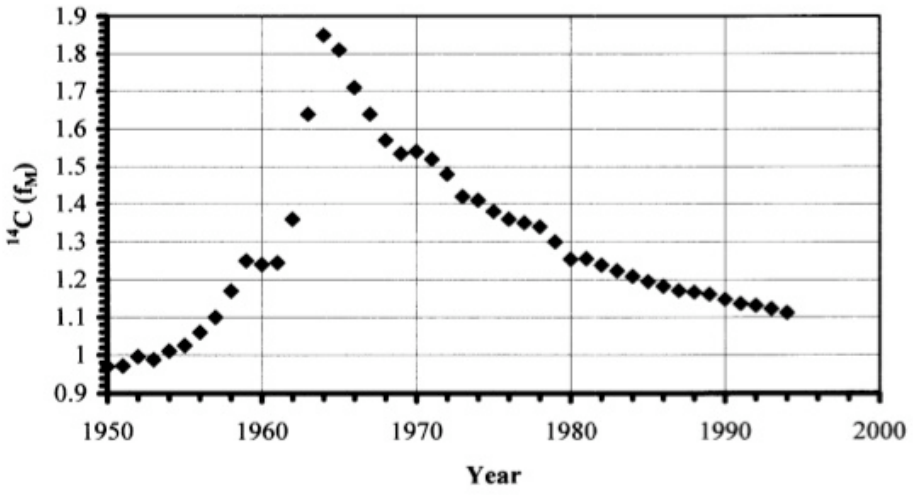

Figure 1.9: Biospheric ^{14}C enhancement in northern hemisphere from atmospheric nuclear testing (reproduced from [Curr02]).

A simple two-source model, based on the discrimination between fossil and contemporary (biomass) sources of carbonaceous aerosol has been widely applied in studies on the aerosol TC fraction [Curr83, Curr89, Curr00, Lewi04] from the beginning of radiocarbon measurements, and more recently, also in studies focused on the EC fraction [Curr02, Slat02, Szid04].

In the two-source model the fossil carbon composition is assumed to be complementary to the biomass carbon one. Therefore, the contribution of the sources to the carbonaceous fraction of interest on the sample can easily be obtained by the

following relations [Curr00]:

$$\begin{aligned} C_{tot} \cdot f_m(C) &= C_{fossil} \cdot f_{m,fossil} + C_{bio} \cdot f_{m,bio} \\ C_{tot} &= C_{fossil} + C_{bio} \end{aligned} \qquad (1.2)$$

where $f_m(C)$ is the measured fraction of modern carbon in the carbonaceous fraction C, present in the sample with a concentration C_{tot}, and C_{fossil} and C_{bio} are the concentrations of C originating respectively from fossil and biomass sources.

The identification of the sources and the evaluation of their contribution to the particulate matter burden of the atmosphere represent the first step towards developing policies for aerosol pollution reduction and prevention. In this perspective, it is very helpful to be able to discriminate between natural and anthropogenic sources since, obviously, it is possible to act only on the latter ones.

The simple two-source model is able to distinguish between fossil and non-fossil sources, thus allowing the quantification of the contribution of fossil fuel combustion. This is an important information, and it can not be obtained by other methods. However, this model is not able to discriminate between natural and anthropogenic sources. In fact, there is no possibility to separate the anthropogenic wood burning contribution to the carbonaceous load from the biogenic one, as both are almost contemporary. This limitation can be overcome if radiocarbon measurements and source apportionment are performed on selected carbonaceous sub-fractions, such as EC and OC (see § 2.4.2).

§ 1.5.2 EC and OC source apportionment: an advanced model

As mentioned in the previous paragraph, recently, some studies based on radiocarbon measurements focused on the source apportionment of the EC aerosol fraction. This particular attention is due both to a special interest on this specific carbonaceous fraction (see § 1.2) and to its peculiarity of being mainly emitted only by anthropogenic sources[5]. In fact, EC is injected into the atmosphere uniquely as primary particles from combustions, either of fossil fuel or biomass.

As EC is not emitted by any biogenic source, the "contemporary" source is without any ambiguity represented by wood (or other biomass) burning. The impact of this latter source on the aerosol load in atmosphere is a debated issue, and its evaluation is

[5] Limits of this assumption will be discussed in the following.

evermore necessary due to the increasing popularity of wood stoves.

With the assumption that the only contemporary source is the wood burning, the (1.1) can be rewritten as follows (the carbonaceous fraction of interest is now EC):

$$\begin{aligned} &\mathrm{EC_{tot}} \cdot f_m(\mathrm{EC}) = \mathrm{EC_{fossil}} \cdot f_{m,fossil} + \mathrm{EC_{wb}} \cdot f_{m,wb} \\ &\mathrm{EC_{tot}} = \mathrm{EC_{fossil}} + \mathrm{EC_{wb}} \end{aligned} \tag{1.2}$$

where, according to the previous used symbols, $\mathrm{EC_{tot}}$ is the concentration of total EC, $\mathrm{EC_{fossil}}$ and $\mathrm{EC_{wb}}$ are the concentrations of EC from, respectively, fossil and wood burning sources and f_m(EC) is the measured fraction of modern carbon on the EC fraction. $f_{m,wb}$ represents the fraction of modern carbon for the burnt wood. Obviously, this is a biomass component that represents a range of years (i.e. the average tree age), therefore adjustments should be made for its lifespan, also taking into account tree growth models [Curr00, Lewi04].

Being $f_{m,fossil} = 0$, the concentrations of EC from respectively fossil and wood burning sources can be easily obtained as follows:

$$\begin{aligned} &\mathrm{EC_{wb}} = \mathrm{EC_{tot}} \cdot \frac{f_m(\mathrm{EC})}{f_{m,wb}} \\ &\mathrm{EC_{fossil}} = \mathrm{EC_{tot}} - \mathrm{EC_{wb}} = \mathrm{EC_{tot}} \cdot \left(1 - \frac{f_m(\mathrm{EC})}{f_{m,wb}}\right) \end{aligned} \tag{1.3}$$

An advanced source apportionment model, based on radiocarbon measurements on both the two separated carbonaceous fractions EC and OC, was proposed by [Szid06]. This model is based on EC source apportionment enhanced by the introduction of an additional information, namely the EC/OC emission ratio for wood burning, that enables the apportionment of the OC fraction among fossil, biogenic and wood burning sources.

For the OC fraction, the (1.1) can be extended to a three-sources model as follows:

$$\begin{aligned} &\mathrm{OC_{tot}} \cdot f_m(\mathrm{OC}) = \mathrm{OC_{fossil}} \cdot f_{m,fossil} + \mathrm{OC_{wb}} \cdot f_{m,wb} + \mathrm{OC_{biog}} \cdot f_{m,biog} \\ &\mathrm{OC_{tot}} = \mathrm{OC_{fossil}} + \mathrm{OC_{wb}} + \mathrm{OC_{biog}} \end{aligned} \tag{1.4}$$

where the previously introduced symbols here have been used for OC. In addition, OC_{biog} and $f_{m,biog}$ represent respectively the concentration of OC from the biogenic source and the fraction of modern carbon for the living biosphere. Obviously, $f_{m,biog}$ is the fraction of modern carbon characterising the living biosphere in the sampling year.

If the EC/OC emission ratio is known for the wood burning source, i.e. if $(EC/OC)_{ER,wb}$ is independently estimated by measurements at the source or by literature data, then the concentration of OC deriving from wood burning can be evaluated starting from EC_{wb}. Therefore, with this additional information, the OC source apportionment relations deriving from the (1.4) are:

$$\begin{aligned} OC_{wb} &= EC_{wb}/(EC/OC)_{ER,wb} \\ OC_{biog} &= \frac{OC_{tot} \cdot f_m(OC) - OC_{wb} \cdot f_{m,wb}}{f_{m,biog}} \\ OC_{fossil} &= OC_{tot} - OC_{wb} - OC_{biog} \end{aligned} \tag{1.5}$$

According to this model, the anthropogenic OC is therefore:

$$OC_{anthropogenic} = OC_{fossil} + OC_{wb} \tag{1.6}$$

The proposed model is sketched in Figure 1.10. The emission pathways for TC, OC and EC are reported in the upper part, in red if coming from a “contemporary” source and in blue if coming from a fossil source. In the lower part of the figure, the advanced source apportionment model is schematised: OC and EC fractions of the sampled carbonaceous aerosols are thermally separated, quantified and their radiocarbon concentration is measured. Since it is known that EC has only one contemporary source, it is easily apportioned between its two sources, fossil and wood burning. Dashed lines indicate the apportionment of the contemporary OC that can be performed on the basis of the additional information on the EC/OC emission ratio for wood burning.

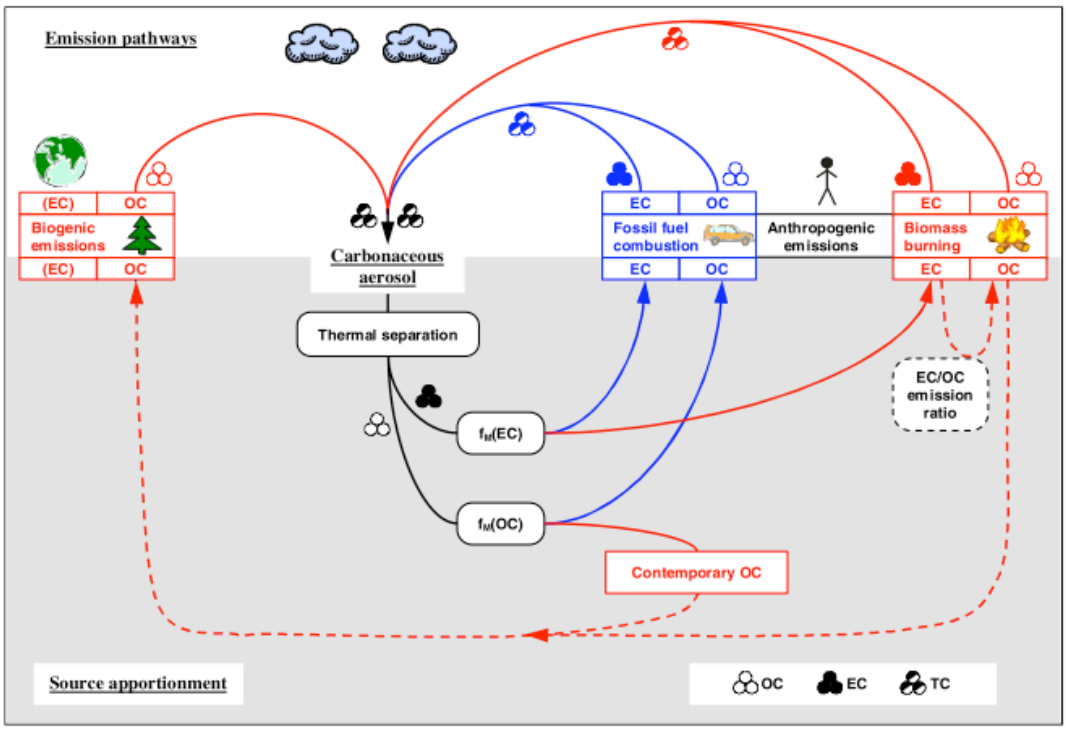

Figure 1.10: Main emissions pathways of OC, EC and TC (upper part of the scheme) and source apportionment according to the advanced model (lower part of the scheme); reproduced from [Szid06].

Finally, it is worthy to emphasise that a TC source apportionment derived from the simple application of the two-source model, i.e. according to the (1.1), can only distinguish between fossil and contemporary sources, but a more detailed TC source apportionment can be performed on the basis of EC and OC source apportionments according to the simple relations:

$$\begin{aligned} & f_m(\mathrm{TC}) \cdot \mathrm{TC} = f_m(\mathrm{EC}) \cdot \mathrm{EC}_{\mathrm{tot}} + f_m(\mathrm{OC}) \cdot \mathrm{OC}_{\mathrm{tot}} \\ & \mathrm{TC} = \mathrm{OC}_{\mathrm{tot}} + \mathrm{EC}_{\mathrm{tot}} \\ & \Rightarrow \mathrm{TC}_{\mathrm{natural}} = \mathrm{OC}_{\mathrm{biog}} \;;\; \mathrm{TC}_{\mathrm{anthropogenic}} = \mathrm{OC}_{\mathrm{anthropogenic}} + \mathrm{EC}_{\mathrm{tot}} \end{aligned} \qquad (1.7)$$

Moreover, the first one of the (1.7) allows the determination of the fraction of modern carbon of one of the carbonaceous fractions (EC or OC) by difference, once the f_m of the other carbonaceous fraction and f_m(TC) have been measured (radiocarbon measurements on TC are easier as the thermal separation phase is avoided).

In conclusion, a source apportionment of the carbonaceous fraction of the aerosol taking into account the three main sources (fossil, biogenic and wood burning) can be performed on the basis of the measurement of the following quantities:

- TC, OC and EC concentrations;
- Fraction of modern carbon (f_m) of EC and OC (or one of these and f_m(TC)).

Limits of the advanced source apportionment model

Source apportionment of EC, and consequently of OC in the advanced model, is based on the assumptions that EC derives from only two sources both anthropogenic, i.e. wood burning and fossil fuel combustion, and that wood burning is the only "contemporary" source.

Actually, three limitations exist for these assumptions:

- Assuming wood burning as an anthropogenic source means neglecting the naturally occurring forest fire as a biogenic EC source;
- One more contemporary source can be represented by combustion of biofuels, i.e. combustible materials derived from processed biomass, commonly produced from plants, micro-organisms and also from organic waste (e.g. biodiesel, bioethanol and biogas), or even from animals[6];
- A complex aerosol source is given by particle emissions of waste incineration facilities.

These limitations very rarely can affect the reliability of the described source apportionment model. In fact, for what concerns natural forest fires, their influence is generally very episodic, therefore it is sufficient taking it into account and rejecting samples possibly collected during such episodes.

As regards biofuels, they do not represent a problem as so far their use constitutes only a negligible share of total global energy consumption. For example, biofuels for transport provided only 0.3% of global final energy consumption in 2006 and 1.8% of total transport fuels in 2007 [UNEP09]. The biofuel use is expected to increase in the future, also because of encouraging policies[7] toward renewable energy sources, therefore this limitation will have to be kept in mind.

Incineration facilities are still also very rare, therefore their contribution to the total aerosol load is generally negligible. Attention should be paid if sampling is performed in proximity of an incineration facility.

[6] In remote rural areas, animal dung is traditionally burnt in place of wood for cooking, heating and agricultural and industrial processes.

[7] All EU countries have a biofuel target, although sometimes only indicative, ranging up to 7% of transport fuels by 2010 (the French one). Emerging economies can have higher targets: India approved a new target of 20% biofuels blending both gasoline and diesel over 10 years [REN09].

Actually, there are increasing concerns over health effects of particles emitted by waste incineration facilities and over the global implications and negative climate impacts of biofuels[8]. Therefore comparison of radiocarbon studies performed before and after the possibly significant introduction of biofuels, or performed on selected carbonaceous chemical fractions, will be potentially very helpful in understanding this issue.

Uncertainties of the advanced source apportionment model

In radiocarbon aerosol source apportionment, ambient carbonaceous particles are assumed as a mixture originating from sources with pure isotopic signals. In particular, for the advanced model, the following fractions of modern carbon have to be indipendently known:

- $f_{m,fossil}$;
- $f_{m,biog}$;
- $f_{m,wb}$.

The further information needed is the EC/OC emission ratio for wood burning:

- $(EC/OC)_{ER,wb}$

Except $f_{m,fossil}$, which can be assumed equal to zero without any uncertainty, all the other data bear some uncertainties, therefore in the following it will be briefly discussed how these uncertainties affect the source apportionment.

- As previously mentioned, the $f_{m,biog}$ value can be derived from long-term time series of $^{14}CO_2$ measurements: for example, in [Szid09], a $f_{m,biog} = 1.055 \pm 0.015$ was assessed for 2005/2006 on the basis of the $^{14}CO_2$ measurements reported in [Levi08];
- $f_{m,wb}$ represents the integral on the tree life, based on a tree growth model [Lewi04], of the biospheric ^{14}C enhancement. As an example, a $f_{m,wb} = 1.16 \pm 0.05$ value was estimated for 30-50 year-old wood cut in 2004, which is assumed to be mainly the wood for residential wood burning in 2005 [Szid09].
- $(EC/OC)_{ER,wb}$ can be evaluated on the basis of literature data on EC/OC emission ratios for wood burning, taking into account only the wood species

[8] These concerns also led to strong reductions of the biofuel targets of energy consumption (in Germany, the biofuel target for road transport, proposed in 2007 to be 20% by 2020, has recently been decreased to a little more than 6% [UNEP09]).

representative of the sampling country. In [Szid06], for residential wood burning, assumed to be the main wood burning source in Switzerland, it was assumed an emission ratio $(EC/OC)_{ER,wb} = 0.16 \pm 0.05$. This information, obtained as an average on many literature data, bears a great uncertainty (~ 32% relative standard deviation), which is essentially due to variability among the considered literature works in wood burning conditions and procedures for the EC/OC determination (it is worth recalling that the EC/OC separation is method-dependent).

Moreover, in evaluating $(EC/OC)_{ER,wb}$ it is very difficult to take into account for agricultural, forestry and private waste burning. However, these activities are very seasonal, therefore a proper programming of the sampling campaign is sufficient to avoid problems related to this issue.

On the basis of the (1.3), the EC source apportionment is only affected by the uncertainties on the quantification of the EC concentration (~ 5÷10% with the thermo-optical method), on the evaluation of $f_{m,wb}$ (~ 4% [Szid09]) and on the AMS measurement of f_m(EC).

Concerning the OC source apportionment, from the relation (1.5) it is clear that the uncertainty on the determination of OC_{wb} is dominated by the ~ 30% contribution from the evaluation of $(EC/OC)_{ER,wb}$. The uncertainty on OC_{biog} is also dominated by the same contribution (in fact, the ~ 5% and ~ 2% uncertainties respectively on the OC_{tot} concentration and on $f_{m,biog}$ are negligible with respect to that). On the contrary, OC_{fossil} is only slightly influenced by the large uncertainty on $(EC/OC)_{ER,wb}$, as can be clearly seen from the observation of a more explicit writing of the last relation in (1.5):

$$OC_{fossil} = OC_{tot} \cdot \left(1 - \frac{f_m(OC)}{f_{m,biog}}\right) + \frac{EC_{tot}}{(EC/OC)_{ER,wb}} \cdot f_m(EC) \cdot \left(\frac{1}{f_{m,biog}} - \frac{1}{f_{m,wb}}\right)$$

where it is evident that the large uncertainty on the last term depending on $(EC/OC)_{ER,wb}$ is weighted with the $(1/f_{m,biog} - 1/f_{m,wb})$ term, whose value is just ~0.09.

In light of the afore-mentioned values, it is clear that relative uncertainties up to 5% on the AMS measurements of the fractions of Modern Carbon of EC and OC will be perfectly acceptable, while relative uncertainties up to ~ 2% may be even negligible.

Such a precision grade is commonly achievable in AMS measurements, or even better, as radiocarbon dating generally needs relative uncertainties not exceeding 1%.

§ 1.5.3 Future perspectives for radiocarbon source apportionment

There is a large uncertainty about the importance of anthropogenic emissions for the total carbonaceous aerosol burden in the atmosphere. In particular biomass burning is an essential issue: emission inventories for such kind of source show significant differences, more than for aerosol of fossil fuel origin [IPCC07]. Many studies demonstrated that the importance of the biomass burning as a carbonaceous aerosol source has been underestimated, both on local and global scale [Szid09b]. Pre-industrial levels of biomass burning aerosols are difficult to quantify, in order to estimate the radiative forcing due to this source [IPCC07].

Many elemental and organic molecular tracers have been proposed and employed to both identify and quantify carbonaceous aerosols sources. Unfortunately, their reliability often suffers from limited atmospheric lifetimes, due to chemical reactivity and highly variable emission factors [Szid06]. On the contrary, radiocarbon guarantees the opportunity of an unambiguous carbonaceous aerosol source apportionment. Due to the crucial role of carbonaceous aerosols in many issues, such as human health and climate change, there is an urgent need for further studies of this kind [Szid09b].

Moreover, as far as climate change is concerned, one of the future challenges of radiocarbon studies on aerosol is focused on the recovery of the history of aerosol carbon, as it is actually freezed in the polar snow and ice [Curr00].

Chapter 2

AMS system and measurements

In this chapter the basic principles of Accelerator Mass Spectrometry (AMS) are reported and a brief description of the main characteristics of the accelerator installed at the LABEC laboratory of Florence is given.

§ 2.1 Introduction

The LABEC laboratory (*LAboratorio di tecniche nucleari per i BEni Culturali, Laboratory of nuclear techniques for Cultural Heritage*) stems from the almost 25 year-long experience of the Florentine research group involved in the field of accelerator-based applications to various fields. It started its "official" activity in 2004, after the successful installation of a new HVEE (High Voltage Engineering Europe) 3 MV Tandetron; it was the first time that the same accelerator was projected to be extensively used for both Ion Beam Analysis (IBA) and Accelerator Mass Spectrometry (AMS). This new accelerator extended the research possibilities with IBA techniques and opened an entirely new possibility of AMS measurements in Florence. Nowadays, AMS and IBA are ordinarily performed in the laboratory. The former one is commonly used for radiocarbon dating, while the IBA techniques are mainly applied in the fields of Cultural Heritage, Environment and Material Science.

IBA techniques allow the determination of sample elemental composition. They are based on the detection of the products of the reactions that happen in the interaction of a beam of accelerated charged particles with the atoms and the nuclei in the sample (target). For the PIXE (*Particle induced X-ray emission*) technique, the detected

products are the X-rays, while for PIGE (*Particle induced γ-ray emission*) and PESA (*Particle elastic scattering analysis*) γ-rays and scattered beam particles are detected, respectively.

In Mass Spectrometry, the separation of ions of different mass, and thus the determination of the sample isotopic composition for a chemical element of interest, is obtained thanks to a magnetic field. In fact, as it is well known, in a magnetic field ions with the same energy and charge state are deflected with different trajectories depending on their mass. Accelerator Mass Spectroscopy (AMS) enhances the selective sensitivity of this technique by coupling the traditional selective elements, such as magnetic and electrostatic analysers, with a particle accelerator. In the AMS, background counts and isobaric interferences are suppressed by using both the source and the accelerator as additional filters [Tuni98].

A scheme of the LABEC accelerator and its beam lines is shown in Figure 2.1. In addition to the AMS beam line, up to now there are five operating IBA beam lines[1]. Among them, two are used for IBA measurements on aerosol samples (see Appendix): the -45° beam line (external beam for aerosol analysis) and the +30° one (multipurpose IBA vacuum chamber).

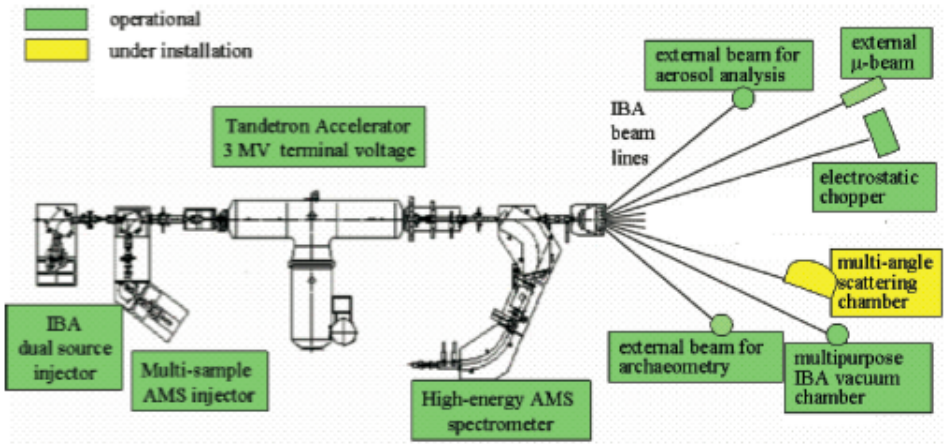

Figure 2.1: Layout of the present Tandem accelerator and beam lines at LABEC.

The accelerator is equipped with two totally independent ion sources for AMS and IBA, so that switching from one operating mode to the other is very simple, with no significant dead times. Actually, the IBA source is a dual one and consists of a Duoplasmatron and of a multipurpose Cs-sputter source. The first one is used to

[1] More details on the LABEC laboratory may be found in [Mand09].

produce high current proton beams or α-beams, the second one is mainly used to produce heavy ion beams (up to now only Carbon and Silicon have been used) or low-intensity proton beams. Conceptually at the reverse than for IBA, where the samples are put at the end of the proper beam line, for AMS measurements the samples have to be put into the AMS source (see § 2.2.1) in the form of solid powder pressed into sample holders (see Figure 2.2).

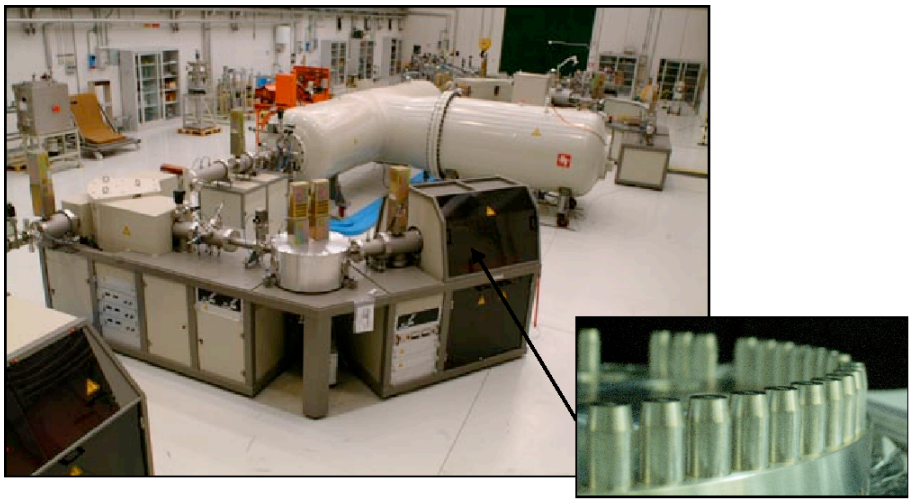

Figure 2.2: The accelerator hall with the AMS source in the foreground; in the small panel the wheel lodging the graphite samples for AMS measurements is shown.

§ 2.2 The AMS system

In the following, the AMS beam line will be briefly described. Although in principle the LABEC AMS system allows the measurement of various isotopes (^{10}Be, ^{14}C, ^{26}Al, ^{129}I), up to now the activity of the laboratory has been focused on radiocarbon and nowadays, to a lesser extent, on iodine.

As such, special attention will be paid to the case of radiocarbon measurements, not to mention that this thesis is indeed focused on this isotope. To this purpose, for the moment, it is sufficient recalling that for radiocarbon measurement it is necessary to determine the ^{14}C sample content. As mentioned in § 1.5, among the three natural isotopes of carbon ^{14}C is the rarest one (the ^{14}C/^{12}C ratio in atmosphere is about $1.2*10^{-12}$). A detailed description of the quantitative determination of radiocarbon by AMS measurements will be given in § 2.3.

The whole AMS beam line[2] is sketched in Figure 2.3.

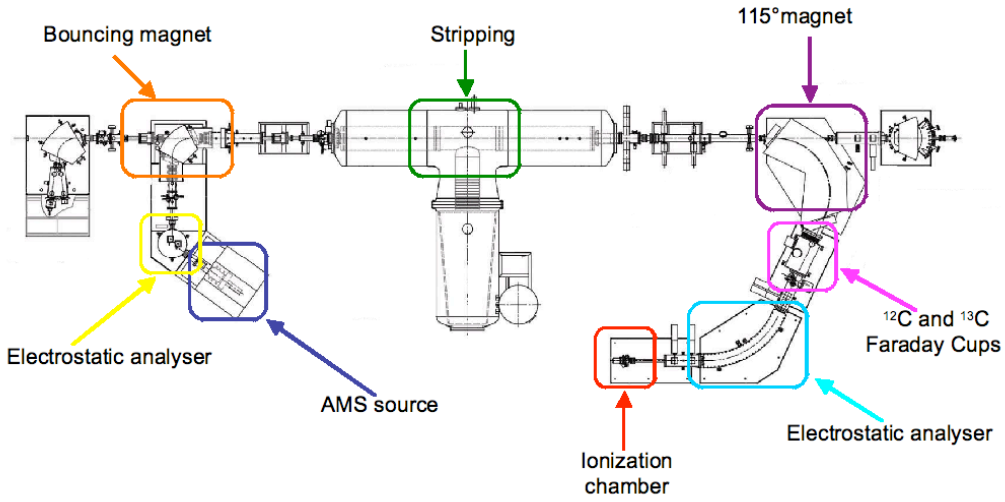

Figure 2.3: The AMS beam line.

§ 2.2.1 The AMS ion source

The AMS source (HVEE model 846B) is a Cs-sputter source with a wheel for the allocation of up to 59 samples, or "cathodes", which can thus be easily changed by means of a mechanical arm without opening the source.

In a sputtering source (see Figure 2.4), caesium vapours (produced by the heating of a caesium reservoir connected to the source itself) are thermally ionised by contact with the so-called ionizer, a metal semi-spherical plate provided with a central hole and kept at a temperature of about 1100°C. The so-formed positive ions are focused by a proper electric field on the target surface, which is kept at a negative voltage with respect to the ionizer. The target surface is cooled in order to condensate a thin Cs layer on it. The sputtered atoms and molecules acquire a negative charge by passing through this thin Cs layer and are thus repelled by the potential of the target. Finally, after having passed through the ionizer central hole, the negative ion beam is accelerated to the extraction electrode and therefore injected into the low-energy side of the beam line. In our case, the sputtered targets are indeed the samples to be measured therefore samples will also be referred to as "cathodes", hereinafter.

In the 846B source, during sputtering, the sample can be moved with respect to the Cs beam, so that almost all the surface can be scanned and it is possible to average out on the possible inhomogeneities.

[2] More details on the AMS beam line may be found [Fedi07].

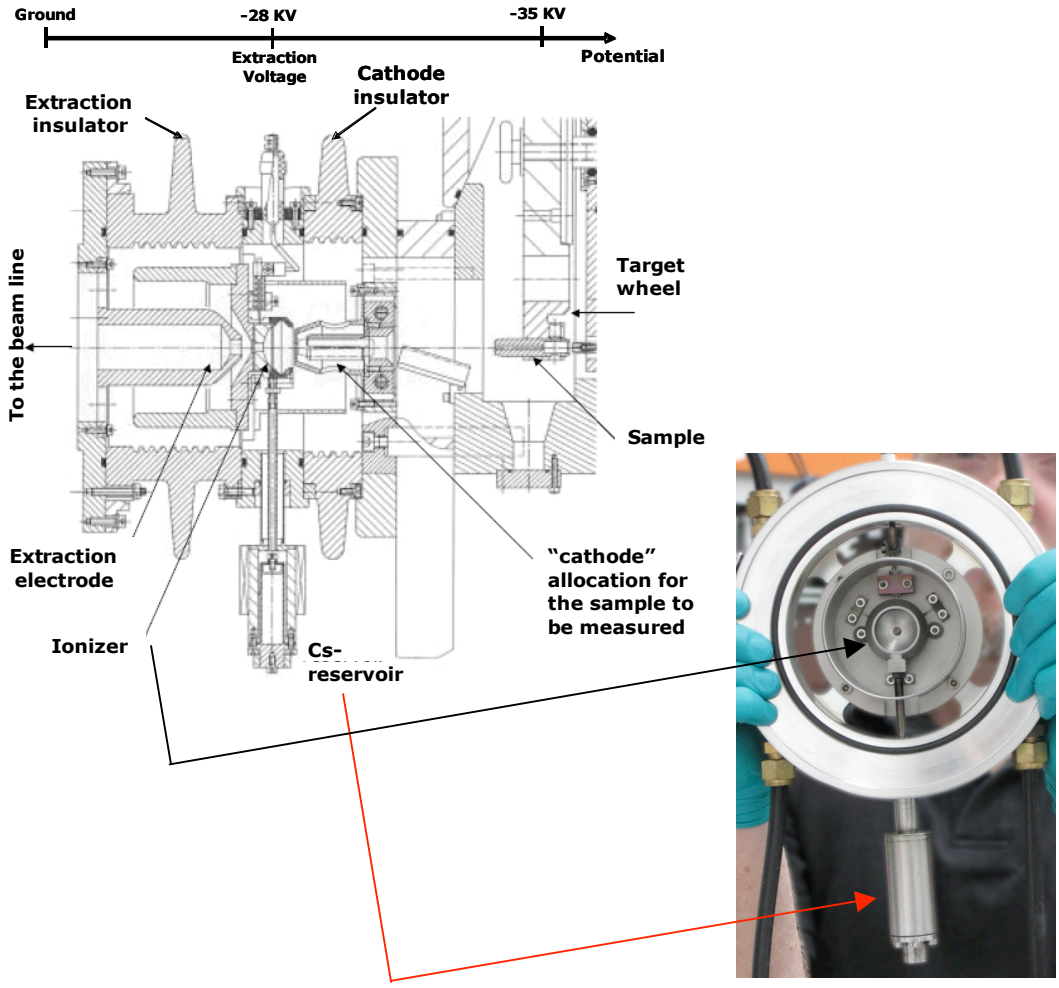

Figure 2.4: Technical drawing of the AMS source (courtesy of HVEE). A detail of the LABEC AMS source is also shown.

As mentioned before, in AMS the source itself acts as a filter for isobars: in the case of radiocarbon, the main interfering isobar is the ^{14}N, and it is suppressed because it does not form any negative ion (in a tandem[3] accelerator, such as the one at LABEC, only negative ions can be injected) [Benn77].

§ 2.2.2 AMS pre-analysis on the low-energy side

In order to inject into the accelerator only ions with the desired mass, energy and charge state, after the source the beam passes through some first pre-analysing components.

[3] See Paragraph 2.2.3.

After the extraction, a first Einzel lens focuses the fragments from the sputtering process towards an electrostatic analyser, which selects ions with a specific energy/charge ratio.

The selection of the mass of the injected ions is then performed by means of a magnet. In fact, the ions passing through a magnetic field B are deflected from the original path with a bending radius r depending only on the mass m of the ion itself, once that the energy E and the charge state q of the ion are fixed:

$$r = \frac{\sqrt{2mE}}{qB}$$

In order to measure the carbonaceous isotopic composition of a sample, a sequential injection of the three masses 12, 13 and 14 into the accelerator is necessary: the switch between the transmitted masses has to be very fast and therefore it can not be achieved by just changing the magnetic field B, because of magnetic hysteresis. So, the sequential injection is achieved by changing the energy E of the ions passing through the magnet. A proper voltage is applied to the magnet chamber (electrically insulated from the beam line) and its sequential changes result in sequential changes of the ion mass transmitted and injected into the accelerator (this is the so-called "bouncing" system). The 90° bouncing magnet is usually set for mass 13, so that switching from a convenient positive voltage to a negative one allows to switch from ^{12}C to ^{14}C. The transition time from a steady voltage to another one is of the order of one tenth of ms. During this time a "blanking" voltage is applied to the beam, just after the bouncing magnet, so that it is completely deflected from the straight path and no spurious particle can be injected into the accelerator.

The sequential injection time laps that are commonly used in Florence for Radiocarbon dating measurements are the following:

$$\Delta t_{14} = 8.5 \text{ ms} ; \Delta t_{13} = 0.6 \text{ ms} ; \Delta t_{12} = 6 \text{ } \mu\text{s}$$

For most of the time, the bouncing magnet injects ^{14}C, while the time laps for the two stable isotopes are inversely proportional to their natural abundances (in nature, the $^{13}C/^{12}C$ ratio is ~1/100), in order to obtain similar beam currents on the high-energy side for ^{12}C and ^{13}C (see § 2.2.4).

§ 2.2.3 The accelerator

As previously mentioned, the accelerator installed at the LABEC is a tandem accelerator with 3 MV as maximum terminal voltage, achieved with a cascade generator

similar to Cockroft and Walton systems. The working principle of a tandem accelerator can be qualitatively described as follows: the particles are injected as negative ions and are accelerated towards a positive high voltage terminal; when they reach it, they change their charge state from negative to positive due to the interaction with matter (stripping of the electrons). After the change of their charge, the particles are accelerated again by the same potential. At the Tandetron of Florence, the stripping medium is Argon gas, injected at the terminal in a channel of 13 mm diameter.

In more detail, stripping is a charge exchange process that consists in the loss of one ore more electrons by an ion passing through matter. Actually, when penetrating a medium, ions may undergo both electron loss and capture. The probabilities for these two processes generally differ and depend on the ions charge state and velocity. Therefore, due to stripping the beam develops an ion charge-state distribution, which evolves towards a dynamic charge-state equilibrium as the ions get deeper into the medium (see Figure 2.5); the medium thickness corresponding to the achievement of the charge-state equilibrium is called "equilibrium thickness" [Hell05].

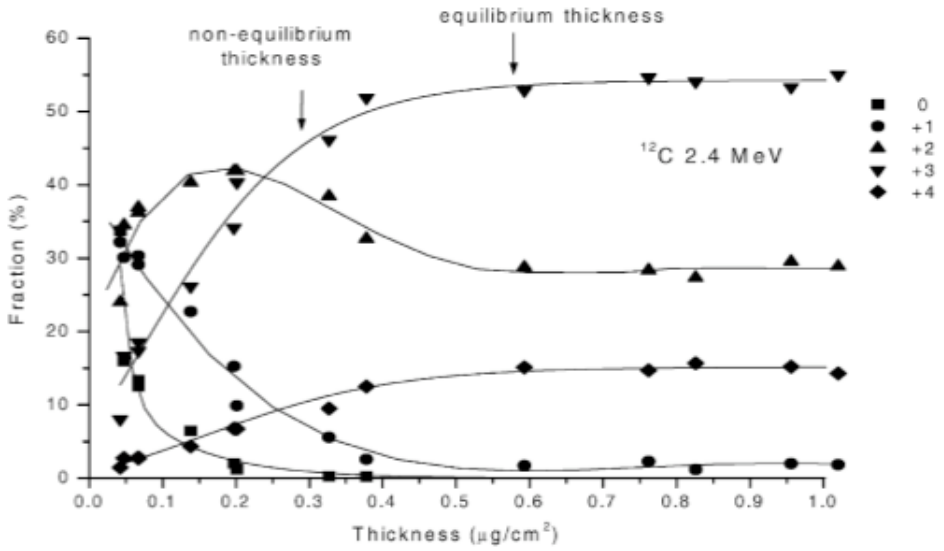

Figure 2.5: Charge-state distribution as a function of the medium (N_2) thickness for ^{12}C ions at a terminal voltage of 2.4 MV (reproduced from [Kiis02].

In the typical AMS measurement conditions at LABEC, i.e. provided an Argon thickness exceeding the equilibrium thickness in the stripping canal and 2.5 MV terminal voltage, the most probable charge state for carbon ions after the stripping is 3+ [Sute90].

As previously mentioned, in AMS measurements the accelerator itself acts as an additional filter to suppress the molecular interfering isobars, such as $^{12}CH_2$ and ^{13}CH; using charge states 3+ (or higher) to eliminate molecular ions is very effective as molecules do not have bound states with such electron configurations [Syna09]. In fact, at such charge states, the molecular bonds get instable because the constituent atoms get repelling each other due to the loss of electrons during the stripping process (*Coulomb explosion*). Therefore, after the accelerator the beam is composed by molecular fragments and carbon ions of the selected mass, all having different energies and charge states.

All along the beam line, both before and after the accelerator, there are focusing and diagnostic systems, such as lenses, electrostatic quadrupoles doublets, steerers, beam profile monitors and Faraday Cups (FC). Another important feature of this machine is the very good vacuum level inside the beam lines (~10^{-7} mbar or better), necessary to avoid charge-exchange processes.

§ 2.2.4 AMS analysis on the high-energy side

At the high-energy side (Figure 2.6), the first selective element for AMS is a 115° magnet, whose field is set to transmit $^{14}C^{3+}$ ions. In order to reduce the residual background due to improbable but still possible charge-exchange processes, the transmitted $^{14}C^{3+}$ beam is made to pass through a 65° cylindrical electrostatic analyser, which selects only ions with the proper energy/charge ratio (in the typical conditions for radiocarbon measurements, it selects ions with 10 MeV/3 ratio, which is the value that only ^{14}C ions having undergone the stripping process exactly at the high voltage terminal may have).

The ^{14}C ions are detected by means of a gas ionisation detector, filled with butane (25 mbar) and with a Mylar entrance window 10×10 mm^2 wide and 125 $\mu g/cm^2$ thick. The detector signals, after being amplified, are acquired only during the ^{14}C arrival time window (determined on the basis of the timing signals from the bouncing system and on the time of flight of the ions through the beam line, 4.5 μs in our case). The detection system, in principle, allows the measurement of ΔE-E spectra. However, for radiocarbon measurements the further discrimination provided by the differential energy loss analysis is not necessary, as the previous filters are sufficient to discriminate the signals of interest; in fact, typically, only the ΔE spectrum is acquired.

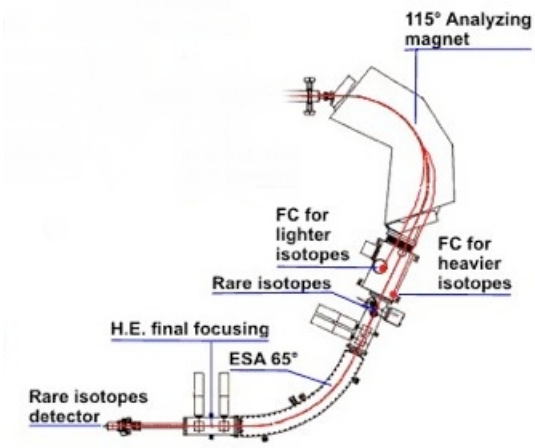

Figure 2.6: AMS high-energy side beam line.

The ^{12}C and ^{13}C ions are deflected in the 115° magnet with different trajectories and are measured by means of two off-axis Faraday Cups.

Actually, the ^{13}C Faraday Cup is composed of two half-plates, very close each other but electrically insulated. In optimal measuring conditions, the magnetic field of the 115° magnet should be tuned so that the ^{13}C ions are bent on a trajectory centred into the Faraday Cup, as the relative paths of the different isotopes are fixed. Thus, the beam current measured on the two half-plates (hereinafter simply "plates") should be the same. The difference between the currents measured on the two plates is called *slit error:* when the ^{13}C beam is aligned with the centre of its Faraday Cup the slit error is zero; otherwise, the slit error is not nil, as the signals from the two plates are different.

AMS measurements usually run for a long time (some days, during both day and night), therefore slight variations of environmental parameters such as temperature, might occur and affect the beam transport. In such cases, the currents measured on the two plates are different, as the ^{13}C beam is not longer centred into the Faraday Cup. The difference between these two signals, i.e. the *slit error,* is sampled with high frequency and it is used as feedback to slightly modify the high terminal voltage in order to restore the correct trajectories through the selective elements (mainly the 115° magnet) on the high-energy side. This feedback system allows the change of the rigidity of the ions, in order to optimise the beam transport, by changing the high voltage applied to the tandem in a range of about ±15 kV with respect to the voltage selected and controlled by the generating Voltmeter[4].

[4] A generating Voltmeter (GVM) is usually used on the electrostatic accelerators to measure the voltage on the terminal, as it produces a signal that is proportional to the terminal voltage itself.

Before starting an AMS run, a fine tuning of the beam is mandatory; for example, as far as the beam tuning at the high-energy side is concerned, the value of the magnetic field of the 115° magnet is chosen in such a way to (see Figure 2.7):

- Centre the ^{13}C beam into its Faraday Cup;
- Have a constant $^{12}C/^{13}C$ current ratio (such ratio is used for data analysis and gives information about the relative paths of the two isotopes);
- Maximise the ^{14}C collection in the gas ionization detector.

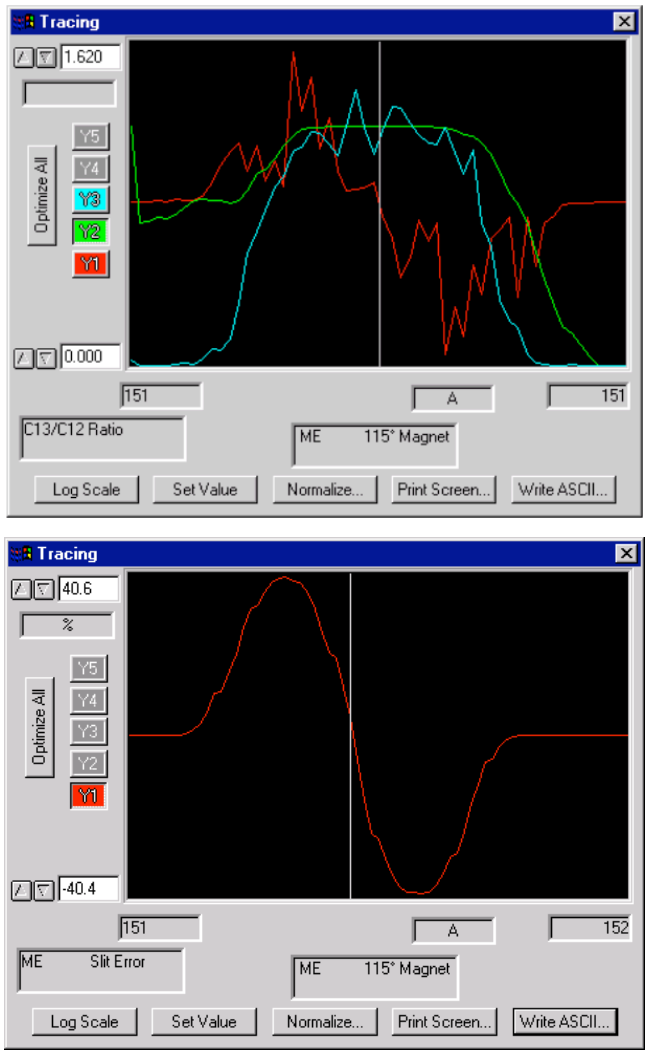

Figure 2.7: Beam tuning at the high-energy side. Upper panel: tracing, with the 115° magnetic field value increasing, of the $^{13}C/^{12}C$ currents ratio (green), radiocarbon counts in the gas ionisation detector (blue) and the slit error (red); the white marked value is the proper value of the magnetic field for correct beam transport.
Lower panel: tracing of the slit error alone, when only ^{13}C is injected.

§ 2.3 Radiocarbon measurements

As mentioned in § 1.5, the aim of a radiocarbon measurement, whatever is its application (dating, aerosol source apportionment or anything else), is to determine the concentration of the 14-mass isotope.

Actually, both radiocarbon dating and aerosol source apportionment relay on the hypothesis that living organisms have the same radiocarbon concentration as in the atmosphere. This implies, for dating, that living organisms have the same age as the atmosphere and, for aerosol source apportionment, that biogenic aerosol are characterised by the same radiocarbon concentration as in atmosphere. Nevertheless, this hypothesis is only approximately true because of isotopic fractionation, since natural biochemical processes occur in preference with the lighter isotopes. Due to isotopic fractionation, living organisms are expected to appear radiocarbon-depleted with respect to the atmosphere. A correction for isotopic fractionation can be done on the basis of the measurement of the $^{13}C/^{12}C$ ratio; in fact, since both ^{13}C and ^{12}C are stable isotopes, this ratio is not time-dependent and is affected only by isotopic fractionation, so this correction is very powerful in radiocarbon dating. Quantitative details will be given in § 2.3.1.

When all the carbon isotopes are measured, i.e. when ^{12}C and ^{13}C are also measured in addition to ^{14}C, AMS is not only a very sensitive technique able to measure the radiocarbon content of small samples, but it also makes possible the contemporary evaluation of the sample isotopic fractionation.

It is worth stressing that the radiocarbon measurement by AMS is not an absolute measurement. Sample isotopic ratios are measured relative to a standard with a known isotopic ratio, from which some cathodes are prepared and put into the source together with the ones prepared from the unknown samples. In other words, the AMS measurement method relies on the idea that unknown samples and standards, measured in a sequential mode under the same conditions, behave in same way in the instrument, thus allowing the determination of the isotopic ratios of the unknown samples by comparison with the isotopic ratios of the standards.

Therefore, in an AMS measurement at our accelerator, the following data are collected:

- Isotopic ratios for the unknown samples: $^{13}R_{smp,meas}$ and $^{14}R_{smp,meas}$;
- Isotopic ratios for the standard material: $^{13}R_{std,meas}$ and $^{14}R_{std,meas}$;

where the following definitions have been used:

$$^{14}R = {}^{14}C/{}^{12}C$$
$$^{13}R = {}^{13}C/{}^{12}C \qquad (2.1)$$

§ 2.3.1 Quantitative AMS data analysis

Without claiming to be exhaustive, a brief overview on the steps leading from the measurement of the three carbon isotopes to radiocarbon data reporting is given hereinafter.

$^{13}C/^{12}C$: isotopic fractionation

By international convention, the fractionation of ^{13}C relative to ^{12}C in a sample was defined as [Keit64]:

$$(\delta^{13}C)_{smp} = \left[\frac{^{13}R_{smp} - {}^{13}R_{PDB}}{^{13}R_{PDB}}\right] \cdot 1000 \qquad (2.2)$$

where $^{13}R_{smp}$ and $^{13}R_{PDB}$ were the $^{13}C/^{12}C$ ratios respectively in the sample and in the so-called PDB standard, a limestone fossil of Belemnitella Americana from the Cretaceous Peedee formation in South Carolina (USA).

Actually, the PDB standard was discontinued and it was replaced in 1983 by the reference Vienna-PDB (VPDB) [Gonf84], which was defined by using NBS19 (*National Bureau of Standards* 19) as a reference material with $\delta^{13}C$ = 1.95 ‰ with respect to VPDB.

By convention, the ^{13}C isotopic fractionation correction factor is expressed for all samples by normalising it to -25‰ with respect to VPDB, being -25‰ the $\delta^{13}C$ of the so-called mean wood.

According to what demonstrated in [Crai54], the ^{14}C fractionation correction factor is given by the square[5] of the ^{13}C fractionation correction factor. With this assumption, for every sample the $^{14}C/^{12}C$ ratio corrected for fractionation ($^{14}R_{smp,corr}$) is related to the

[5] Actually, the square relation was demonstrated for natural processes. However, since there is no reliable experimental evidence for the true value of the exponent, and because this uncertainty is irrelevant in light of the analytical precision of ^{14}C measurements, the square relation is accepted as a sufficient approximation [Mook99].

measured $^{14}C/^{12}C$ ratio ($^{14}R_{smp,meas}$) by the following, generally used, approximated equation:

$$^{14}R_{smp,corr} \cong {}^{14}R_{smp,meas} \cdot \left[1 - 2 \cdot \frac{25 + (\delta^{13}C)_{smp}}{1000}\right] \tag{2.3}$$

Reporting ^{14}C data

Since the very beginning of radiocarbon measurements, it was agreed that all laboratories should report their results, i.e. the measured $^{14}C/^{12}C$ ratios, as relative to an internationally accepted value, which was conventionally assessed to be the isotopic ratio in AD 1950, i.e. the 95% of a specific batch of oxalic acid (OxAcI) produced by the US National Bureau of Standards (NBS). Nowadays, this standard is out of stock and has been substituted by a new batch of oxalic acid (OxAcII), provided by the US National Institute of Standard and Technology (NIST, formerly NBS).

Radiocarbon concentration is usually expressed in *percent of Modern Carbon* (pMC). Although some confusion about the use of this term exists, the most adopted definition is the following one[6] [Proc72, Stui77, Mook99, Rom00]:

$$(pMC)_{smp} = \frac{^{14}R_{smp,corr}}{0.95 \cdot {}^{14}R_{OxAcI,corr}} \cdot 100 \tag{2.4}$$

where both $^{14}R_{smp,corr}$ (the sample $^{14}C/^{12}C$ ratio) and $^{14}R_{OxAcI,corr}$ (the NBS OxAcI $^{14}C/^{12}C$ ratio) are intended to have been measured at the same time (or time-corrected to be referred to the same measurement time) and to have been already corrected for isotopic fractionation according to relation (2.3). In this way, pMC is defined as a time-independent value, relating the sample isotopic ratio to the international reference value, namely the 95% of the OxAcI isotopic ratio. It is important to notice that, by this definition, radiocarbon concentrations are normalised to the "modern" concentration of the reference year 1950.

After OxAcI, many reference materials have been produced, and their isotopic ratios

[6] Here, the definition of pMC is reported according to the aforementioned nomenclature, which is typical in AMS measurements. The earlier definition is:

$pMC = A_{SN} / A_{ON} \times 100$

where A_{SN} is the measured and $\delta^{13}C$-corrected sample activity and A_{ON} is 95% of the measured and $\delta^{13}C$ -corrected activity of NBS OxAcI.

have been certified in pMC, according to equation (2.4). As previously mentioned, nowadays the most used normalisation standard is the NIST OxAcII, whose radiocarbon content is certified to be (134.06±0.04) pMC [Stui83].

Radiocarbon concentration in an unknown sample expressed in pMC is thus simply obtained by the following relation:

$$(\mathrm{pMC})_{\mathrm{smp}} = (\mathrm{pMC})_{\mathrm{std}} \frac{{}^{14}\mathrm{R}_{\mathrm{smp,corr}}}{{}^{14}\mathrm{R}_{\mathrm{std,corr}}} \tag{2.5}$$

where $(\mathrm{pMC})_{\mathrm{std}}$ is the certified radiocarbon content for the measured standard.

As mentioned in §1.5.1, some laboratories report their radiocarbon data as *fraction of Modern Carbon* (f_m); this term is simply related to pMC, as defined in (2.4), by the relation:

$$(f_m)_{\mathrm{smp}} = \frac{(\mathrm{pMC})_{\mathrm{smp}}}{100} \tag{2.6}$$

§ 2.3.2 Measurement-induced isotopic fractionation

As previously mentioned, fractionation effects occur in nature leading to variations in the equilibrium distributions of the isotopes of carbon. It is possible to take into account these effects and to correct for them by measuring the $\delta^{13}C$ for the samples.

Moreover, since the late 1990s, many AMS laboratories have reported a dependence of the measured isotopic ratios on sample size, often when dealing with small size samples [Vand97, Brow97, Pear98]. Although there has been debate whether this effect is due to real isotopic fractionation [Pear98], to a "blank shift" as a result of dead carbon contaminations [Brow97] or to a combination of the two causes [Alde98], the occurrence of isotopic fractionation effects during radiocarbon AMS measurements has been so far ascertained [Nade04]. The causes of such effects can be numerous; without claiming to be exhaustive, the "more popular" ones are reported:

- Incomplete graphitisation;
- Fractionation in the negative ion production by sputtering;
- Space charge effects inside the machine.

Concerning fractionation during graphitisation, [Vand97] showed that graphite produced by reactions that failed to reach completion is depleted both in ^{14}C and ^{13}C. A

similar result was found in [Hua04], where it is also stressed that this effect can be corrected using the $\delta^{13}C$ measured during the AMS run, if both unknown samples and standards undergo to the same processes.

Fractionation inherent to the negative ion production by sputtering was hypothesised by [Nade87], but later excluded on the basis of further experiments performed at the Leibniz-Labor AMS system, based on a HVEE 3 MV Tandetron accelerator equipped with a 846B model Cs-sputter ion source [Nade04]. Since the same model of source is installed also on the LABEC AMS system, these results can be directly applicable to our case too.

Space charge effects are indicated to be the primary isotopic fractionation cause by [Pear98, VonR98]; quantitative details on the beam dynamics are there given. The argument can be qualitatively summarised as follows: Coulomb repulsion affects lighter isotopes more strongly, so it is possible that ^{12}C detection is less efficient relative to ^{14}C detection. This effect can be less relevant for small samples with respect to large samples, for which the fractionation is compensated during the AMS system tuning[7], with the net effect of an apparently lower $^{14}C/^{12}C$ ratio with sample size decreasing.

A confirmation to this theory can be found in [Nade04], where extracted current intensity, and not directly the sample size, is clearly shown to determine the fractionation. Obviously, the extracted current intensity is related to the sample size, but the target properties are demonstrated to be better described by the C/Fe ratio, i.e. by the sample concentration inside the iron powder (used as catalyst for graphitisation and also necessary to provide cohesiveness to the sample bead pressed inside the aluminium sample holder).

In short, AMS measurements appear to be prone to machine-induced isotopic fractionation, especially when dealing with small samples. However, it is possible to compensate effectively for machine fractionation by measuring samples relative to size-matched standards, as it is demonstrated in [Pear98, VonR98, Nade04]. In this manner, all the cathodes give very similar extracted currents. Therefore, with the "matching-size" method, unknown samples and standards behave in the same manner in the instrument; thus, the determination of the isotopic ratios of the unknown samples by comparison with the isotopic ratios of the standards is possible.

[7] Tuning of the AMS machine is commonly performed with large samples (~1 mgC).

§ 2.3.3 Radiocarbon measurements at LABEC

At LABEC, samples are prepared following the matching-size method (i.e. samples and standards have the same size): although there is still some debate about the profitability of this method with respect to the non-matching one [Sant07], we conservatively decided to follow this method in order to prevent possible machine-induced fractionation effects (see § 2.3.2).

For every radiocarbon measurement run, many cathodes are prepared from the standard NIST OxAcII for normalization, and from "dead" graphite for blank evaluation and subtraction. The overall accuracy of the measurements is constantly checked by putting into the ion source also some cathodes prepared from reference materials such as the C7 oxalic acid provided by IAEA.

One measurement of all the samples allocated into the target carrousel is called "batch". During each batch, in order to average over possible inhomogeneities, every sample is sputtered for 30 s in nine points[8] (called "blocks"), with an overall measurement time of ~ 6 min (including the sample positioning times).

Batches are commonly allowed to run until at least 40000 counts on each OxAcII standard cathode are collected, thus reducing the counting statistics error below 0.5%. The number of performed batches is therefore chosen on the basis of the extracted current and, possibly, on the radiocarbon content of the "unknown" samples (this is especially important for radiocarbon dating, when a high precision is typically needed).

^{14}R and ^{13}R of "unknown" samples are normalised to the average values of ^{14}R and ^{13}R of the standards measured within the same batch. After having verified that the variations between the batches can be fully explained by statistics (see the discussion below about uncertainties), the normalised ^{14}R and ^{13}R of "unknown" samples are finally averaged over all the batches. It is also possible to normalise the ^{14}R and ^{13}R of the "unknown" samples to the standards ones when all these ratios have already been averaged over all the batches. As the AMS measurement method relies on the stability of all system parameters in order to compare unknown samples with standards, the first procedure is preferred because it allows the compensation for possible slight variations of the experimental parameters during the whole time necessary to perform the desired number of batches (as an example, performing 10 batches on 25 samples takes about 25h). Obviously, if no variation occurs, the two procedures are perfectly equivalent.

[8] Both sputtering spots and times can be easily changed by the user.

Radiocarbon concentrations, expressed in pMC, are obtained by correcting the measured $^{14}C/^{12}C$ ratios for isotopic fractionation ($^{13}C/^{12}C$ ratios are also measured in the same run from Faraday Cups at the exit of the 115° magnet). After background subtraction, the corrected $^{14}C/^{12}C$ ratios are normalised to the isotopic ratios measured for the NIST OxAcII standards.

Uncertainties

As previously mentioned, during each batch every sample is sputtered in nine points. Therefore, for every sample, the uncertainty on the ^{14}R measurement in a single batch is due to the statistical uncertainty on radiocarbon counts, to the sample superficial inhomogeneities and to the reading error on the ^{12}C current measurement (this contribution is totally negligible with respect to the other two).

The uncertainty on $^{14}R_{av}$ (i.e. the average of ^{14}R over all the performed batches) is due to the uncertainty on the ^{14}R measurement in every single batch and to the variability among the batches. The variability among the batches is determined by the variations in the machine parameters and, to a lesser extent, by the bulk inhomogeneities of the sample. This variability is the main contribution to the uncertainty on $^{14}R_{av}$ when dealing with standard samples (i.e. with contemporary samples). For "unknown" samples, this contribution may be less important than the one coming from the ^{14}C counting statistical uncertainty, depending on their radiocarbon content.

Concerning the ^{13}R ratio, the contributions to the uncertainties on both its single measurement and its average over all the batches ($^{13}R_{av}$) are analogous to those for ^{14}R, once the ^{14}C counting statistical uncertainty is substituted by the reading error on the ^{13}C current measurement. The latter contribution is always negligible with respect to the other involved ones. Therefore, the uncertainty on ^{13}R as measured in a single batch is always dominated by the sample superficial inhomogeneities while the uncertainty on $^{13}R_{av}$ is dominated by both sample inhomogeneities and, mainly, by the variations in the machine parameters.

As previously mentioned, pMC values of unknown samples are calculated batch-by-batch, normalising their ^{14}R and ^{13}R to the averaged values of ^{14}R and ^{13}R over all the standards within the same batch (batch-by-batch normalisation). In this manner, the contribution to the pMC uncertainty coming from the variability of the machine parameters among the batches is minimised. As a consequence, if bulk inhomogeneities

are negligible, the pMC uncertainty should be fully explained by the statistical contribution on the unknown samples ^{14}R (calculated according to the Poisson statistics expected for ^{14}C counting measurement). Therefore, for every sample the dispersion of the pMC values on the batches (calculated as the standard deviation of the mean) should reflect the statistical uncertainty. Actually, these two values are always compared in order to check whether they are of the same order of magnitude. This condition is almost always verified and in these cases the uncertainty on pMC is conservatively chosen as the maximum between these two values. However, if discrepancies arise, special attention is paid to investigate possible causes (e.g. samples inhomogeneities or transitory machine problems[9]). When the singled out causes affect only a few batches, it may be sufficient to reject the data from those batches.

[9] For example, when dealing with very small samples possible transitory problems may arise by the accelerator stabilization system embedded in the ^{13}C Faraday cup (see § 5.2.2).

Chapter 3

The AMS aerosol sample preparation laboratory

In this chapter the new sample preparation laboratory for the aerosol samples, especially developed, installed and tested during this PhD activity, is described.

§ 3.1 Introduction

The realization of a proper sample preparation line is one of the key points to be developed in order to perform AMS measurements, and which sample preparation line may be the "proper" one depends on the typology of the samples and on the aim of the work.

As far as the radiocarbon measurements are concerned, a "typical" sample preparation line is essentially based on four parts (Figure 3.1): the cleaning of the carrier gases[1], the combustion of the sample, the selection and collection of the produced CO_2 and the conversion of this gas to solid samples (graphitisation[2]) to be injected into the AMS source.

Moreover, it is worthy to recall the importance of cleanliness during the preparation of samples for radiocarbon measurements. Carbon is everywhere, so it is necessary to be very careful and to follow very strict protocols for the cleaning of the laboratory materials and instruments to get rid of contamination effects.

[1] This first phase can be neglected if very pure gases are supplied; the "acceptable" purity of the gases depends on the sample preparation protocol adopted (see §3.2.1).
[2] This latter phase is not necessary in case of accelerators equipped with a gas ion source.

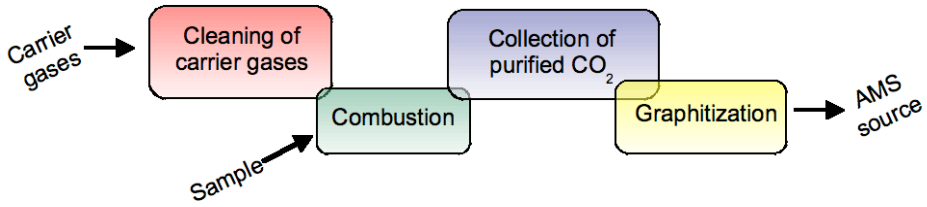

Figure 3.1: Scheme of a sample preparation line for radiocarbon measurements.

As discussed in § 1.5, radiocarbon measurements on aerosol samples have been carried out since the 1960s, but it is only with the advent of AMS that the analytical technique gained the sensitivity necessary to measure the radiocarbon content in the small quantities of aerosol sampled with the desired resolution both in temporal scale and size-segregation (see § 1.3). Recently, great interest has been shown for the potentiality of performing radiocarbon measurements on the separate carbonaceous fractions and an advanced source apportionment model based on these measurements was proposed (see §1.5.2). Presently, only the Laboratory for Radiochemistry and Environmental Chemistry at the Paul Scherrer Institute (Switzerland) is equipped with a proper sample preparation line for this purpose and currently performs this kind of measurements [Szid09]. A few other laboratories, such as ours, are working in order to implement similar facilities (e.g. NIES-TERRA [Uchi09]).

Before starting to design our sample preparation laboratory, the Swiss facility was extensively studied, and single details were deeply discussed with the research team operating it during a visit to the laboratory itself. This study was very useful, and many ideas for the new facility stemmed from it. Since the beginning, it was clear that relevant variations needed to be done in order to match the requirements for the radiocarbon measurements in our laboratory. In fact, the samples prepared at the Swiss laboratory are currently analysed in Zurich mainly by means of an AMS system equipped with a gaseous source, which allows the measurement of very small carbon quantities (~10 μg C). Conversely, our AMS system only supports solid cathodes, and when we started this work it had been used only to measure "medium-size" samples (~600 μg C) for radiocarbon dating. In Florence a sample preparation laboratory has already been developed and it is currently running in order to prepare samples of this size starting from materials such as wood, bones, carbons and paper that have to be dated.

During this PhD work, a new sample preparation line was designed having in mind the fulfilment of the following requirements:

- The line should produce solid samples to be inserted in the LABEC AMS source; thus, an integrated combustion-graphitisation line is required.
- The line should be as flexible as possible in a wide sample size input range, i.e. it should allow the proper preparation of samples with size of the same order of those used for dating and at the same time should assure the possibility of reducing the samples size as much as possible in order to maximise the aerosol sampling resolution both in temporal scale and size-segregation. However, the chosen size should always match the LABEC AMS system requirements (the issue of a decrease of the sample size is discussed in detail in Chapter 5). The adopted strategy counts on both the use of a relatively large combustion oven (with respect to the one installed on the Swiss line) as well as the efficiency maximisation, which assures the feasibility of the production of smaller samples.
- The line should be equipped with properly fitted devices for the collection and the purification of the produced CO_2 and the efficiency of these devices should be maximised.
- The line should allow the thermal separation between OC and EC; to this aim, a combustion oven able to perform specific thermal evolutions with fast changes in both combustion temperature and atmosphere (oxidising and/or inert) is required. It is worthy to stress that the already running sample preparation line for radiocarbon dating does not satisfy this condition, as the combustion is accomplished by a commercial elemental analyser.

§ 3.2 The new sample preparation line for aerosol samples

The new sample preparation line for aerosol samples has been set up in the frame of the INFN-NUMEN project (*National Institute for Nuclear Physics – NUclear Methods for the ENvironment*), in collaboration with the Physics Department of the University of Milan. A schematic representation of the line is shown in Figure 3.2 and a detailed description of all its parts is given in the following paragraphs.

In order to avoid any contamination, the line was built up with clean materials such as quartz and 316 stainless steel. In particular, quartz was chosen because of its high temperature resistance and it was used in all the "hot" parts of the line (temperatures ranging from 600°C up to 900°C) All the others parts (tubes, valve bodies, fittings)

were made by 316 stainless steel, which can be manufactured much more easily and therefore is an optimum material to produce a line in which leaks have to be minimised under both in-vacuum and in-flow conditions.

The connections between stainless steel parts were made by means of fittings equipped with stainless steel ferrules. The connections to quartz parts were made with Swagelok Ultra-Torr Vacuum fittings whose Viton o-rings were replaced with Kalrez 8900 o-rings, since this elastomer is much more resistant to high temperatures (Kalrez 8900 is certified to have an outgassing rate $<2.7*10^{-7}$ mbar·Liter·sec^{-1}·cm^{-2} up to 290°C).

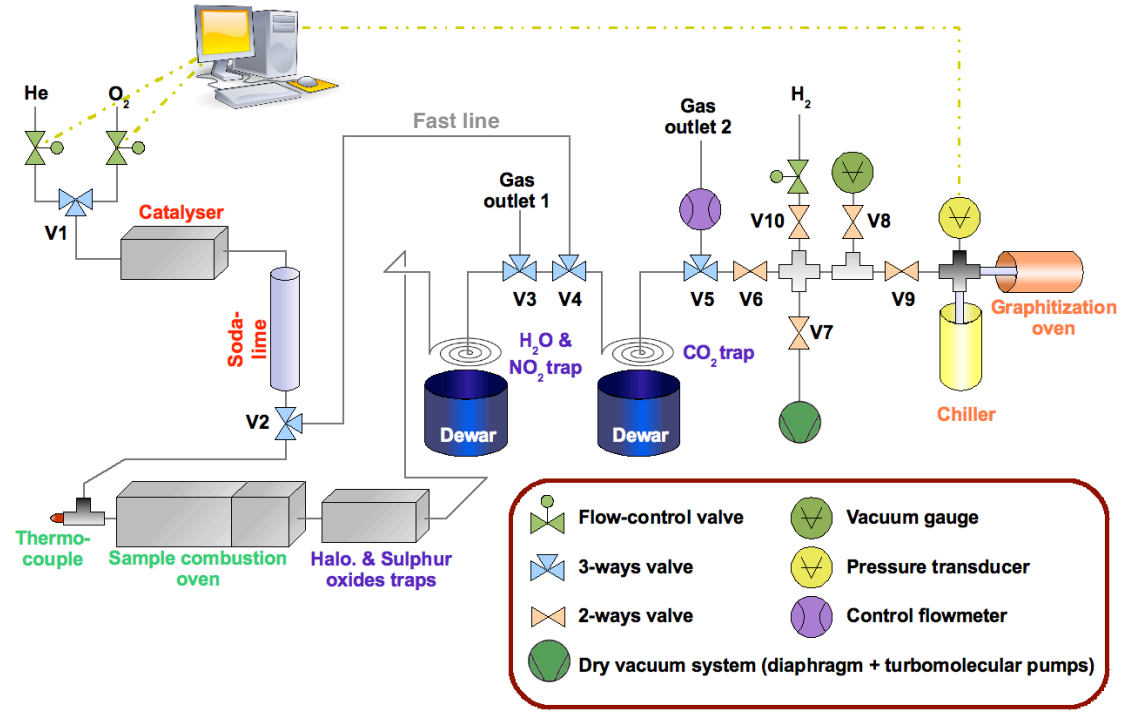

Figure 3.2: Scheme and picture of the preparation line for aerosol samples.

Both quartz and stainless steel parts were previously cleaned by means of ultrasonic baths (first in a 50% acetone/water solution and then in ultra-pure water); afterwards, stainless steel parts were heated in-vacuum for at least 8 hours at 100°C, while quartz parts were kept for 4 hours at 900°C in the air.

§ 3.2.1 Cleaning of the gases

In this new line, the two injected gases, namely Helium and Oxygen, both act as carrier gas and create the proper atmosphere for the combustion. In fact, as is discussed in § 3.3, the combustion protocols for EC/OC thermal separation rely on various steps at different temperatures and different atmospheres; in the following, these gases will be simply called "carrier gases".

Two thermal mass-flow controllers, just at the entrance into the line, set helium and oxygen flows (see Figure 3.3). For proper combustion and EC/OC separation, prompt and accurate gas selection and flow regulations are required. The EL-FLOW series mass flow controllers from Bronkhorst installed in the new line were calibrated for the gases of interest and meet the requirements about accuracy, cleanliness and fast response.

The carrier gases are supplied by gas bottles of high-purity helium (99.998%) and oxygen (99.999%). In any case, in order to avoid any possible contamination, the carrier gases are previously cleaned. This is very important because the combustion protocols (for all the carbonaceous fractions of the aerosol) count on a long time of collection of the produced gas (~ 30 min). Furthermore, it is also necessary to wait for a relatively long time (up to ~ 45 min) to overcome the inertia of the line in establishing the right temperatures and saturate with the proper gas before starting with the combustion. In all this time, there would be the risk of collecting contaminant CO_2, if present. Therefore, it is clear that it is mandatory to remove any contaminant from the carrier gases, even if present in very low quantity.

This purpose is achieved by making the entering gases pass first through a Copper Oxide catalyser kept at 700°C, in order to oxidise any carbonaceous gas to CO_2, and then through an irreversible soda lime trap, which adsorbs all the possible CO_2 (see Figure 3.3).

The catalyser is formed by a cylindrical quartz furnace (10 mm inner diameter, 220 mm long, see Figure 3.4) filled for 140 mm with CuO; it is kept at the proper temperature by means of a commercial heating element, consisting in an iron-chrome-aluminium wire embedded in a ceramic fibre insulator. The case housing the heater and

the furnace provides also an accommodation for a thermocouple, which allows the temperature control. The signal from the thermocouple is read by a PID (proportional-integral-derivative) controller, whose output controls a static relay connecting the heater to its power supply. The case is made of high-temperature resistant Aluminium, and it is stuffed with insulating fibres.

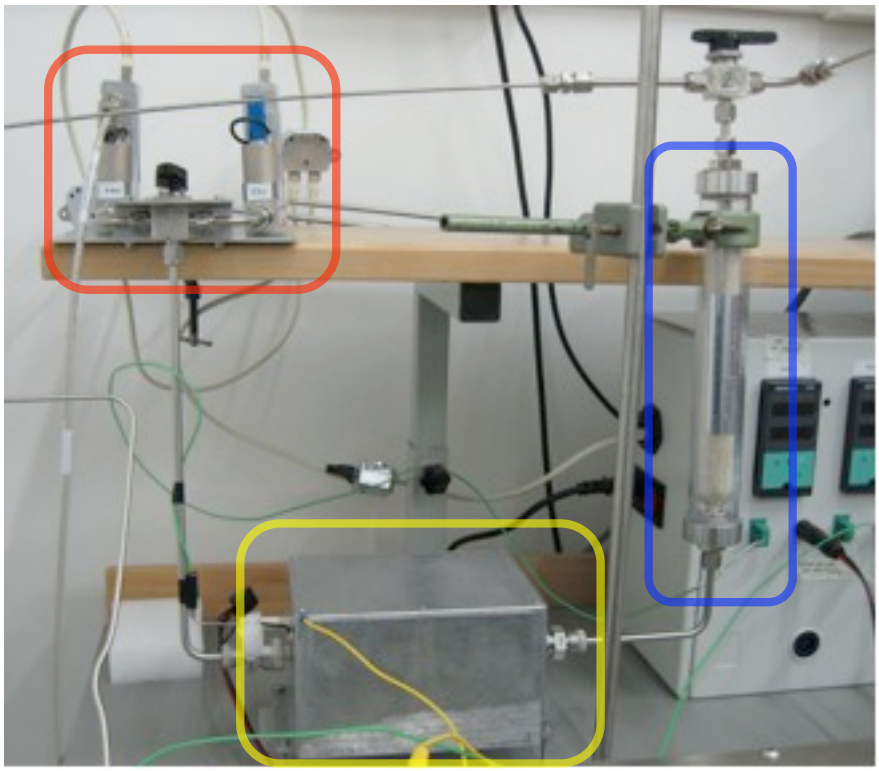

Figure 3.3: Flow setting and cleaning of the carrier gases. Helium and oxygen flows are set by mass-flow controllers (red), and then pass through an oxidising oven (yellow) and a soda-lime trap (blue).

The catalysis efficiency issue was investigated by means of measurements performed by the research group of Milan in the frame of the NUMEN project: a 100% catalysis efficiency can be obtained at a minimum working temperature of 650°C when the furnace (10 mm inner diameter) is filled with CuO for at least 6 cm.

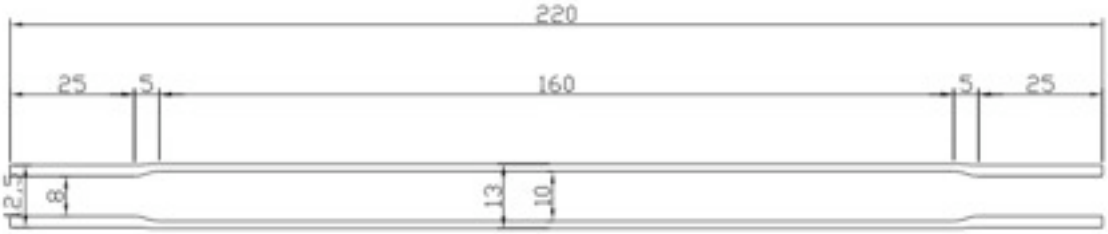

Figure 3.4: Scheme of the oxidising oven furnace; dimensions are expressed in millimetres.

§ 3.2.2 Combustion oven

In order to be able to perform a thermal separation between EC and OC, the combustion oven has to satisfy some specific requirements, which are listed as follows:

- *Temperature uniformity:* the furnace should be characterised by a good temperature uniformity (differences from the selected temperature should be less than 5°C) in all the region lodging the aerosol sample to be sure that the whole sample will undergo the same thermal evolution.
- *Flash heating:* as it is known by literature [Cach89], charring is minimised by flash heating, i.e. by a very fast increase of the temperature (~200°C/min); therefore an essential requirement is an oven with a low thermal inertia, able to perform the flash heating.
- *Presence of a catalyser:* in order to ensure that all the gaseous combustion products yield to their most common oxides, an oxidant catalyser such as Copper Oxide has to be placed as close as possible to the sample combustion zone. The oxidation state is very important for the subsequent phase of purification and collection of the CO_2, based on thermal traps, as condensation temperatures depend very strictly on the formed gas (in particular, it is important that the possible CO evolves to CO_2 to be subsequently trapped[3]).
- *Temperature control:* for thermal evolution, it is very important to know exactly the temperature at which the sample is effectively kept; therefore it is necessary to be able to position a thermocouple as close as possible to the sample itself.
- *Furnace dimensions:* the furnace should be as small as possible, to reduce its thermal inertia and the time needed to establish an equilibrium condition after changes of the carrier gas or in its flux. Obviously, the final dimensions will be a compromise between this requirement and the minimum quantity of aerosol sample to be put inside the furnace, which will need a minimum space available.

All these requirements are not easily satisfied by commercial ovens, so, after a long and unsuccessful research on the available solutions "ready-to-install", we decided to design a "homemade" oven. The core of this oven is a "double" quartz furnace, i.e. a

[3] The boiling temperature of the CO is ~82 K, i.e. lower than the O_2 one; therefore, it would not be trapped and it would flow away towards the gas outlet together with the carrier gases (see § 3.2.3).

furnace composed by two butt-welded quartz tubes of different diameters and lengths. The wider tube, the so-called "main furnace" lodges the "sample boats", two quartz semi-cylinders where the punches of each aerosol sample are put. The second tube is filled with CuO grains (see Figure 3.5). The two tubes are thermally insulated by means of ceramic fibre blankets, so that the catalyser can be kept at the working temperature of 700°C while the main furnace is heated according to the chosen thermal program.

Figure 3.5: The combustion oven: on the left the main furnace, on the right the CuO catalyser furnace, both wrapped by heating coils.

No commercial heater was able to satisfy the requirements about dimensions and, as far as the heating of the "main furnace" is concerned, temperature uniformity and fast temperature increase. Therefore, we opted for two homemade heaters consisting of two stainless steel heating coils wrapped around the two tubes. Great care was given to optimise the temperature uniformity along the 12 cm-long zone of the main furnace lodging the sample boats, so that at 400°C differences between the temperatures measured along the tube with a 1 cm step and the selected temperature were always below 5°C.

Concerning the requirement about dimensions, the minimum volume necessary for the aerosol samples was estimated on the basis of the following considerations:

- In light of the experience gained by the research group working in Florence with the AMS system, the goal of being able to measure cathodes with a quantity of graphite halved with respect to the one usually pressed for radiocarbon dating (~600 μg) reasonably appeared to be achievable. Assuming for the new sample preparation line the same efficiency obtained for the already running sample preparation line (~75%), the quantity of

carbon to be introduced into the line should be ~400 μg. The assumption of obtaining the same efficiency is reasonable and to some extent conservative. In fact, we would expect to obtain something better thanks to some optimisations introduced in the perspective of working with samples smaller than the ones for dating purposes.

- In an urban background site, a typical PM_{10} concentration in air is ~30 $\mu g/m^3$, corresponding to a ~150 $\mu g/cm^2$ aerosol concentration on the filter when sampling is performed by means of standard samplers (see § 1.3). The average carbon content of the aerosol accounts for ~30% of the total mass, therefore ~50 $\mu g/cm^2$ of carbon can be expected on the loaded filter. As the EC fraction typically constitutes ~20% of the carbon load, only 10 $\mu gC/cm^2$ would be expected to be EC[4] in an urban background aerosol sample.

Therefore, in order to perform an AMS measurement on the EC fraction alone (thus for the scarcest carbonaceous fraction), it would be necessary to introduce ~ 40 cm^2 of the loaded filter, i.e. ~ 8 circular punches with a 25 mm diameter.

We planned to insert the 8 punches into the oven by putting them into two semi-cylindrical sample boats to be superimposed to form a cylinder whose external diameter fits the inner diameter of our furnace (23 mm). This configuration maximises the extension of the loaded filter that can be inserted in the finite volume of the oven[5] as to properly expose the aerosol deposition surface to the gaseous atmosphere. The sample boats were designed to be 120 mm long, that is exceeding the 100 mm corresponding to 4 punches of a 25 mm diameter in line (see Figure 3.6). In this manner, the sample positioning inside the oven is not critical (centring the punches in the sample boat we can be sure that they will be lodged inside the part of the oven with uniform temperature). Concerning the whole length of the main furnace it was chosen larger than the 120 mm needed for the sample boats in order to take into account border effects and the space for handling the clamp closing the Rotulex joint mounted at the entrance of the main furnace. Moreover, some centimetres between the last loop of the heating coil and the joint would be necessary in any case to avoid the heating of the

[4] This value lays on the upper limit of the loads to be considered "typical", anyway, as this kind of measurements, being highly time-consuming, will not "ordinarily" performed, this is a value easily obtainable choosing the proper sampling methods and durations.

[5] Rectangular or square punches are not used, as the circular geometry is the proper one for water-soluble compounds extraction (this operation is compulsory for EC analysis; see § 3.3).

Kalrez o-ring mounted on the joint up to temperatures higher than 300°C (maximum temperature at which the Kalrez compound is certified not to degas).

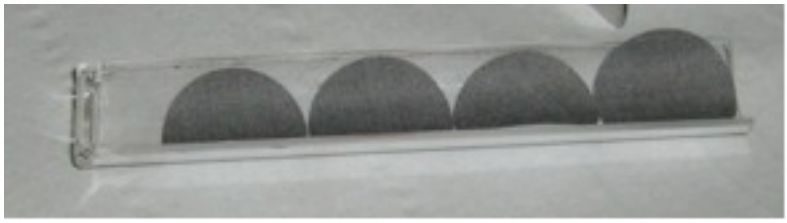

Figure 3.6: Sample boat loaded with four 25 mm diameter punches sampled by an aerosol loaded quartz fibre filter.

In order to reduce the overall oven thermal inertia and encumbrance, the dimensions of the second tube constituting the oven, i.e. the one dedicated to lodge the CuO catalyst, were chosen in order to just slightly exceed the minimum amount of CuO necessary to a have a 100% catalysis efficiency (a 10 mm inner diameter furnace, like this one, should be filled with CuO for at least 6 cm; see §3.2.1).

Final dimensions are reported in the scheme shown in Figure 3.7.

As concerns the temperatures of the two tubes constituting the oven, they are regulated by means of two commercial couples PID-relay (identical to the one used for the catalyser described in §3.2.1) connected to two thermocouples, one for each tube. In the case of the catalyst tube, the thermocouple is put in contact with the tube by passing through a nozzle sealed on top of the tube itself. Regarding the main furnace, as previously mentioned, the important requirement is to be able to control the effective temperature inside the main furnace. Therefore a type K (chromel-alumel) thermocouple is inserted through the Rotulex joint cup and it is positioned along the main furnace axis, just in the middle of the two sample boats. The connection of the joint cup to the previous part of the line and to the thermocouple is made by means of a Swagelock Ultra-Torr Tee connection (see Figure 3.8).

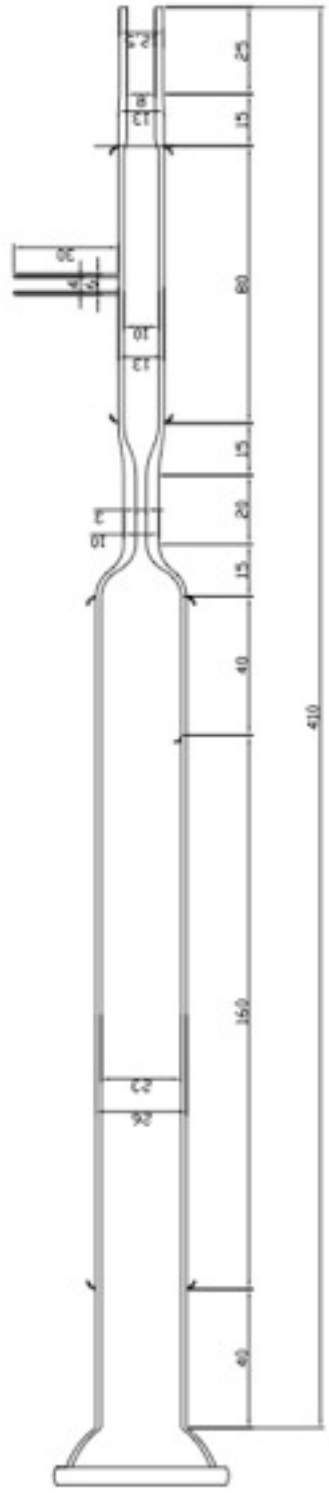

Figure 3.7: Scheme of the furnace of the combustion oven; dimensions are expressed in millimetres.

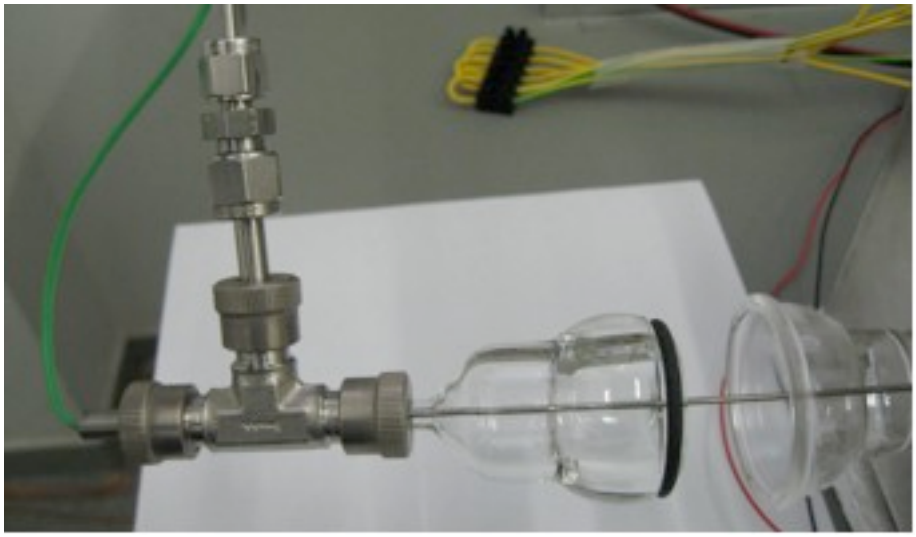

Figure 3.8: Main furnace closing cup, with the thermocouple to be inserted inside the same furnace.

§ 3.2.3 Purification and collection of the produced CO_2

During the combustion, not only CO_2 is produced, but also aqueous vapour, nitrogen oxides (NO_x), halogens and gaseous sulphur oxides. Therefore, the gas stream outgoing from the combustion oven is a mix of all these gases and obviously the carrier gas. In order to transfer only CO_2 into the graphitisation reactor at the end of the line, the gas stream has to be purified, removing all the "undesired" gases, and the CO_2 has to be collected, separating it from the carrier gas flux.

To this purpose, our new sample preparation line counts on some chemical and thermal traps, which are passed by the gas stream in the following order:

- Chemical trap for halogens
- Chemical trap for gaseous sulphur oxides
- Thermal trap for aqueous vapour and NO_x
- Thermal trap for CO_2 collection

Chemical traps

The removal of gaseous sulphur oxides and halogens is achieved by means of two chemical reagents usually used in gas-chromatographic columns, i.e., respectively, AgV and EA-1000, both supplied by Perkin Elmer. For both the reagents, the working temperature is ~800°C, so they were put inside the same furnace, separated one from the other by some quartz wool. The design of the furnace and of the whole oven (Figure 3.9) is identical to the design of the catalyser necessary for the cleaning of the gases (see

§3.2.1): a “modular” solution is very useful both for the set up of the line and for its maintenance.

The furnace is filled for one half with AgV and for the other half with EA-1000. As for the catalyst CuO, the chemical trap quantities were chosen on the basis of measurements performed by the research group of the Physics Department of Milan involved in the NUMEN project.

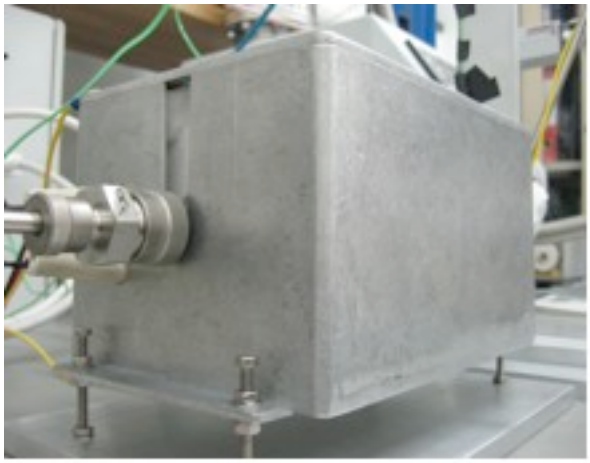

Figure 3.9: Chemical traps oven.

Thermal traps

After the removal of halogens and gaseous sulphur oxides, the gas stream still contains not only the CO_2 but also aqueous vapour, nitrogen oxides and obviously the carrier gas (helium or oxygen depending on the chosen thermal program and therefore on the carbonaceous fraction of interest). These gases can be separated by means of thermal traps on the basis of their different thermo-dynamical properties. In Table 3.1, phase change temperatures at 1 atm pressure are listed for water, CO_2, O_2, He and NO_2 (which is the form of NO_x that we expect to find after the gases produced during the combustion have passed through the oxidising catalyser). In Table 3.1, it is clear that a first thermal trap working at a temperature of ~215K would surely remove both aqueous vapours and NO_2 without trapping the CO_2. In fact, such a temperature is well below the melting temperatures of both aqueous vapours and NO_2 and lays approximately 20K above the CO_2 sublimation temperature.

As concerns the CO_2 collection, a second trap working at ~115K would perfectly comply with the requirement of trapping the CO_2 but not the carrier gas (which ever it

is, He or O_2): in fact, such a temperature is well below the CO_2 sublimation temperature and well above the O_2 and He boiling temperatures.

Gas	Melting temperature (K, at 1 atm)	Sublimation temperature (K, at 1 atm)	Boiling temperature (K, at 1 atm)
H_2O	273.15	-	373.2
NO_2	**262.0**	-	294.2
CO_2	-	**194.4**	-
O_2	54.8	-	**90.2**
He	-	-	4.2

Table 3.1: Phase change temperatures at 1 atm pressure for water, CO_2, O_2, He and NO_2 [Stre71, Fern84, Fand99, Feis06]

The reported phase change temperatures are relative to the atmospheric pressure; in any case, if the maximum overpressure in our line (~ 1.5 atm) is considered, the increase in the phase change temperature is less than 10 K , as shown in Figure 3.10 and Figure 3.11). Such an increase would not affect the correct functioning of the thermal traps, with the (conservatively) chosen working temperatures.

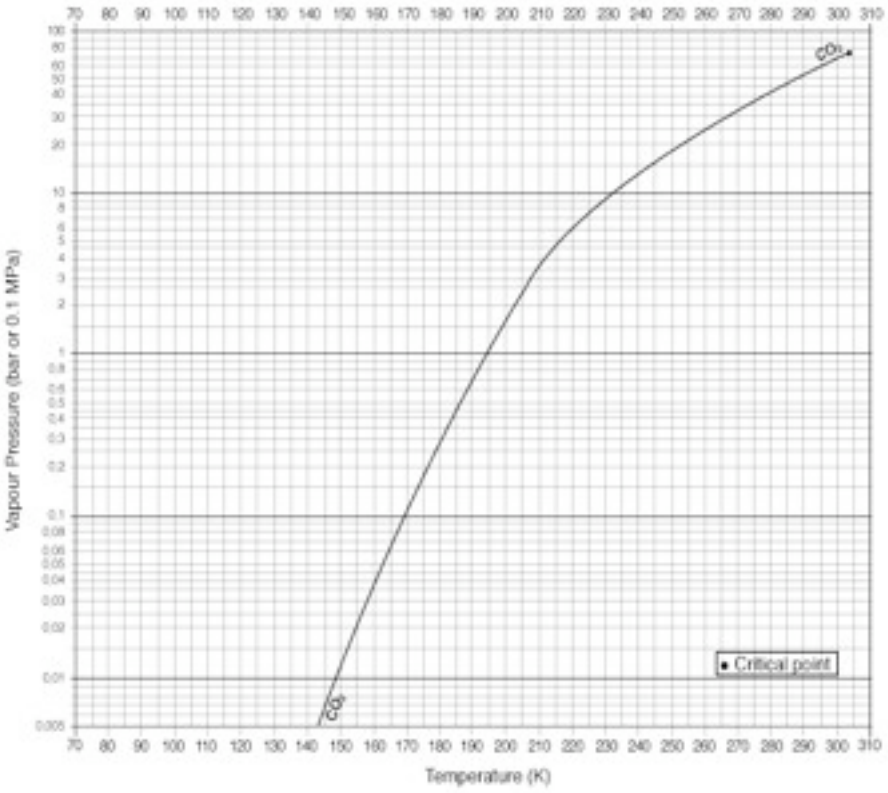

Figure 3.10: CO_2 vapour pressure at 1 atm [http://encyclopedia.airliquide.com/encyclopedia.asp].

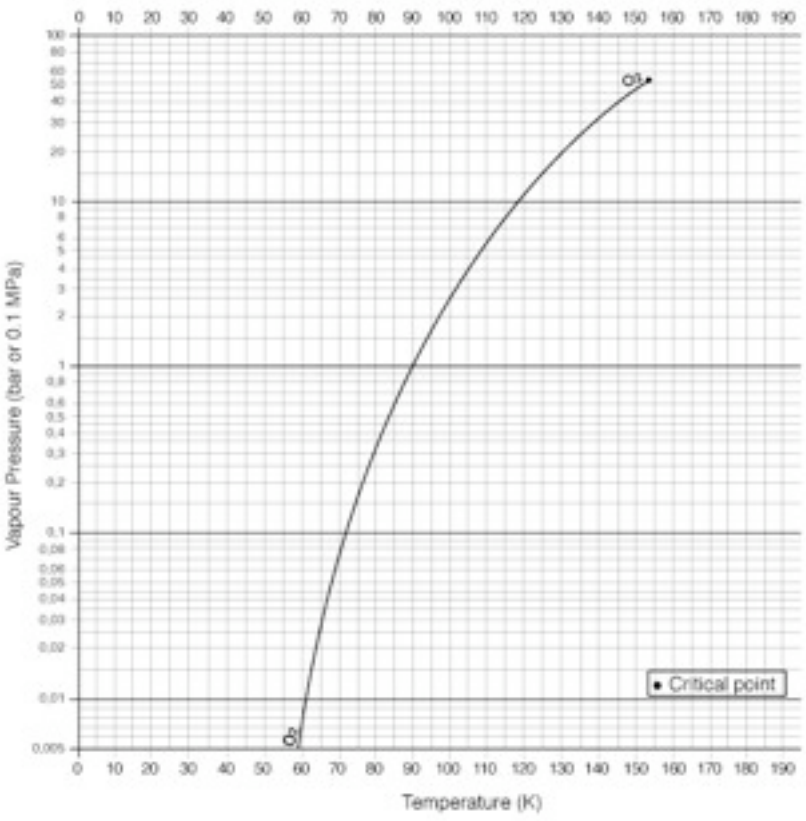

Figure 3.11: O_2 vapour pressure at 1 atm [http://encyclopedia.airliquide.com/encyclopedia.asp].

As regards the production of the traps, the first one (working temperature: ~215K) could quite easily be made by means of an ethanol and dry ice bath [Szid04], but the creation of the second one (working temperature: ~115K) was not so easy to obtain. No commercial trap working at such temperature was found; the solution adopted in [Szid04], namely a double chamber bath, with stirred 2-methylbutane filling the inner chamber partially frozen by liquid nitrogen put in the outer chamber, was avoided because of safety requirements for 2-methylbutane handling (2-methylbutane is harmful for inhalation and therefore it should be handled under an extractor fan).

The thermal trap for CO_2 produced for this line is homemade and is based on an "original" working principle (we are not aware of any commercial trap working this way, not even described in literature). In a Dewar partially filled with liquid nitrogen, a temperature gradient becomes established between the surface of the liquid nitrogen, at 77K, and the top (entrance), at ambient temperature; therefore it is possible to produce a thermal trap working at the desired temperature by positioning a coil at the proper height into the Dewar. In order to get a uniform temperature inside the coil, this one was made bending a stainless tube (6 mm OD) to obtain a flat spiral with ~18 cm external

diameter (see Figure 3.12). Since the coil is connected to the line, the distance between the spiral and the surface of the liquid nitrogen can be regulated by lifting up and down the Dewar with a proper manually controlled elevator. A resistive thermal device, precisely a PT100, connected to the spiral, allows monitoring the temperature.

Figure 3.12: CO_2 thermal trap; in the foreground the PT100 for temperature control.

The efficiency of the trap was verified measuring the infrared (IR) absorbance during the CO_2 trapping and release phases (see Figure 3.13) and it turned out to be 98±2%.

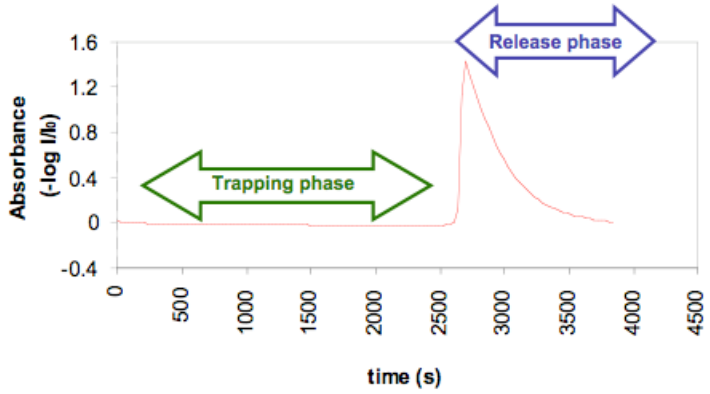

Figure 3.13: Test of the CO_2 trap efficiency: a plot of the IR absorbance measurement during both the trapping phase and the release phase is shown.

The good result obtained for the CO_2 trap convinced us to make the trap for aqueous vapour and nitrates removal on the basis of the same working principle, with the further advantage of getting rid of dry ice supply and ethanol/dry ice bath preparation. The only difference between the two thermal traps lies in the dimensions: the Dewar used to cool the coil acting as trap for water vapour and nitrates removal is smaller than the one for CO_2 trapping. In fact, as the working temperature is less critical, a higher temperature gradient does not affect the correct functioning of the trap, while the smaller diameter of the Dewar really helps to reduce the line encumbrance.

As previously mentioned, the thermal trap for CO_2 was designed to collect the CO_2 and at the same time to allow the carrier gases to flow out. On its way out, the gas stream passes through a flow-meter (rotameter) in order to control the gas flow that is expelled outside, so that any possible loss along the whole line may be detected.

When the combustion is completed and all the produced CO_2 is collected, every thermal program (see § 3.3) schedules a 5 min cleaning time while a 100 cc/min He flux removes the O_2 in the coil. In order to minimise the time necessary to remove the O_2 from the coil volume, a "fast line", which starts immediately after the part of the line dedicated to the carrier gas cleaning and is connected to the valve at the entrance of the coil, was introduced. In this way, the cleaning process is focused only on the CO_2 trap, while the cleaning of the whole line, requiring much more time, is delayed to "dead times", such as the time necessary for the graphitisation (during such time no new combustion can be started).

Just after this cleaning process, the valves at the entrance and at the exit of the CO_2 trap are closed. Inside the coil there is a small amount of condensed CO_2 while the whole coil volume is filled with He. In order to remove this last "undesired" gas, and to introduce only CO_2 into the graphitisation reactor, the coil is connected to the vacuum system in the last part of the line (see 3.2.4) and the carrier gas is pumped away. This last part of the line is dedicated to the graphitisation, a process in which H_2 is involved: therefore we conservatively preferred to avoid any O_2 introduction in this part, and we added the coil cleaning process after the combustion phase.

After connecting it to the vacuum system, the coil is initially evacuated until reaching a pressure of ~ 4÷6 mbar; then the coil is dipped into the liquid nitrogen and evacuated down to ~ $6*10^{-4}$÷$8*10^{-4}$ mbar. As it is shown in Figure 3.11, at ~ 5 mbar the boiling temperature of O_2 is ~ 60K, i.e. less than the liquid nitrogen temperature (77K), so there is no risk of trapping possible gaseous O_2.

§ 3.2.4 Graphitisation

The last part of the line (sometimes called "graphitisation line") is dedicated to the conversion from gaseous CO_2 to solid graphite; it is important to stress that, unlike the upstream parts of the line, working with a gas flux, this last part should be kept under in-vacuum conditions.

Many reactions for the graphitisation are known, however, we decided to reduce the CO_2 to graphite according to the well-known Bosch reaction[6] (e.g. [Voge84], [Lowe87]):

$$CO_2 + 2H_2 \xrightarrow{Fe,600°C} C + 2H_2O$$

The choice of this reaction was driven by two factors:

- This reaction is suitable also for the production of small samples (<100 μg C): [Sant07, Stei06, Hua04, Pear98]
- The same reaction is used at the LABEC for the preparation of samples for radiocarbon dating [Fedi07].

The core of this last part of the line is the graphitisation reactor (Figure 3.14), which is designed around a Swagelok Ultra-Torr ¼' Tee union modified to lodge a pressure transducer: it is connected at one side to the upstream line, while housing two quartz vials into the other two connections.

As the reaction occurs at 600°C, one of the two vials is heated by means of an insertable oven, set up and controlled as the ones for the catalyser in the carrier gas cleaning part of the line (see § 3.2.1) and for the chemical traps (see § 3.2.3). The only differences consist into dimensions (the graphitisation oven has a smaller inner diameter to better fit the vial dimensions, namely 6 mm diameter) and design of the case, optimised for oven insertion.

Water is produced in the reaction and, if not removed, it can back react with the graphite, inhibiting the reaction progress. Therefore, the second vial acts as a "cold-finger", where the water produced during the reaction is cryogenically trapped; the vial cooling is obtained by means of a homemade device (based on [Fedi04]) consisting in two Peltier modules thermally connected in series. The working temperature of the trap

[6] Actually, the cited reaction occurs in two steps, with CO formed as an intermediate product.

is -30°C, suitable to trap aqueous vapour at very low pressure (however, unlike the boiling temperature, the melting temperature does not strongly depend on the pressure).

Figure 3.14: The graphitisation reactor. The graphitisation oven is visible on the right, the Peltier chiller on the bottom.

A low-vacuum capacitive pressure transducer from Data Instruments lodged on the upper part of the reactor allows the monitoring of the pressure trend during reaction (the reaction is completed when all the CO_2 has been converted into graphite, and thus when the pressure settles on a constant value; see Figure 3.15).

As mentioned in § 3.2.3, the "graphitisation line" is provided with a Leybold compact dry vacuum system, based on a turbomolecular pump backed by a diaphragm forepump (oil diffusion pumps were avoided because of the possible contamination deriving from malfunctioning). The vacuum level is measured by means of a Leybold pressure gauge, combining both rough and high vacuum measurements.

After the connection of the CO_2 trap coil to the "graphitisation line" (see § 3.2.3), this vacuum system pumps away the remaining He; when a good vacuum level is reached (~ $6*10^{-4} \div 8*10^{-4}$ mbar), the trapped CO_2 is cryogenically transferred into the reactor and quantified by means of a pressure measurement.

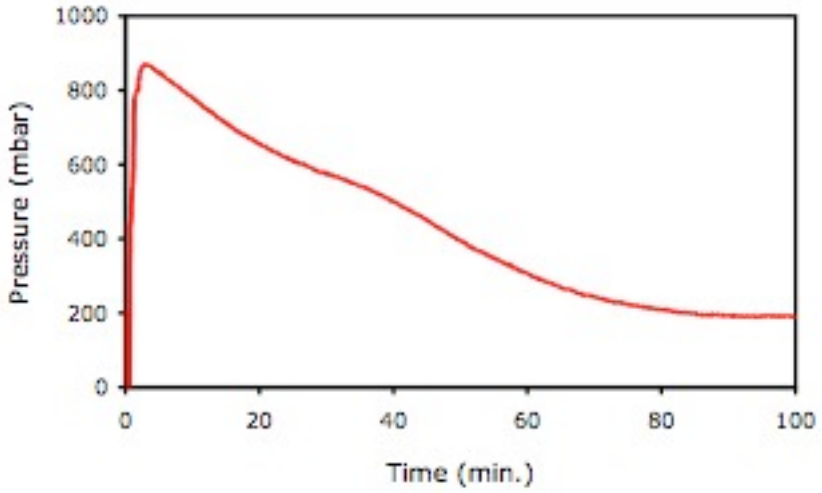

Figure 3.15: Typical graphitisation curve, i.e. typical pressure time trend inside the reactor during graphitisation. The pressure decreases as the reaction proceedes; when the pressure settles on a constant value, the reaction is completed.

The H_2 for the reaction, to be added in a double quantity with respect to the CO_2, is supplied by a gas generator, producing 99.999% pure H_2 by hydrolysis of deionised water. H_2 flux is regulated thanks to a Swagelok metering valve.

The reaction occurs only if a catalyst, namely Fe, is present: according to [Fedi07, Sant07b], iron powder (Alfa Aesar, 99.9+%, <10 μm) is used. After the insertion into the graphitisation reactor, the iron powder has to be activated. The so-called "activation" counts on two phases: first, the iron powder is heated up to 600°C under dynamic vacuum conditions for 30 min, then it is kept at 350°C with ~800 mbar of H_2 for 30 min more[7]. Finally, the reactor is evacuated and it is ready for the CO_2 introduction.

§ 3.3 Sample preparation protocols

A sample preparation procedure was developed, in order to optimise the sample preparation itself and to maximise the reproducibility of the results. Such procedure is schematically reported in this paragraph; as concerns the phases of sample pre-treatment and combustion, a distinction on the carbonaceous fraction of interest will be necessary.

The sample preparation procedure counts on the following steps (number of valves refers to Figure 3.2):

[7] During the first phase, the iron powder degases. Residual carbonaceous traces from the iron are removed through the formation, during the second phase, of CH_4 that is pumped away later.

- Insertion of (3.0±0.1) mg of iron powder into a weighted vial;
- Insertion of the aforementioned vial into the graphitisation reactor;
- Activation of the iron powder (§ 3.2.4);
- Opening of the valves along the line so that the gas stream passes through the combustion oven (thus closing on the "fast line") and exits through the gas outlet 2, just at the end of the CO_2 trap coil;
- Heating of the first catalyser and traps ovens, respectively to 700°C and 800°C, while a 200 cc/min He flux is set;
- Introduction of the aerosol sample into the main furnace;
- Cleaning of the line with a 200 cc/min He flux for 20 min;
- Insertion of the first thermal trap[8] (for aqueous vapour and nitrates, working temperature ~ 215 K);
- Insertion of the second thermal trap (for CO_2 collection, working temperature ~ 115 K);
- Setting of a 100 cc/min O_2 flux and heating up to 700°C of the catalyser positioned just after the main furnace, in the combustion oven;
- Combustion of the sample according to the chosen thermal program (see in the following);
- Setting of a 100 cc/min He flux and opening of the valves 2 and 4 on the "fast line": the cleaned He is flowed through the CO_2 trap coil alone for 5 min; in the meanwhile, all the heaters except the first catalyser's one are switch off;
- Closure of the valves 4 and 5; switching off of the first catalyser's heater; 100 cc/min He flux is flowed through the ovens in order to enhance heat dissipation (the He stream exits from the line through one way of the valve 3);
- Opening of the valve 6 and control of the vacuum level inside the "graphitisation line" (during this phase it should be ~ 4÷6 mbar, that is the vacuum level obtained with the only forepump switched on);
- Opening of the valve 5 and pumping away of the He volume contained in the coil;

[8] Between the insertion of a thermal trap and the following one it is necessary to wait some minutes, necessary to reach a thermal equilibrium inside the Dewar, and, therefore, inside the coil.

- Immersion of the coil into liquid nitrogen when pressure decreases to the initial value (~ 4÷6 mbar); switching on of the turbomolecular pump;
- Closure of the valves to the vacuum system and to the pressure gauge (valves 7 and 8) when the vacuum level reaches the value ~ $6*10^{-4}$÷$8*10^{-4}$ mbar; cryogenic transfer of the trapped CO_2 to the graphitisation reactor;
- Closure of the valve 9; quantification of the CO_2 with a pressure measurement (inner reactor volume ~ 6 cm^3);
- Selection of the desired quantity of CO_2 (the possible exceeding CO_2 is pumped away);
- Cryogenic trapping of the CO_2; opening of the valves 9 and 10 and introduction of a H_2 amount double with respect to the CO_2 quantity;
- Closure of the valve 9; insertion of the oven previously heated to 600° and of the Peltier based chiller, already at -30°C;
- Monitoring of the pressure inside the reactor;
- Switching off of the graphitisation oven once the pressure has settled down on a constant value;
- Removal of the vial containing the graphite coated iron powder and measurement of its total weight;
- Preparing for the next sample preparation or line stand-by.

It is worthy to emphasise that this procedure is quite time consuming and only one or, at the most, two samples per day may be prepared with this protocol. For every radiocarbon measurement, many cathodes from standard samples and "dead" graphite have to be prepared for normalisation and blank evaluation, as discussed in § 2.3.3. As a consequence, the preparation of the samples for an AMS run of a few days may require a one-month work.

As previously mentioned, the combustion of the sample and the possible needed pre-treatment depend on the carbonaceous fraction of interest. Actually, it is mandatory to stress that, as far as OC and EC are concerned, both pre-treatment and combustion procedures are currently under test. Only some more AMS measurements focused on this topic will allow the validation of the described procedures.

Total Carbon

No pre-treatment is needed (a previous acidification is not necessary because carbonates can be neglected in mid-latitude aerosols [Chow02]); combustion is achieved heating the sample at 800°C for 20 minutes in a 100 cc/min oxygen flow.

Organic Carbon

As well as for TC, no pre-treatment is needed; OC separation may be achieved heating the sample in oxygen stream at low temperature (340°C, [Szid04b]); combustion time is still under evaluation (estimated range: 10÷20 minutes).

If the water insoluble fraction of OC (WINSOC) is of interest, a previous water extraction of the water-soluble compounds is needed.

Elemental Carbon

Previous water extraction of the soluble compounds is mandatory in order to minimise charring; EC combustion may be achieved in oxygen stream at high temperature (650°C, [Szid04b]) after complete removal of OC. OC thermal removal protocols, based on a flash heating up to ~350÷400°C in oxidising atmosphere and a combustion at such temperature for 0.5÷2 h, are currently under study. It is worth noting that the OC removal is a very critical point. Since the radiocarbon content is much higher in the OC with respect to the EC, even tiny OC residuals can significantly affect the measurement of the EC radiocarbon content.

§ 3.4 From the graphite to a cathode

The iron powder coated by fluffy graphite is pressed into aluminium capsules with a 2.0 mm diameter (see Figure 3.16). This operation, apparently very easy, requires gaining some manual experience, and the efficiency of this process is difficult to evaluate (some graphite can be lost during the transfer, e.g. because not totally removable from the vial inner surface). Moreover, sometimes, some samples can be "lost" during this process, as it is quite difficult to recover the graphite after a failure in the pressing process.

As it will be discussed in § 5.2.1, this is one of the processes generating some problems in preparing "small" samples.

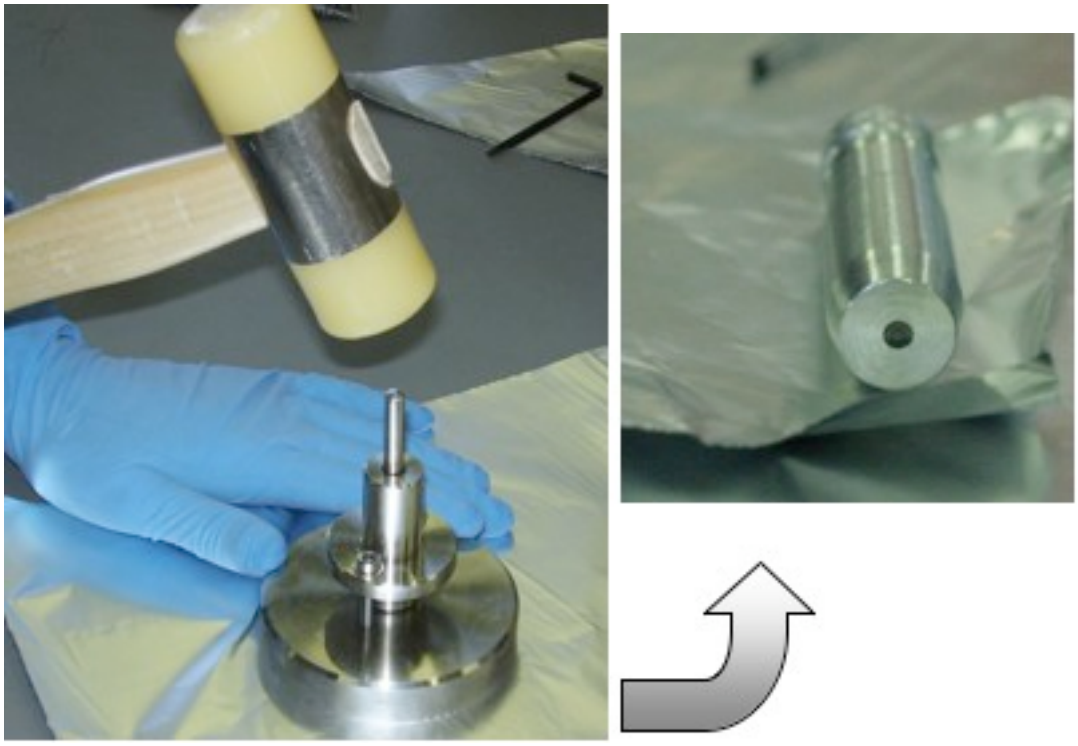

Figure 3.16: Pressing a sample inside the aluminium sample holder (left) and the produced cathode (right).

§ 3.5 Behind and beyond this line

As for every experimental work, and especially for the realization of new equipments, behind a description of the new apparatus, like the one given in this chapter, there is much more. There are many tests, many attempts, many projects, many technical problems and unfortunately, sometimes also some failures. Actually, we could almost state that this sample preparation line is the optimisation of a first prototype, due to the numerous changes performed after every preliminary test. It is worthwhile to stress that every test was very time-consuming, as each one of them required the preparation of many samples just changing one parameter at a time (and only one or at the most two samples per day may be prepared!). Finally, behind this chapter there are all those "non-working things" that you will never find in literature, but they are what will mainly help to understand the object you are trying to create.

In particular, "behind" this line there are various prototypes for the ovens and the main furnace, and some problems with hydrogen generators (see § 5.2.1).

Beyond this line, again as for every experimental work, there are possible future improvements, which are briefly listed hereinafter:

- Optimisation and validation of the EC and OC measurement protocols;
- Reduction of the graphitisation reactor volume in order to better control the process in the case of smaller samples;
- Insertion of a thermal trap (working temperature: 77K, that is easily feasible with a coil dipped into liquid nitrogen) on the inlet of the H_2, in order to get rid of any possible contamination (mainly water vapour);
- Duplication of the graphitisation reactor in order to increase the cathode throughput by having two reactors working in parallel;
- Duplication of the CO_2 trap (in addition to the graphitisation reactor duplication): two collection-graphitisation systems working in parallel allow, in principle, the preparation of cathodes from the CO_2 evolved from the same sample during different phases of the chosen thermal program.

As far as the EC/OC separation is concerned, it is important to emphasise that there is a long way to go yet. In fact, the validation of the protocols currently under evaluation will need the preparation of many other samples to be analysed by AMS measurements, since the parameters to be investigated are numerous (e.g. combustion temperatures and times, gas fluxes) and their variability ranges are quite wide.

Chapter 4

Characterization and first tests on the new line

Before beginning to use a new line to prepare "real" samples, it is mandatory to proceed to a full characterization of the line itself, to a control of the suitability of the produced samples for AMS measurements and, finally, to test the reliability of the obtained results.

These tests were performed on samples slightly smaller (~75%) than the samples routinely prepared for radiocarbon dating measurements, thus starting from the very beginning with a first step towards the reduction of the sample size.

§ 4.1 Efficiency of the aerosol sample preparation line

The efficiency of the sample preparation line is not a parameter used in the quantitative analysis of AMS data. Nonetheless, the estimate of the efficiency is very important, especially in the perspective of working with small samples, as the aerosol ones are (especially if the EC fraction is of interest). When dealing with small samples, the collection of as much carbon as possible from the filters is mandatory, i.e. the maximisation of the efficiency of the whole process leading from an aerosol loaded filter to a cathode to be put into the AMS source is required.

The overall efficiency of the sample preparation line can be evaluated as the ratio between the produced graphite mass and the carbon quantity introduced into the combustion oven:

$$\eta = \frac{W_{graph}}{W_{C,in}} \tag{4.1}$$

This efficiency obviously includes the efficiencies for every single process such as combustion, trapping, transfer and graphitisation. Unfortunately, some of the efficiencies of these processes are very difficult to evaluate singularly. Only two data can be known, in order to give a possible "a priori" estimate of the resulting "overall" efficiency η: the CO_2 trap efficiency was measured and its value turned out to be 98±2%, as reported in § 3.2.3. Moreover, from the experience gained by the research group working at LABEC on radiocarbon dating, the efficiency of the graphitisation with the used reaction and catalyst (Alfa Aesar iron powder, <10 μm) was estimated approaching the 100%. On the basis of these data, we would expect a high efficiency for our line[1] (unless combustion problems arise).

In order to characterise the line, we checked the reproducibility of combustion, trapping and transfer processes as a whole (hereafter called, broadly speaking, "transmission" process), and we estimated the efficiency according to the (4.1).

§ 4.1.1 Reproducibility of combustion, transfer and trapping

In order to check the reproducibility of the processes occurring in the first part of the line, namely all the processes before the graphitisation, the measured pressure of the collected CO_2 in the graphitisation reactor was related to the introduced carbon load. In more detail, these tests were carried out burning in the oven some samples of NIST Oxalic Acid II (OxAcII), "dead graphite" (Alfa Aesar graphite) and aerosol-loaded filters. The OxAcII is the primary standard material used for radiocarbon measurements (see § 2.3.1); its carbon content, according to stoichiometry[2], is ~27%. The graphite is simply elemental carbon, thus its carbon content is 100% of the mass. The samples from these two materials were introduced into the combustion oven after having been weighted. As concerns the aerosol samples, they were loaded into the oven in the form of 1.5 cm^2 punches; the carbon content was measured by thermo-optical measurements (see § 1.4.1) on another 1.5 cm^2 punch from the same sample. For these tests, the protocol for TC analysis (see § 3.3) was followed. The pressure was measured by the pressure transducer installed on the graphitisation reactor, as described in § 3.2.4.

[1] As reported in §3.2.2, the overall efficiency of the sample preparation line dedicated to radiocarbon dating is ~75%: this value, smaller than an ideal 100% efficiency, can be mainly ascribed to the transfer process of the CO_2 from the Elemental Analyser (EA), where combustion is performed, to the "graphitisation line". This is somehow intrinsic of this specific combustion method and of the large volumes characterising this graphitisation line. Therefore, with a different combustion oven as ours and with reduced volumes, we could expect to get rid of it.

[2] Oxalic acid stoichiometric formula: $C_2H_2O_4$.

In Figure 4.1, the transmission (i.e. the efficiency of production, transfer and collection of the CO_2, expressed as mbar/mgC) is reported as measured for 14 samples of OxAcII, 4 samples from "dead" graphite and 5 aerosol samples. The uncertainties on the measured values are evaluated as the square root of the sum-of-the-squares of the contributions coming from the pressure measurements and the carbon mass measurements (for the aerosol samples this last contribution also includes the ~10% uncertainty on the thermo-optical measurement of the carbon content; see § 1.4.1).

As far as the OxAcII samples are concerned, the reproducibility of combustion, trapping and transfer processes as a whole appears to be good (the relative standard deviation is less than 4%). The data dispersion is larger than the uncertainty on the single measurement but this can be explained by the fact that all the operations required by the sample preparation protocol are manually performed (e.g. valve opening and closure). The average value for the CO_2 measured in the graphitisation reactor as a function of the carbon loaded into the oven turns out to be (310±3) mbar/mgC.

The data dispersion is larger than the error bars (not visible in the chosen scale) also for the "dead" graphite samples. In particular, the transmission measured for the TEST33 sample is significantly lower than for the other samples: this can be due to graphite losses after the weighting procedure. In fact, the Alfa Aesar graphite is a very fine powder and some grains might have been lost during the transfer into the oven. The transmission for the "dead" graphite samples is of the same order than the one measured for the aerosol samples.

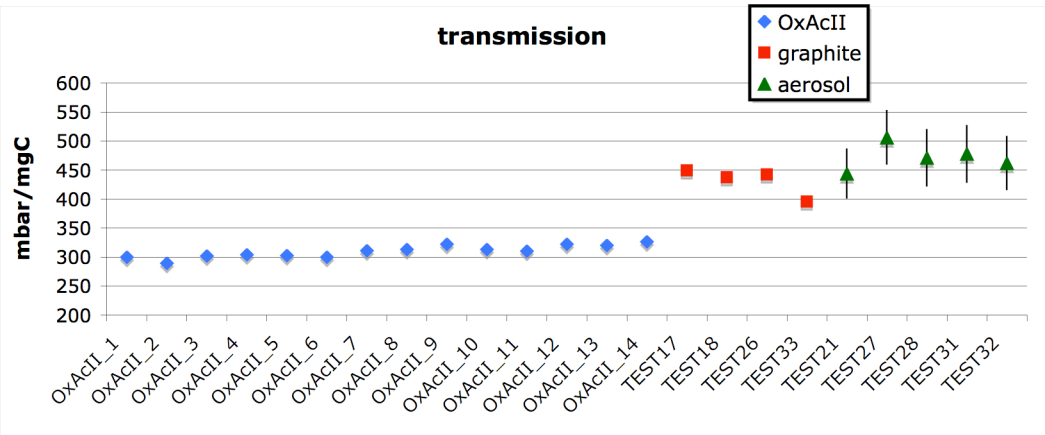

Figure 4.1: CO_2 pressure in the graphitisation reactor for mg of Carbon introduced into the main oven, for various typologies of samples.

However, in Figure 4.1, the most relevant and surprising feature is the striking difference between the transmission for the OxAcII samples and the transmission for the samples of "dead" graphite and aerosol. Such a different transmission depending on the sample material was not expected, as the combustion should be completely achieved during the chosen combustion time (20 min).

The observed discrepancy with respect to the combusted material was hypothesised to be due to the hygroscopicity of the oxalic acid. This hypothesis was verified by thermo-optical measurements performed with the Sunset Laboratories analyser (see § 1.4.1). To this aim, some solutions were prepared dissolving a weighted quantity of OxAcII into a known milli-Q water volume. The thermo-optical measurements gave as a result a (18±2)% carbon content for our "humid" OxAcII (much less than the stoichiometric 27%, coherently with the hypothesis of water absorption by the OxAcII). Taking into account hygroscopicity, the observed discrepancy in the transmission is solved, as shown in Figure 4.2. The larger error bars on the corrected transmission values for OxAcII samples are due to the experimental uncertainties associated with the thermo-optical measurements.

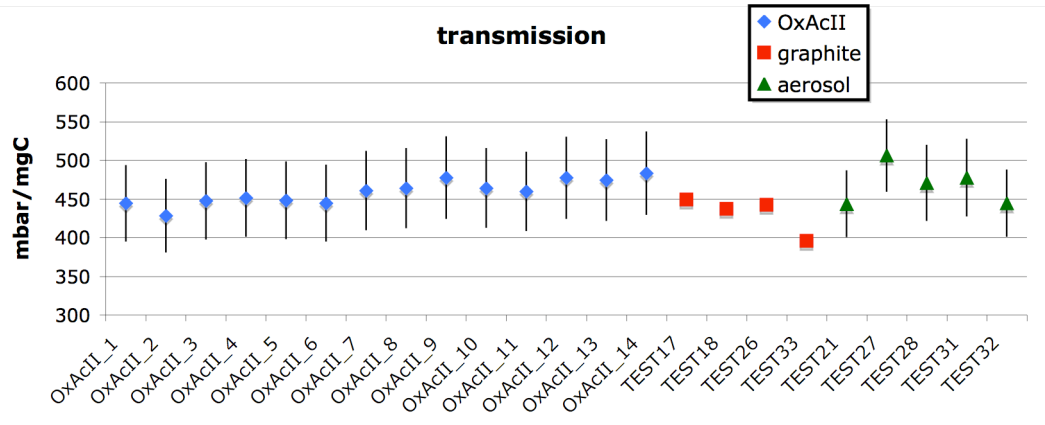

Figure 4.2: Transmission for various typologies of samples; transmission for OxAcII samples was corrected for oxalic acid hygroscopicity.

The average transmission is reported in Table 4.1, taking into account either the samples from OxAcII alone or all the samples (from OxAcII, graphite and aerosol). This distinction was made in order to take account of possible problems in the evaluation of the burnt carbon load for aerosol and "dead" graphite samples. In fact, for aerosol samples this evaluation might be affected by sample inhomogeneities while for

graphite samples, as previously mentioned, it might be affected by possible losses due to its very fine grains.

Sample	Mean transmission (mbar/mgC)	St. dev. of the mean (mbar/mgC)
OxAcII	459	4
OxAcII, graphite, aerosol	456	5

Table 4.1: Measured transmission averaged over the samples prepared from the OxAcII alone and over the samples from OxAcII, graphite and aerosol.

In brief, the reproducibility of the transmission was verified for the various typologies of the samples of interest; it is worth stressing that, when the final protocols for EC and OC fractions will be defined, only the reproducibility of combustion will need to be verified again.

§ 4.1.2 Overall efficiency of the sample preparation line

The overall efficiency of the line, resulting from all the efficiencies characterising all the processes leading from an aerosol loaded filter to the graphite to be pressed into a cathode, is quantified according to the (4.1).

Although any possible dependence from the sample material had been almost conclusively excluded on the basis of the observations on transmission (see § 4.1.1), the topic of the efficiency was investigated not only by means of OxAcII combustions but also taking some data for samples from "dead" graphite and from aerosol loaded quartz filters.

Samples were converted to graphite according to the protocol described in § 3.3, using the combustion method for TC analysis. The quantity of CO_2 selected for graphitisation was chosen as to give a (200±5) mbar pressure[3] in the graphitisation reactor. According to the experience gained by the radiocarbon dating research group, such a quantity should correspond to 400÷450 μg of produced graphite, hence according to Table 4.1 it would yield an overall efficiency of at least 90%. Anyway, at this step, this datum has to be considered only indicative, since the graphitisation reactor mounted on our new line is indeed very similar to those of the line for the preparation of samples for radiocarbon dating but, however, it is not calibrated.

[3] All the prepared samples were also used for the first tests at the LABEC accelerator (see § 4.2), so great care was also given to produce samples with the same size (see § 2.3.3).

In Figure 4.3 the masses of the produced graphite are reported as obtained by the difference between the final mass[4] of the vial containing the graphite coated iron powder and the initially measured masses of the vial and the iron powder. Error bars were calculated as the sum of the uncertainties on the single mass measurements of the vial alone, the iron powder and the vial containing the graphite coated iron powder. The mass measurements bring along great uncertainties. They were performed with a Sartorius analytical balance (model CP225D), with a 0.01 mg reading precision in the range of interest (less than 40 g); the measurement reproducibility was tested and the standard deviation in the range of interest turned out to be ~0.02 mg (in accordance with the certified reproducibility).

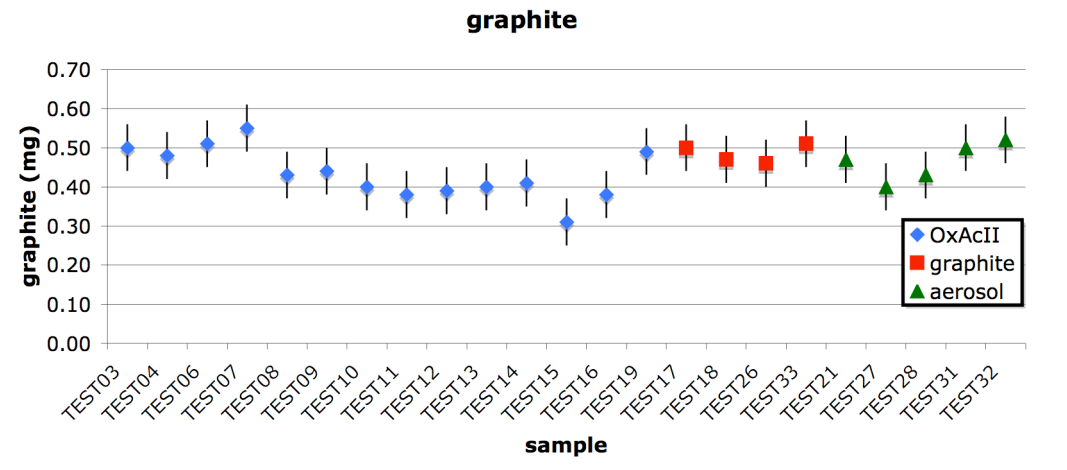

Figure 4.3: Produced graphite from the graphitisation of (200±5) mbar of CO_2 (produced by the combustion of various sample typologies). Error bars were calculated as the sum of the uncertainties on the single mass measurements of the vial alone, the iron powder and the vial containing the graphite coated iron powder (see text).

The average value of the produced graphite over all the samples taken into account is 0.45±0.01 mg, in agreement with the expected value, estimated on the basis of the radiocarbon dating team experience. The data dispersion is quite good (the relative standard deviation is ~13%) and also includes the variability in the CO_2 amounts selected for graphitisation (ranging between 195 and 205 mbar). The data variability is mainly to be ascribed to the graphitisation process itself. However, another possible contribution is given by the balance instability due to microclimatic changes as a function of time. Actually, the weightings of the vial alone and of the iron powder were

[4] Data for samples TEST01, TEST02 and TEST05 were not taken into account because the vials were touched without wearing gloves when removing them from the line after graphitisation, thus altering their final weight.

generally done in a different day with respect to the weighting of the vial containing the graphite coated iron powder.

This result is important since it means that the produced graphite is a well reproducible quantity: with the new line we are able to produce samples all characterised by the same size, thus fulfilling the requirements of the matching-size method (§ 2.3.2).

The introduced carbon load was evaluated on the basis of the considerations reported in § 4.1.1: for OxAcII and "dead" graphite the amount of carbon is ~18% and 100% of the weighted sample, respectively. Aerosol samples, whose areal carbon content was previously estimated by thermo-optical analysis, were introduced in the form of punches of known area. Due to the difficulty of sampling a very precise quantity of material to be burnt, the introduced sample mass was always slightly exceeding the quantity really necessary to produce the chosen CO_2 quantity to be graphitised (i.e. 200±5 mbar). Therefore, the carbon load equivalent to the actually selected CO_2 quantity was derived, for each sample, on the basis of its measured transmission.

Finally, the overall efficiencies were calculated for every sample; they are reported in Figure 4.4. Error bars represent the square root of the sum-of-the-squares of the uncertainties on the produced graphite mass, the selected CO_2 quantity and the transmission[5]. The average efficiency is reported in Table 4.2, again taking into account all the samples or the samples from OxAcII alone. As previously mentioned, this distinction was made in order to take account of possible problems affecting the evaluation of the carbon load for aerosol and graphite samples.

A ~100% overall efficiency for the new sample preparation line is indeed a good result, not only because this result assures that all the processes are well controlled and optimised, but mainly because it guarantees that we do not lose anything during the sample preparation: this is especially important in the perspective of drastically reducing the sample size.

[5] Actually, these quantities cannot be considered completely independent. As previously mentioned, the transmission is calculated dividing the quantity of collected CO_2 by the carbon content of the burnt sample. Thus, the uncertainty on the efficiency is due to the uncertainties on the masses of both the produced graphite and the burnt sample, on the pressure measurement of the CO_2 both collected and selected and, finally, on the evaluation of the sample carbon content. The relative uncertainties on the pressure measurements and on the sample mass are negligible with respect to the other two, being at least one order of magnitude smaller. Therefore, the root-sum-of-squares of the uncertainties is reduced to the root-sum-of-squares of the uncertainties on the produced graphite mass and on the sample carbon content, two quantities absolutely independent. For graphite samples, the relative uncertainty on the efficiency substantially coincides with the one on the produced graphite mass.

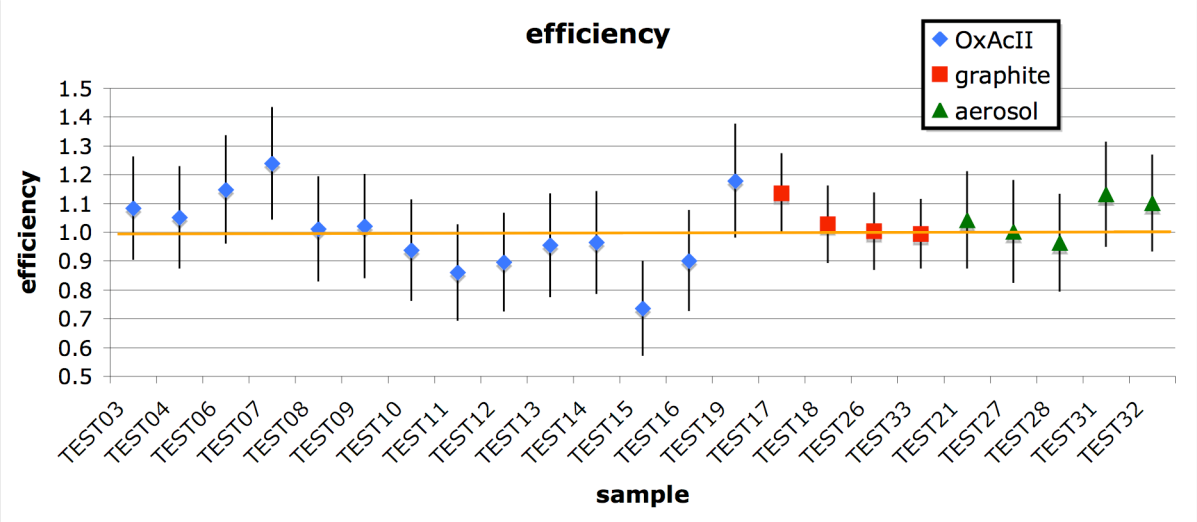

Figure 4.4: Overall efficiency for the preparation of some samples of different typologies with the new sample preparation line for AMS measurements on aerosol samples.

Sample	Mean efficiency	St. dev. of the mean
OxAcII	1.00	0.04
OxAcII, graphite, aerosol	1.02	0.02

Table 4.2: Measured efficiency averaged over the samples prepared from the OxAcII alone and over the samples from OxAcII, graphite and aerosol.

§ 4.2 First tests at the LABEC accelerator

In order to verify the reliability of the sample preparation procedure with the new sample preparation line, several cathodes, all having the same size (~450 μgC), were produced and analysed by AMS measurements.

The 25 prepared cathodes are listed in Table 4.3: samples from OxAcII were used to check the reproducibility of the results; cathodes from dead carbon samples, namely Alfa Aesar graphite, were analysed to investigate the background of our measurements; cathodes from the reference material C7 from IAEA (International Atomic Energy Agency) were employed to check the reliability of the attained results.

During the measurements 10 batches were acquired, in order to collect at least 40000 counts on every OxAcII cathode[6] (see § 2.3.3).

[6] Actually, 40000 counts were collected on every OxAcII cathode except two ones, which resulted to be depleted (see § 4.2.1).

Sample label	Sample
TEST01	OxAcII
TEST02	OxAcII
TEST04	OxAcII
TEST05	OxAcII
TEST06	OxAcII
TEST07	OxAcII
TEST09	OxAcII
TEST10	OxAcII
TEST11	OxAcII
TEST12	OxAcII
TEST13	OxAcII
TEST14	OxAcII
TEST15	OxAcII
TEST16	OxAcII
TEST19	OxAcII
TEST17	Alfa Aesar graphite
TEST18	Alfa Aesar graphite
TEST26	Alfa Aesar graphite
TEST33	Alfa Aesar graphite
TEST22	IAEA C7
TEST25	IAEA C7
TEST29	IAEA C7
TEST30	IAEA C7

Table 4.3: Samples put into the ion source to perform reproducibility and reliability tests.

§ 4.2.1 Reproducibility

Fifteen OxAcII standards prepared according to the protocol reported in § 3.3, were put into the accelerator ion source for AMS measurements.

Figure 4.5 shows the behaviour of the measured cathode current for this set of samples, batch by batch. Cathode current is the current provided by the power supply to keep constant the voltage applied to the cathode[7]; it is proportional to the current of the sputtered negative ions leaving from the cathode and it is therefore a good proxy of the extracted ion currents (i.e. it shows the same behaviour). The produced set of standards is characterised by a good uniformity of the extracted currents: this property is a mandatory requirement to perform high precision AMS measurements, as it allows the compensation for isotopic fractionation effects occurring inside the accelerator machine (see § 2.3.2).

[7] For a detailed source description see § 2.2.1.

The slightly decreasing behaviour of the cathode currents with the batch number increasing, i.e. with the time running, is probably due to some source stabilization effects.

The measured ^{14}R ($^{14}C/^{12}C$) and ^{13}R ($^{13}C/^{12}C$) are reported for all the standards and for every batch, in Figure 4.6. No important trend is observed with the batch number increasing, i.e. with the sputtering depth increasing. This suggests a good spatial uniformity of the sample graphite pressed into the cathode and also indicates that none of the samples collapsed during the measurements. Error bars are not reported for the sake of clarity. Uncertainties on ^{14}R are of the order of 1÷2% for all the samples; uncertainties on ^{13}R are not visible in the chosen scale. For both ^{14}R and ^{13}R, the data dispersion on the batches is larger than the uncertainties on the data themselves: this is due to variations in the machine parameters or to possible small inhomogeneities of the samples (see § 2.3.3). These variations can indeed be likely since each batch can last even some hours (e.g. 3.5 h for these specific measurements).

It is worthwhile to stress that the normalization of the samples to the standards "batch by batch" (see § 2.3.3) allows to take into account the effects on both the isotopic ratios and the cathode currents and to compensate for them.

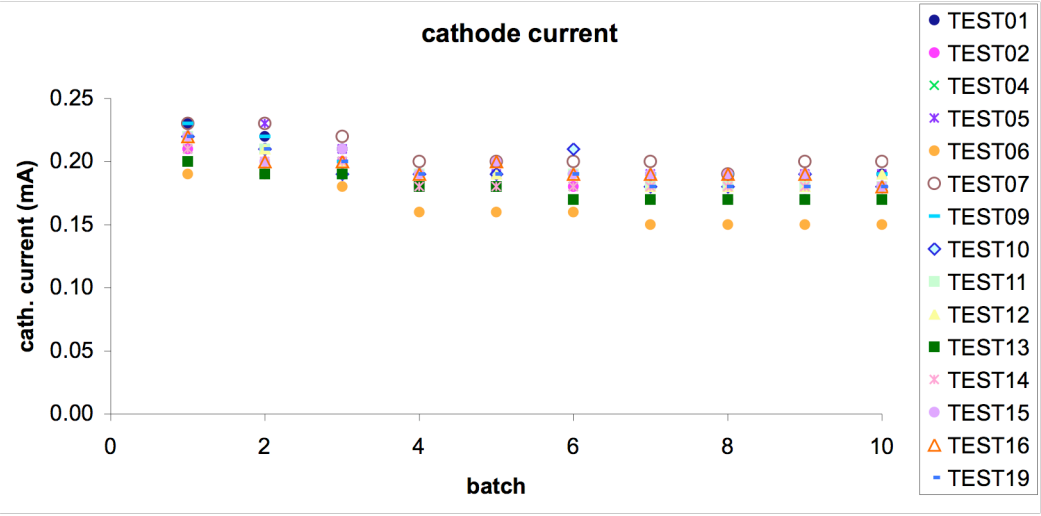

Figure 4.5: Cathode current for all the standards, batch by batch.

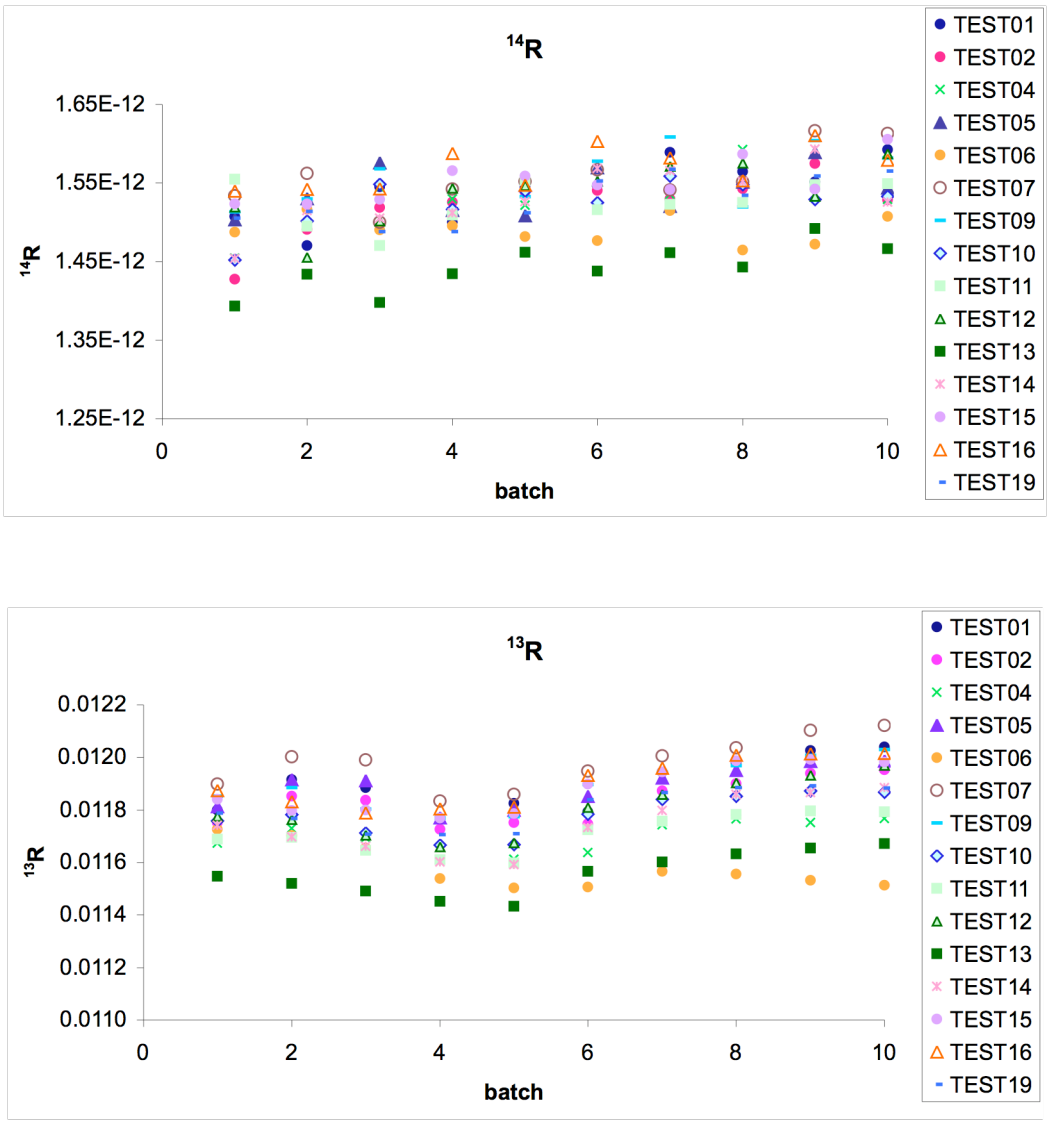

Figure 4.6: Measured ^{14}R and ^{13}R for all the standards, batch by batch.

The $^{14}R_{av}$ and $^{13}R_{av}$ (i.e. the average of the ^{14}R and ^{13}R ratios over all the performed batches; see § 2.3.3) are reported in Figure 4.7 for all standard samples. Error bars represent the standard deviation of the mean[8].

Two samples (TEST06 and TEST13, see also Figure 4.6) clearly appear to have smaller $^{14}R_{av}$ compared to the others. Such an effect might be explained by considering a "real" ^{14}C depletion in the samples themselves due to fractionation effects occurred during sample preparation (e.g. as a consequence of an incomplete graphitisation) or to some dead carbon contamination. However, the most reliable explanation appears to lay in the dependence of the measured isotopic ratios on the extracted currents (see § 2.3.2).

[8] In fact, as discussed in detail in § 2.3.3, for the standards the statistical uncertainty is negligible with respect to variability among the batches.

In fact, nothing peculiar occurred during sample preparation, and the measured efficiencies for these two samples do not substantially differ from the ones measured for the other samples (see Figure 4.4), so contaminations or incomplete processes are thought to be improbable. On the contrary, we can observe that the cathode currents over the 10 batches for TEST06 and TEST13 were systematically lower than for the other standards (see also Figure 4.5). The extracted currents depend on the sample size, so, as the produced graphite was almost the same for all the samples, we hypothesized that maybe some losses could have occurred during the pressing process.

On the basis of these considerations, reproducibility was studied either taking into account all the samples or discarding the two "depleted" ones, i.e. TEST06 and TEST13: data are summarized in Table 4.4.

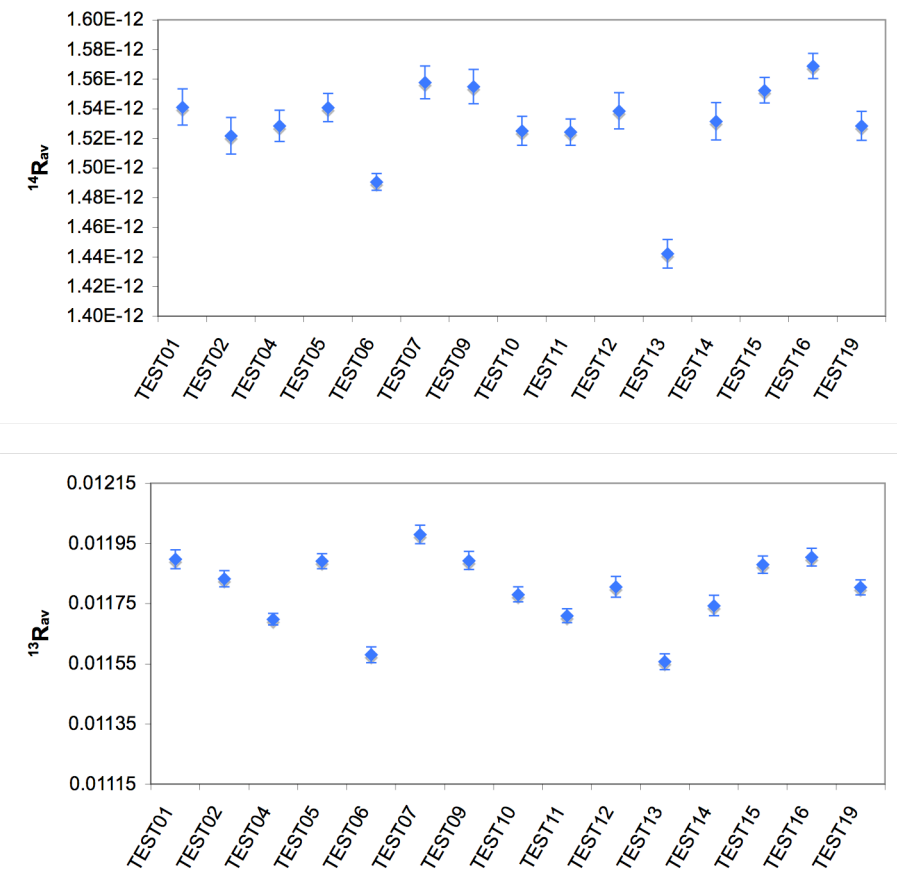

Figure 4.7: $^{14}R_{av}$ and $^{13}R_{av}$ for all the standards; error bars represent the standard deviation of the mean over the 10 batches.

The attained reproducibility has to be compared with the precision[9] specification guaranteed by the accelerator supplier High Voltage Engineering Europe. The precision is quantitatively evaluated as the ratios between the standard deviation of the mean (σ^{mean}) and the averaged R_{av} over all the measured standards. In the accelerator final commissioning tests, the protocol stated that the $^{14}R_{av}$ and $^{13}R_{av}$ on a set of modern standard samples would have to be measured with a precision better than 5‰ and 3‰, respectively. As far as $^{13}R_{av}$ is concerned, the reproducibility is better than the guaranteed precision either discarding or not the two "depleted" samples. For $^{14}R_{av}$, this condition is fully verified only if TEST06 and TEST13 are discarded; however, the reproducibility measured taking into account all the standards is just slightly worse than expected, therefore the two samples TEST06 and TEST13 were not discarded and were used for the subsequent blanks and reference materials data processing.

Samples	$^{14}\mathbf{R_{av}}$	σ_{14}^{mean}	$\sigma_{14}^{mean}/^{14}\mathbf{R_{av}}$	$^{13}\mathbf{R_{av}}$	σ_{13}^{mean}	$\sigma_{13}^{mean}/^{13}\mathbf{R_{av}}$
All	1.5298E-12	0.0079E-12	5.2 ‰	0.011797	0.000031	2.7 ‰
All - (TEST06,13)	1.5395E-12	0.0041E-12	2.7 ‰	0.011832	0.000023	2.0 ‰

Table 4.4: $^{14}R_{av}$ and $^{13}R_{av}$ as obtained by the average over all the standards or over all the standards except TEST06 and TEST13. σ_{14}^{mean} and σ_{13}^{mean} are the standard deviations of the mean of $^{14}R_{av}$ and $^{13}R_{av}$, respectively.

Coming to conclusions, the reproducibility of sample preparation with the new sample preparation line was tested; the overall reproducibility of sample preparation and sample AMS measurement satisfies the supplier guaranteed precision parameters for AMS measurements.

By considering the behaviour of the two samples TEST06 and TEST13, further investigations are needed to improve the graphite pressing process.

§ 4.2.2 Background

Although the background topic for radiocarbon aerosol source apportionment is much less critical than for radiocarbon dating[10], it is nevertheless important to take this

[9] As "precision" we mean here the reproducibility of the measured isotopic ratios over a given series of measurement runs.

[10] In radiocarbon dating background is a very important issue, as it represents the limit to the maximum age of the samples that can be dated. Therefore, high background can constitute a limitation to measure very old samples. On the contrary, as is discussed in the text, for aerosol source apportionment it is very

issue under control. Therefore, in order to check the background of our measurements, four cathodes from a nominally dead carbon material, namely Alfa Aesar graphite, were prepared following the same sample preparation protocol used for all the other samples and reported in § 3.3 (see Table 4.3).

Unfortunately, the sample TEST33 collapsed just after the first batch, as it could be clearly seen as the extracted currents dramatically decreased. This fact is probably due to an improper pressing of the graphite coated iron powder into the aluminium sample holder, leading to a scarce resistance to sputtering and in-vacuum conditions.

The average background level measured on the three remaining samples is reported in Table 4.5. The uncertainty was calculated as reported in § 2.3.3.

pMC	tRC (years BP)
0.43 ± 0.03	43740 ± 520

Table 4.5: Background level for AMS measurement on samples prepared with the new sample preparation line. The conversion to radiocarbon age (tRC) is reported for easier comparison with other facilities.

For comparison, the machine contribution to the background can be estimated as about 0.05 pMC, corresponding to 60,000 years BP [Fedi07].

The obtained background level is very good, and it does not represent a limitation for our measurements. In fact, the minimum radiocarbon concentration values we will deal with are expected to be ~1÷2 orders of magnitude higher. The minimum values we expect to deal with are those measured in the case of major importance of fossil sources, i.e. for the analysis of the EC fraction in an aerosol sample collected in an urban site. For example, a study on particulate matter collected in Göteborg reported radiocarbon concentrations in the range ~ 5÷17 pMC for the EC fraction in an urban site, rising over 35 pMC for a rural site, while radiocarbon concentration in the OC fraction were always found to be well above 50 pMC [Szid09].

§ 4.2.3 Accuracy test with a reference material

The attained accuracy of both sample preparation and measurement was tested by means of some cathodes prepared from the reference material C7 provided by IAEA.

unlikely to deal with samples with a pMC near to the background level, even for EC samples, mainly coming from fossil sources.

The IAEA C7 is oxalic acid and its ^{14}C activity and $\delta^{13}C$ are certified as follows [LeCl98]:

- pMC = 49.53 ± 0.12;
- $\delta^{13}C$ = -14.48‰

This reference material is characterised by a radiocarbon content of the same order of the one expected for aerosol samples (see § 5.1): therefore, the accuracy was tested for samples quite similar to the ones of interest.

Unfortunately, only two of the four prepared cathodes produced extracted currents of the same order of the currents observed for the standards, while the remaining two cathodes were characterises by lower, very similar currents, as shown in Table 4.6.

Sample	Cathode current (mA)
Standards	0.191 ± 0.010
TEST25, TEST29	0.189 ± 0.002
TEST22, TEST30	0.174 ± 0.001

Table 4.6: Average cathode currents for all the standards and for samples from IAEA C7.

As already described in details in § 2.3.3, radiocarbon concentrations for these "unknown" samples were obtained normalising their ^{14}R isotopic ratios, already corrected for isotopic fractionation[11] and background, to the ^{14}R isotopic ratios measured for the standards. Uncertainties were calculated as reported in § 2.3.3. Results are summarised in Figure 4.8; IAEA C7 certified concentration is also reported for comparison with a continuous line (±1 σ uncertainty in dashed lines).

Results for samples TEST25 and TEST29 (which were characterised by cathode currents very similar to the ones observed for standards) are well consistent with the certified value, while the radiocarbon concentrations measured for the other two samples TEST22 and TEST30, characterised by lower cathode currents, are ~2.5σ far from the certified value.

[11] It is worth recalling that ^{13}R are also measured in the AMS beam line.

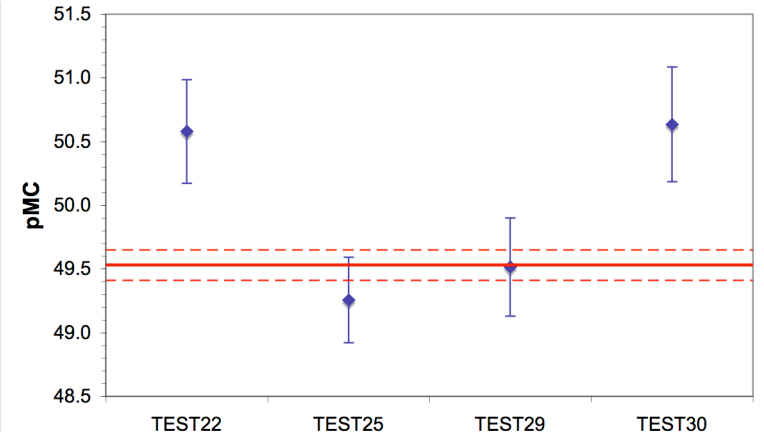

Figure 4.8: Measured radiocarbon concentrations in samples from IAEA C7; normalization to ^{14}R ($^{14}C/^{12}C$) and ^{13}R ($^{13}C/^{12}C$) isotopic ratios on standards. IAEA C7 certified concentration and ±1 σ uncertainty are reported with continuous line and dashed lines, respectively.

The hypothesis that some machine fractionation effects (§2.3.2) have occurred during AMS measurements finds a confirmation by performing a different normalization procedure. As reported also in [Pear98], space charge effects affect lighter isotopes more strongly. Therefore, neglecting the "vanishing" ^{12}C, i.e. normalizing the unknown samples on the basis of the isotopic ratio $^{14}C/^{13}C$, might increase the reliability of the results, as the fractionation effects would be less evident. Obviously, in order to perform such normalization, an additional information is needed: $\delta^{13}C$ has to be known, that is independently measured (e.g. by conventional mass spectrometry measurements) or independently certified (such as in our case for IAEA C7). Results obtained normalising the $^{14}C/^{13}C$ ratios, corrected for background and isotopic fractionation (on the basis of the certified $\delta^{13}C$), to the $^{14}C/^{13}C$ ratios measured for the standards are shown in Figure 4.9. With this normalization procedure, all our samples are well consistent with the certified value.

It is important to remark that, when $\delta^{13}C$ is assumed to be equal to the certified one, possible isotopic fractionation effects occurring during sample preparation are assumed to be negligible: this hypothesis is reliable, as isotopic fractionation effects during graphitisation were observed only in case of reactions that failed to reach completion [Vand97, Hua01] and this is not what we observed during sample preparation.

The effect of the different normalization procedure was more evident on the samples characterised by lower cathode currents (TEST22 and TEST30), with a net result of having measured pMC values less scattered over the whole set of samples, thus

confirming that the processes causing the observed pMC behaviours have been determined.

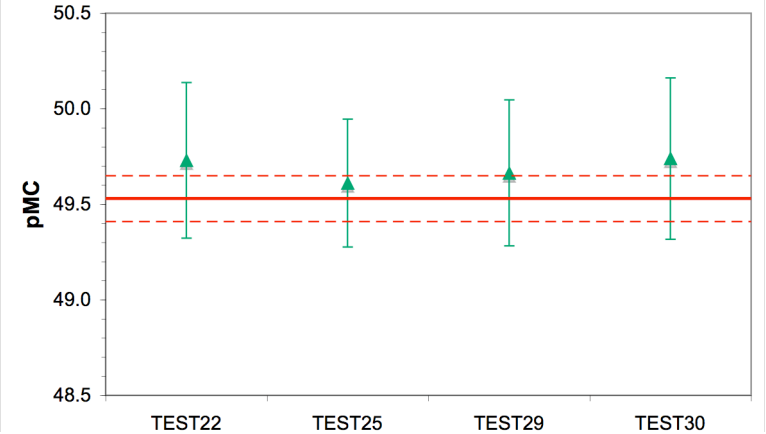

Figure 4.9: Measured radiocarbon concentrations in samples from IAEA C7; normalization to $^{14}C/^{13}C$ isotopic ratios on standards. IAEA C7 certified concentration and ±1 σ uncertainty are reported with continuous line and dashed lines, respectively.

It is worth stressing that the recourse to a different normalization procedure was very helpful to investigate the causes of the slight discrepancies observed between the measured and certified ^{14}C concentrations in some IAEA C7 samples, but it is not necessary for aerosol samples. In fact, also with the "usual" normalization procedure, the deviation of the measured value from the "true" one, assumed to be the certified one, hardly exceeds 1 pMC, which corresponds to a 2% error on the ^{14}C concentration. Such an error is surely acceptable, if even not completely negligible, due to the uncertainties on the quantities in the source apportionment relations (see § 1.5.2).

In summary, measurements on samples prepared from the reference material IAEA C7 proved the reliability of both our sample preparation and measurement procedures: with this last test, the new sample preparation line was validated for TC analysis. After this full characterization, it will be possible to act on the combustion parameters in order to investigate the EC/OC separation issue, namely to determine the proper combustion protocols, having all the other parameters of the line under control.

Chapter 5

Challenges and first results with the new line

In the first part of the chapter, first results from tests and measurements performed on 450 μgC cathodes prepared from some aerosol samples are reported.

In the second part, some preliminary results about sample-size reduction opportunities at LABEC are presented. In fact, as mentioned in the previous chapters, the reduction of the sample size is a key point for radiocarbon aerosol source apportionment, as this results in greatly improved sampling resolution (both in temporal scale and size-segregation) and chemical resolution (i.e. the possibility of analysing separate carbonaceous fractions).

§ 5.1 Measurements on aerosol samples

First tests on aerosol samples were performed on filters specially sampled for this purpose: PM_{10} aerosol was collected in Milan for 24÷48h during July 2008 in a urban background station by means of a Digitel DHA-80 HV sequential sampler on Munktell quartz fibre filters with 15 cm diameter (see § 1.3).

The carbon load on the filters was evaluated by performing thermo-optical measurements with the Sunset analyser (see § 1.4.1), thus allowing the insertion of a proper quantity of filter in the sample preparation line: in order to obtain a cathode containing ~450 μgC, 12÷15 cm^2 of loaded filter were burnt for each sample. Samples were prepared according to the protocol for TC analysis reported in § 3.3 and measured as described in § 2.3.3.

Results for these measurements are reported in Table 5.1, both as pMC and f_m; uncertainties were evaluated as described in § 2.3.3. The shown TC source

apportionment is performed on the basis of the two-source model relations (1.2), which can be written as follows for TC:

$$\frac{\mathrm{TC}_{\mathrm{fossil}}}{\mathrm{TC}_{\mathrm{tot}}} \cdot \frac{f_{m,fossil}}{f_m(\mathrm{TC})} + \frac{\mathrm{TC}_{\mathrm{bio}}}{\mathrm{TC}_{\mathrm{tot}}} \cdot \frac{f_{m,bio}}{f_m(\mathrm{TC})} = 1$$
$$\frac{\mathrm{TC}_{\mathrm{fossil}}}{\mathrm{TC}_{\mathrm{tot}}} + \frac{\mathrm{TC}_{\mathrm{bio}}}{\mathrm{TC}_{\mathrm{tot}}} = 1 \qquad (5.1)$$

where $f_{m,fossil}$ = 0, as reported in §1.5.1. The fraction of modern carbon for "contemporary" samples was assumed to be $f_{m,bio}$ = 1.055 ± 0.015, according to [Szid09, Levi08]. It is worth to highlight that the assumed $f_{m,bio}$ does not take into account any compensation for the lifespan of some contemporary sources such as wood burning.

The fossil source appears to account for ~50% or even less during summer, and these results are very likely as they well agree with others studies on this issue (e.g. [Lewi04]). The fossil source contribution appears to be the same for the FV12 and FV13 samples, which were collected during consecutive days. A significantly lower contribution is found for the sample FV3, which was collected ten days before. This variation may be explained by a change, in those ten days, in the aerosol sources or in the meteorological conditions. As previously mentioned, these filters were specially sampled for test purposes, so no much additional information is available. Nonetheless, the performed source apportionment appear to be likely as abrupt changes in the sources contributions are not probable, if no abrupt change in the meteorological conditions occurs, while changes on a ten-days time scale are very common.

Sample	pMC	f_m	TC_{bio}/TC_{tot}	TC_{foss}/TC_{tot}
FV3	67.3 ± 0.6	0.673 ± 0.006	0.638 ± 0.011	0.362 ± 0.011
FV12	53.7 ± 0.4	0.537 ± 0.004	0.509 ± 0.008	0.491 ± 0.008
FV13	52.2 ± 0.7	0.522 ± 0.007	0.495 ± 0.010	0.505 ± 0.010

Table 5.1: Measured fraction and percent of Modern Carbon for filters sampled in Milan.The TC source apportionment was performed assuming $f_{m,bio}$ = 1.055 ± 0.015 [Szid09, Levi08]. Uncertainties on the TC_{bio}/TC_{tot} and TC_{fossil}/TC_{tot} ratios were evaluated as the root-sum-of-squares of the uncertainties on f_m and $f_{m,bio}$.

Moreover, in the last months we participated to an intercomparison on radiocarbon measurements on carbonaceous aerosol organised by Dr. Soenke Szidat from the Laboratory for Radiochemistry and Environmental Chemistry at the Paul Scherrer

Institute (Switzerland) within the frame of the EUCAARI project (*European Integrated Project on Aerosol Cloud Climate Air Quality Interactions*). Due to the limited availability of the intercomparison samples (a fraction of every sampled filter was supplied to each involved laboratory), before sampling and shipping the samples, every laboratory participating into the intercomparison was asked for the minimum sample size to be provided, in order to supply to every laboratory the fraction matching their minimum requirements. In this way, the duration of the aerosol sampling was selected in order to get a total amount of aerosol sufficient for all the laboratories and the partitioning of the sampled filter was calibrated on the necessities of the involved laboratories.

The following samples were shipped to our laboratory:

- 3 aerosol samples collected on quartz fibre filters;
- 2 "blank" quartz fibre filters, i.e. filters not loaded as they did not undergo to aerosol sampling.

In Table 5.2, a summary of the sample preparation outcome is reported[1].

Sample	Sample preparation summary
Blank1	*Insufficient amount of collected CO_2*
Blank2	*Insufficient amount of collected CO_2*
Sample1	*Problems during combustion- no cathode produced*
Sample2	Four TC cathodes produced
Sample3	Two TC cathodes produced

Table 5.2: Summary of the sample preparation outcome for intercomparison samples.

When burnt, the unloaded filters ("blank filters") produced less than 50 mbar of CO_2, i.e. less than a quarter of the CO_2 pressure corresponding to the desired 450 μg quantity of graphite, therefore no cathode was prepared from these samples[2]. The supplied loaded samples were really "unknown", i.e. nothing about them was known, not even the aerosol load, but they were supposed to be just enough to produce one 450 μgC cathode each. Therefore, the whole Sample1 was burnt, without making any previous TC determination by Sunset analyser to avoid wasting necessary material; actually, the aerosol load was much more than expected, and the catalyser and the traps, calibrated for smaller amounts of produced gases, did not work properly (as it was

[1] Original sample name is not reported, as the results of this exercise are still not published.
[2] It is worth recalling that only the matching-size method allows the compensation for machine-induced isotopic fractionation effects (see § 2.3.2).

clearly seen by observing the colourful collected mixture of gases). Due to this experience, for Sample2 and Sample3 a previous TC estimate was performed and more cathodes were produced.

The measured percent of Modern Carbon for the prepared cathodes is shown in Figure 5.1: the reproducibility of both sample preparation and measurement is well evident, as all the data are in agreement among them.

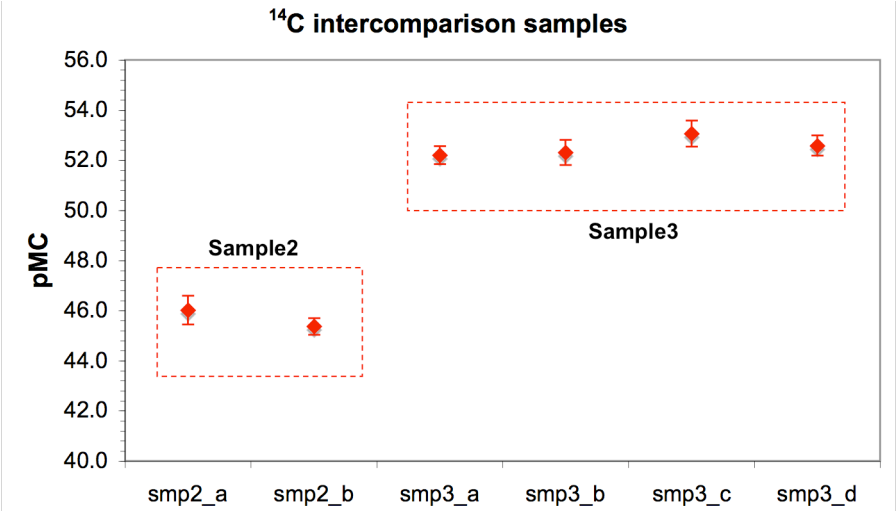

Figure 5.1: Measured pMC for cathodes prepared from the ^{14}C intercomparison samples. Uncertainties were evaluated as reported in §2.3.3.

Final results for this exercise are reported in Table 5.3. Conservatively, the reported final results were not evaluated as the average of the results for all the produced cathodes. Actually, for both Sample2 and Sample3, the reported result coincides with the result of one of the measured cathodes, once it was verified that such result did not significantly differ from the average of the results over all the produced cathodes. For both the samples, this specific cathode was critically chosen on the basis of its behaviour under measurement (cathodes characterised by low ^{14}R and ^{13}R dispersion and giving extracted current very similar to the standard samples one were preferred).

Sample	pMC	f_m
Sample2	45.4 ± 0.3	0.454 ± 0.003
Sample3	52.3 ± 0.5	0.523 ± 0.005

Table 5.3: Results for the radiocarbon intercomparison on aerosol samples.

Further information on the reliability of our measurements on aerosol samples are expected to come from this intercomparison, when all the results from all the involved laboratories will be revealed.

§ 5.2 Towards smaller samples

As reported in detail in § 1.5, since the very beginning of radiocarbon aerosol source apportionment studies, the sample size turned out to be a really crucial topic: nowadays, the challenge for modern radiocarbon aerosol studies is represented by "radiocarbon speciation", i.e. the determination of the spatial and temporal distribution of ^{14}C in individual compounds and chemical fractions [Curr00]. In fact, a complete chemical-physical characterization of the aerosol load on the filter would be very helpful to fully understand the impact of aerosol sources. To this aim, the reduction of the sample size to a quantity "as small as possible" is obviously desirable, as this would result in a greater number of analyses performable on the same sample, and in an improved sampling resolution both in temporal scale and size-segregation. Furthermore, it would be possible to analyse the quartz fibre filters usually collected on a daily basis by the Italian Regional Environmental Agencies with conventional LV samplers (see § 1.3).

As already mentioned, at the LABEC laboratory radiocarbon measurements for dating purposes are commonly performed on samples containing ~600 μg C. Such a quantity properly fits dating requirements, as very rarely taking a sample with such carbon content from an archaeological find represent a problem[3], but it definitively exceeds the requirements for aerosol source apportionment.

As already discussed in Chapter 4, tests performed to check the reliability of the new sample preparation line can be considered as a first step toward sample size reduction: such tests were carried out on samples containing ~450 μg of carbon, thus ~25% smaller than cathodes used in routine dating measurements. Anyway, 450 μg of carbon are still a quite large mass for aerosol source apportionment purposes, as they can constitute a real constraint not only for temporal sampling resolution but also for studies on aerosol in remote areas (with lower atmospheric aerosol loads) or analyses focused on specific aerosol chemical fractions. Since the main oven may contain up to ~ 40 cm^2

[3] It is worth to stress that, to obtain a cathode containing ~600 μg C, the sample taken from the find may be also larger, depending on its carbon concentration; as an example, in case of bones, ~500 mg of sample are needed.

of filter (see §3.2.2), the value of 450 μgC corresponds to a minimum detectable amount of ~ 11 μgC/cm^2. This latter value, in turn, corresponds to 2.7 μgC/m^3 and 2.3 μgC/m^3 concentrations in the air for a daily sampling using respectively a LV sampler[4] (2.3 m^3/h) or a Digitel sampler (30 m^3/h; see §1.3). These limits correspond to typical EC concentrations in urban areas: they do not allow the analysis of the EC fraction in remote/rural areas on a daily basis, or in polluted areas with time resolution better than one day.

When sample size is considerably reduced, both the feasibility of the sample preparation and the accuracy of the AMS measurements have to be checked. In fact, many effects such as graphitisation inefficiencies, scarce cohesion of the graphite bead or low ion currents can get involved with the net effect of producing inaccurate results. Therefore, two sets of samples containing ~ 225 μgC and ~110 μgC (corresponding to reductions by 50% and 75%, with respect to the already decreased sample size of 450 μgC) were prepared and measured by AMS.

§ 5.2.1 Small samples preparation

Samples were prepared with the new sample preparation line described in Chapter 3. Although some problems, mainly during graphitisation, have been reported in literature to occur when decreasing the sample size, in our case no special problem might be expected, due to the choice of a graphitisation reaction commonly used in laboratories preparing samples down to 10 μgC (see § 3.2.4) and to the attained high efficiency of the line (~100%, see § 4.1).

For both selected quantities (namely 225 μgC and 110 μgC), the following samples were prepared according to the protocol reported in § 3.3: OxAcII standards for normalization, Alfa Aesar graphite samples for blank evaluation and IAEA C7 reference material samples to check the accuracy of the measurements.

Samples containing ~225 μgC (corresponding to ~100 mbar of collected CO_2 inside the graphitisation reactor) were prepared first, but not in optimal conditions. In fact, due to a fault in the H_2 gas generator, we were forced to use another H_2 gas generator, which was available in the laboratory. Such H_2 gas generator is conceptually different from the one installed on the graphitisation line, as it does not produce H_2 by hydrolysis, but by a

[4] Actually, in parallel sampling would be necessary with this kind of samplers as the filter area is only ~13 cm^2.

reaction involving a water solution of sodium borohydride. Although the certified purity of the produced gas was equal for the two instruments, with this new generator the purity of H_2 appeared to be out of control and many incomplete or very slow graphitisation reactions were observed. Graphitisation curves for samples graphitised with H_2 produced by the two generators are shown in Figure 5.2: the different behaviour of graphitisation reaction depending on H_2 quality is evident. The second curve is very slow, and the residual gas pressure is higher, thus implying a lower efficiency of conversion to graphite.

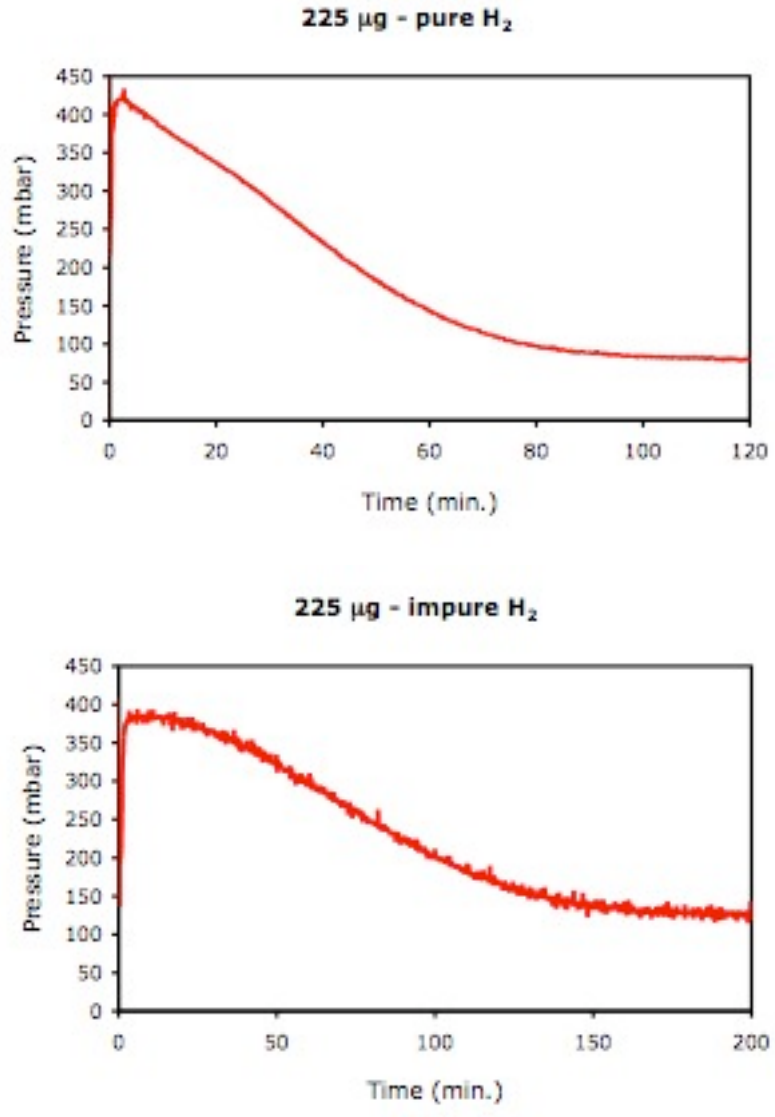

Figure 5.2: Graphitisation curve for a sample containing ~ 225 µgC in case of pure H_2 by the hydrolysis gas generator (upper graph) and in case of uncontrolled H_2 purity (sodium borohydride gas generator, lower graph). Note the different ranges of the time scales.

Unfortunately, due to beam time schedule, there was no opportunity to prepare other samples of this size.

Samples containing ~110 μgC (corresponding to a ~50 mbar CO_2 pressure inside the graphitisation reactor) were prepared only when the hydrolysis H_2 gas generator was available again, after reparation. No problem was experienced during the preparation of these samples, and graphitisation reactions always achieved completion; a typical graphitisation curve for samples of this size is shown in Figure 5.3.

One problem in preparing smaller size samples appeared clear when pressing the mixture of graphite and iron powder into the aluminium sample holders: in some cases we did not succeed, or we hardly succeeded, in reducing them to a coherent bead.

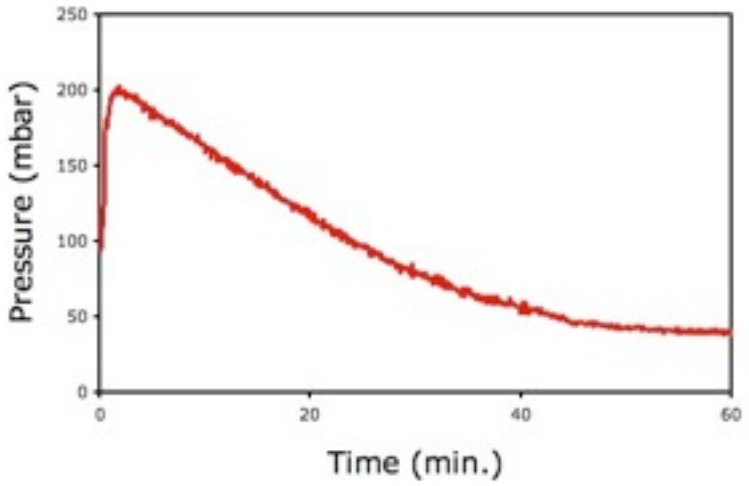

Figure 5.3: Graphitisation curve for a sample containing ~110 μgC.

Despite all the aforementioned experimental difficulties, 22 cathodes were prepared and loaded into the ion source for AMS measurements. They are listed in Table 5.4.

Size	Sample label	Sample
225 µgC	SMAL01	OxAcII
	SMAL02	OxAcII
	SMAL03	OxAcII
	SMAL12	OxAcII
	SMAL05	OxAcII
	SMAL04	Alfa Aesar graphite
	SMAL06	Alfa Aesar graphite
	SMAL14	Alfa Aesar graphite
	SMAL07	IAEA C7
	SMAL08	IAEA C7
	SMAL09	IAEA C7
110 µgC	SMAL19	OxAcII
	SMAL20	OxAcII
	SMAL21	OxAcII
	SMAL15	Alfa Aesar graphite
	SMAL16	Alfa Aesar graphite
	SMAL17	Alfa Aesar graphite
	SMAL18	Alfa Aesar graphite
	SMAL23	IAEA C7
	SMAL25	IAEA C7
	SMAL26	IAEA C7
	SMAL27	IAEA C7

Table 5.4: Samples loaded into the ion source to perform tests on the reliability of the AMS measurements performed for samples with reduced size (namely 225 µgC and 110 µgC).

§ 5.2.2 AMS measurements of small samples

As far as AMS measurements are concerned, the reduction of the sample size can result in reduced extracted currents. If the sample reduction is considerable, as in this case[5], even the measurement of these extracted currents may be critical.

In more detail, the ^{14}C measurement does not constitute a problem with sample size decreasing. In fact, ^{14}C beam intensity depends on the "sample age" even more than on sample size, and the gas ionisation detector used for ^{14}C measurement (see § 2.2.4) successfully cope with the detection of signals from even "almost dead" samples.

As far as ^{12}C and ^{13}C are concerned, a limit to their measurement comes from the read-out electronics noise: in fact, in absence of any beam accelerated trough the AMS system, the two Faraday cups devoted to the measurement of these isotopes give a reading of about 10 pA.

[5] It is worth recalling that the quantities taken into account are reduced by more than 60% and 80% with respect to the usual sample size for radiocarbon dating.

Moreover, some concern is aroused by the accelerator stabilization system embedded in the ^{13}C Faraday cup. In this regard, it is useful to recall that the ^{13}C Faraday Cup is composed by two plates and that the *slit error*, i.e. the difference between the currents on the two plates, controls a feedback mechanism which acts on the terminal voltage in order to restore the correct isotopes trajectories inside the AMS system (see § 2.2.4). This feedback mechanism is necessary to compensate for possible changes in environmental parameters such as temperature (AMS measurements on real samples are usually performed with daylong runs). This feedback, which can provide corrections up to about 15 kV with respect to the selected terminal voltage, might cease to work properly when the sum of the currents on the plates of the ^{13}C Faraday cup are too low. Actually, the minimum current needed to have the feedback mechanism correctly operating appears to be of the order of some hundreds of pA; below this limit, the accelerator stabilization system might switch off. Working with currents lying just above this limit is not suitable. In fact, if the stabilization system switches off on one sample (which might give a lower current due to small variability between the samples), the restoring of the correct trajectories on the next sample is very critical: in such conditions it is no longer possible to compensate for possible changes in environmental parameters and the entire batch might be compromised.

Routine measurements for radiocarbon dating revealed that measurements performed with currents down to ~ 1 nA still produce accurate results and do not incur in any problem, neither due to the switching off of the stabilization system nor caused by the read out electronics noise.

In order to perform the measurements with ion currents still above this suitable limit of 1 nA even on samples of reduced size, two options were possible:

- Increasing the Cs temperature in the ion source, thus enhancing the sputtering of the sample;
- Increasing the injection times[6] for ^{12}C and ^{13}C, thus increasing the charge collected by the Faraday Cup and the current reading, as the Farady cup is read out by electronics with a 10 Hz frequency, i.e. every 10 complete cycles of the bouncing magnet (a complete bouncer cycle lasts 10 ms).

[6] As already described in § 2.2.2, carbon isotopes are injected into the accelerator not continuously, but following a duty-cycle in which ^{14}C injection time is predominant. It is worth to recall that injection times are selected by choosing different times for the cycle of the bouncing magnet ("bouncing times").

The first option was discarded as it presents two disadvantages: having abundant Cs vapours in the source may dirty it; moreover, enhancing sputtering on samples whose resistance is already known to be scarce is not a good idea, as it increases the probability of making them to collapse.

As far as the second option is concerned, it is useful to stress that for every block, i.e. for each one of the nine points where the surface of the sample is sputtered, ~3000 complete bouncing cycles are performed. During these cycles, the Faraday cups are read-out ~300 times and the measured current is therefore the average of these readings (i.e. of the discharge current of the RC circuit associated to the Faraday cups). A reliable "a priori" estimate of the expected current from sample with reduced size was very difficult, therefore, in order to provide that measurements would run with ^{12}C and ^{13}C currents in the estimated suitable range of ~ 1÷10 nA, tests on small samples were performed with two different bouncing time conditions, i.e. not only with the usual bouncing times but also with a cycle with doubled time windows for ^{12}C and ^{13}C:

- Usual bouncing times: Δt_{14} = 8.5 ms, Δt_{13} = 0.6 ms, Δt_{12} = 6 μs;
- Bouncing times with doubled time windows for ^{12}C and ^{13}C: Δt_{14} = 8.5 ms, Δt_{13} = 1.2 ms, Δt_{12} = 12 μs.

225 μg samples

Measurements on samples containing ~225 μgC were allowed to run until 6 batches were performed for each bouncing time condition. ^{12}C and ^{13}C currents were generally well above the ~ 1 nA limit, for both the bouncing time conditions (i.e. for usual bouncing times and for bouncing times with doubled time windows for ^{12}C and ^{13}C).

As previously mentioned, the preparation of these samples was heavily affected by problems concerning H_2 purity. The bad conditions experienced during graphitisation were indeed translated into bad precision measurements. A high cathode current variability and a very unsatisfactory reproducibility on Oxalic Acid samples were observed: for example, the $^{14}R_{av}$ ratios (see §2.3.3) are reported in Figure 5.4 for all the standard samples, for each bouncing time condition.

The reproducibility issue in standard measurements is quantitatively summarised in Table 5.5, as obtained by the ratio between the standard deviation of the mean σ_{14}^{mean} (σ_{13}^{mean}) and the averaged $^{14}R_{av}$ ($^{13}R_{av}$) over all the measured standards; the reference values, i.e. the precision guaranteed by the accelerator supplier (HVEE) on modern

samples for accelerator acceptance tests, are also reported. It is worth recalling that, during the tests for the characterization and validation of the new sample preparation line, such values were respected (see § 4.2.1), while on these samples they are not achieved, and in some cases we are really very far from them.

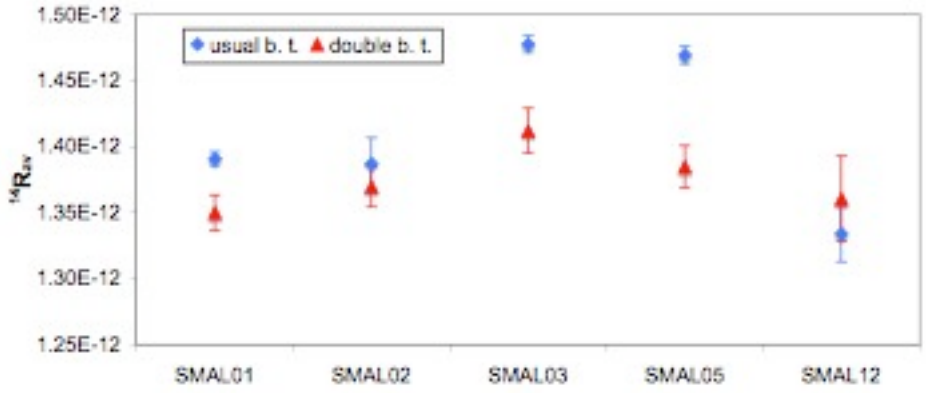

Figure 5.4: $^{14}R_{av}$ for the standards, measured both with usual bouncing times (usual b. t.) and with doubled time windows for ^{12}C and ^{13}C (double b. t.); error bars represent the standard deviation of the mean over the performed batches (see §2.3.3).

Bouncing times	$\sigma_{14}^{mean}/^{14}R_{av}$	Ref. value	$\sigma_{13}^{mean}/^{13}R_{av}$	Ref. value
Usual	19 ‰	< 5 ‰	8 ‰	< 3 ‰
Double	8 ‰		8 ‰	

Table 5.5: Reproducibility of $^{14}R_{av}$ and $^{13}R_{av}$ measurements as obtained by the corresponding ratio between the standard deviation of the mean (σ^{mean}) and the averaged R_{av} over all the measured standards; reference values are the precision specification guaranteed by HVEE for accelerator acceptance tests.

The observed irreproducibility may be regarded as the result of isotopic fractionation effects possibly occurring in various moments during preparation and/or measurement. The observed isotopic fractionation is hypothesised to be mainly due to fractionation effects occurred during sample preparation, and precisely during the phase of CO_2 reduction to graphite due to H_2 impurity. These effects result in a very poor reliability, as it is evident in Figure 5.5, where the measured percent of Modern Carbon for the reference material IAEA C7 are shown (uncertainties were evaluated as reported in §2.3.3). The accordance with the certified concentration (reported with continuous line, while dashed lines represent the $\pm 1\sigma$ uncertainty) is decidedly unsatisfactory.

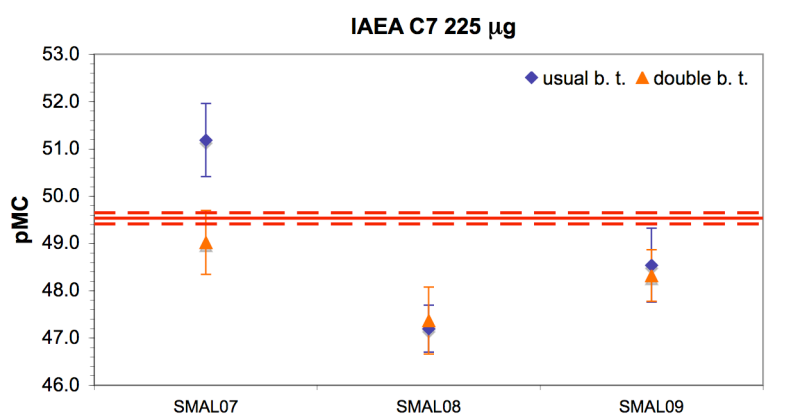

Figure 5.5: Measured radiocarbon concentrations in samples from IAEA C7 for both the bouncing times conditions; normalization to ^{14}R ($^{14}C/^{12}C$) and ^{13}R ($^{13}C/^{12}C$) isotopic ratios on standards. The uncertainties are evaluated as described in §2.3.3. The IAEA C7 certified concentration and ±1σ uncertainty are reported with, respectively, continuous line and dashed lines, respectively.

In the case of the SMAL07 sample, the different pMC measured with the two bouncing times conditions is probably due to sample consumption (measurement with doubled bouncing times for ^{12}C and ^{13}C were performed first); this hypothesis is also confirmed by a decreasing trend in extracted currents with the number of batch increasing.

Figure 5.6 shows the measured percent of Modern Carbon for the reference material IAEA C7 as obtained by the normalization on the basis of the $^{14}C/^{13}C$ isotopic ratios (see § 4.2.3).

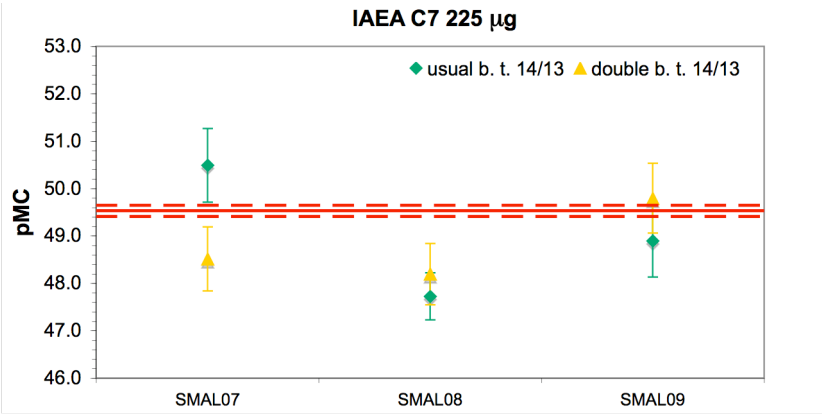

Figure 5.6: Measured radiocarbon concentrations in samples from IAEA C7 for both the bouncing times conditions; normalization to $^{14}C/^{13}C$ isotopic ratios on standards. The uncertainties are evaluated as reported in § 2.3.3. The IAEA C7 certified concentration and ±1σ uncertainty are reported with, respectively, continuous line and dashed lines, respectively.

The accordance with the certified value, although still poor, is slightly better than with the usual normalization, thus meaning that a contribution to the observed isotopic fractionation comes also from machine induced fractionation effects. However, the major contribution to the observed isotopic fractionation appears to be given by effects occurred during graphitisation.

All things considered, on the basis of these data no clear information on the feasibility of measuring samples containing ~225 μgC can be derived. Nonetheless these measurements were instructive to understand the negative effects produced by problematic graphitisation processes.

110 μg samples

The initial doubts (see § 5.2.1) on the possible scarce graphite bead cohesion with the sample size decreasing found a confirmation during measurements on samples containing ~110 μgC. In fact, some of the prepared samples listed in Table 5.4, dramatically collapsed as soon as they were inserted into the ion source, or as they were first sputtered by the Cs beam: in particular, samples labelled as SMAL20, SMAL21 (standards), SMAL17 (blank) and SMAL25 (IAEA C7) did not achieve to be measured.

Moreover, the SMAL26 sample collapsed, or "finished", just after 5 batches with the "double" bouncing times, and therefore did not achieve to be measured with the usual bouncing times. For all the other (not collapsed) samples, 7 batches were acquired for each bouncing time condition.

Anyway, after measurement, most of the samples were almost exhausted as it is macroscopically visible in Figure 5.7: the bead surface is heavily excavated, and in the central part the aluminium pin behind is visible.

The study of the sample consumption under Cs beam sputtering is important to evaluate the maximum level of precision that is achievable for samples of this size: in Table 5.6, the sum of the ^{14}C counts on the total 14 batches performed are reported for samples labelled as SMAL19 (standard), SMAL23 and SMAL27 (IAEA C7). Statistical uncertainties are also reported (on the basis of Poisson statistics). If the uncertainty on the standard isotopic ratio can be reduced to be negligible by performing measurements on a large number of standards (providing that they are all consistent among each others), the statistic uncertainty on ^{14}C counts of the unknown sample constitutes an intrinsic limit to the precision with which its pMC can be measured. From data in Table

5.6 we can therefore estimate that, for half-modern samples containing ~110 μgC, a ~1% minimum uncertainty on the measured pMC value has to be taken into account. Anyway, as stressed in § 1.5.2, such uncertainty would be surely acceptable for aerosol source apportionment purposes.

Figure 5.7: Some of the cathodes containing ~110 μgC after AMS measurements.

Sample label	Sample material	^{14}C counts	$\sigma_{14}/^{14}C$
SMAL19	OxAcII	22245	6.7 ‰
SMAL23	IAEA C7	7365	11.7 ‰
SMAL27	IAEA C7	16740	7.7 ‰

Table 5.6: Statistical uncertainties on ^{14}C counts for 110 μgC samples of modern or half-modern radiocarbon content.

^{12}C and ^{13}C currents were generally above the ~ 1 nA limit for the measurements performed with bouncing times with doubled time windows for ^{12}C and ^{13}C; currents slightly below such limit were observed for some blocks[7] on some samples when measured with usual bouncing times (the measured currents were anyway always > 0.5 nA).

Blank values[8] for the three measured graphite samples are reported in Figure 5.8: the values obtained with the two different bouncing times conditions are in good agreement.

The measured blank value turned out ~4 times higher than the one found during the tests for the characterization of the new sample preparation line (see § 4.2.2). This

[7] As described in § 2.2.1, samples are sputtered in 9 different points on the surface, called "blocks".
[8] We have to acknowledge that normalization was performed relative to only one standard.

increased blank may be however explained by the reduced sample size: the same "absolute" amount of modern contamination would in fact result in a higher blank value as the sample size is decreased. Such "blank shifts" have been indeed reported in literature (e.g. [Brow97]). It is worth noting that in most of the cases these black values are adequate for aerosol source apportionment purposes: for example, radiocarbon concentrations in the OC fraction have always been found to be well above 50 pMC [Szid09]. However, in the worst case, i.e. as far as the EC analysis in sampling sites dominated by fossil sources (like traffic) is concerned, these blank values may be limitative. As a consequence, this issue needs to be better investigated in order to further reduce all the possible contamination sources.

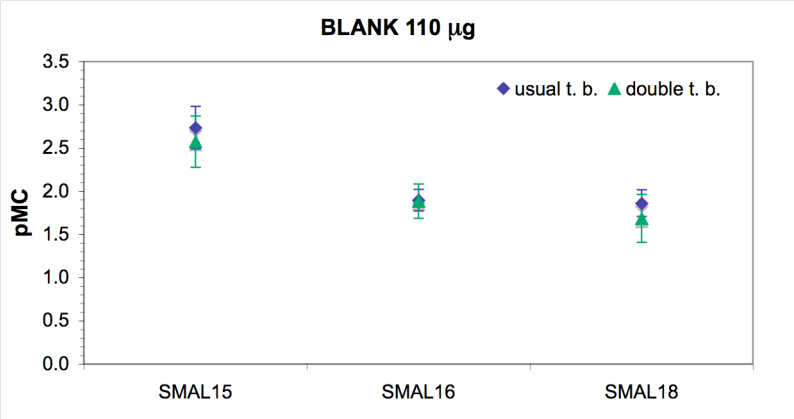

Figure 5.8: Percent of Modern Carbon for blank samples, namely produced from Alfa Aesar graphite, measured both with usual bouncing times (usual b. t.) and with doubled time windows for ^{12}C and ^{13}C (double b. t.). The uncertainties were evaluated as reported in §2.3.3.

Results for cathodes prepared from the reference material IAEA C7 are reported in Figure 5.9. The uncertainties were evaluated as described in § 2.3.3: the dispersion of the pMC values on the batches (calculated as the standard deviation of the mean) was checked and it turned out to be of the same order of the statistical uncertainty. Actually, in most of the cases, the data dispersion exceeded the statistical uncertainty. This confirms that sample cohesion and homogeneity are aspects of the small sample preparation that have to be improved, since presently they are more critical than the limit on the counting statistics.

The results from the measurements performed with different bouncing times conditions are in satisfying agreement among them and also with the certified value. The SMAL26 sample did not achieve to be measured with usual bouncing times as it "finished" just after 5 batches with "double" bouncing times, which were performed

first (the relevant sample consumption also explains the higher uncertainty on this measure).

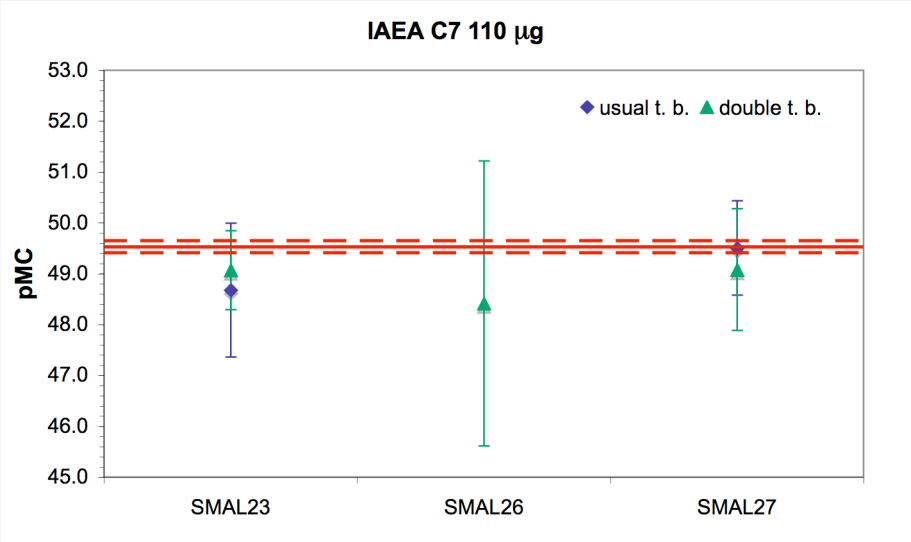

Figure 5.9: Measured radiocarbon concentrations in samples from IAEA C7 for both the bouncing times conditions; normalization to ^{14}R ($^{14}C/^{12}C$) and ^{13}R ($^{13}C/^{12}C$) isotopic ratios on standards. The uncertainties were evaluated as described in § 2.3.3. The IAEA C7 certified concentration and ±1σ uncertainty are reported with, respectively, continuous line and dashed lines, respectively.

Coming to conclusions, from these measurements we can deduce that, for sample size down to ~110 µgC, there is no problem in ^{12}C and ^{13}C current measurement, as the results obtained for the two different bouncing times conditions are in good agreement for both blanks and IAEA C7 reference material.

Moreover, the accuracy for AMS measurements on samples of this size appears good, as the measured pMC values of IAEA C7 samples are consistent with the certified value within 1σ. Although we have to acknowledge that we have used only one normalization standard, the results of these tests are very encouraging and promising on the possibility of further decreasing sample size.

§ 5.2.3 Future implementations for small samples preparation

As mentioned in § 3.5, for the further reduction of the sample size, the graphitisation reactor will need to be modified in order to reduce its volume and, therefore, to increase the gas pressure of the collected CO_2. In fact, the Bosch reaction is pressure-dependent [Smit09]; moreover, reducing the sample size, the quantification of the produced CO_2 and the graphitisation reaction monitoring are less accurate and affected by noise as the sensibility limit of the pressure transducer is approached.

Moreover, as one of the main experienced problems consists in the difficulty of obtaining resistant graphite beads inside the sample holders, the possibility of reducing the diameter of the small housing into which the graphite is pressed shall be taken into account. However, the reduction of the diameter (from the actual 2 mm) is technically very arduous if no other modification of the sample holder is made. Therefore, in the perspective of further reducing the sample size a specially designed target holder will have probably to be developed, as already done in other laboratories using HVEE sources model 846B [Smit09].

In this light, we are also considering the opportunity of increasing the iron powder quantity. In fact, although the increased catalyst amount surely results in a decrease of the extracted currents and might also represent an additional source of contamination, it enhances the resistance of the graphite bead to sputtering. In this manner, sample collapsing during the measurements is less probable [Sant07]. As a consequence, the measurement of samples of this size for a longer time and the analysis of smaller samples might be possible.

Final remarks and future perspectives

In this work, a sample preparation line for AMS radiocarbon measurements of the carbonaceous fractions of the atmospheric aerosols was designed and realised. With this facility, carbonaceous particulate matter collected on quartz fibre filters may be turned into graphite cathodes matching the LABEC AMS system requirements: the carbon within the sample is converted by combustion into CO_2, which is then isolated, collected and converted into graphite.

To fulfil all the desired and necessary requirements, most of the parts of the line demanded original homemade solutions. The whole apparatus was optimised to be as flexible as possible as concerns both the size of the input material and the choice of the thermal evolution during the sample combustion. The homemade furnace fulfils all the requirements for the preparation of samples from TC or segregated carbon fractions (namely, OC and EC): in particular, it is characterised by a good temperature uniformity and it is able to perform accurate and prompt thermal evolutions. Original homemade cryogenic traps accomplish the CO_2 isolation from all the other gases produced by the aerosol combustion.

In the perspective of reducing the sample size, the line was optimised in order to maximise its efficiency. In fact, the sample size reduction is a key point for radiocarbon aerosol source apportionment, as this results in greatly improved sampling resolution both in temporal scale and size-segregation (i.e. aerosol collection in separated dimensional classes) and chemical resolution (i.e. the possibility to analyse EC and OC separately). The optimisation of every process involved in the sample preparation (combustion, CO_2 collection and purification, graphitisation) and the leak minimisation led to an overall efficiency of the order of 100%.

The reproducibility and the reliability of the sample preparation procedure with the new sample preparation line were checked by AMS measurements on several cathodes produced from standards and reference materials according to the protocol for TC analysis developed in the present work. As described in Chapter 4, AMS results for these samples were found to be well reproducible and accurate.

Some first tests were then carried out on aerosol samples collected in Milan especially for this purpose. The radiocarbon content in the TC fraction was evaluated and the results appeared likely as they well agree with others studies on this issue. The feasibility of radiocarbon measurements on the TC fraction is a decisive step, since it allows comparing the results for aerosol samples prepared and measured at LABEC with the results obtained in other laboratories. In this regard, it is worthwhile to emphasise that we have participated to an international intercomparison on radiocarbon measurements on aerosol samples. The results coming from this exercise will surely be very helpful in order to check the goodness of our aerosol sample preparation procedure.

Finally, some first tests on the reduction of the sample size were carried out. It is worthwhile to recall that the size of the samples routinely analysed at LABEC for radiocarbon dating (~600 μg C) is too high for aerosol source apportionment. The new sample preparation line proved to be able to produce samples as small as ~100 μg C and the AMS measurements performed on these small samples gave very encouraging results.

As far as radiocarbon measurements on the separate EC and OC fractions are concerned, both sample pre-treatment and combustion protocols are currently under test. The validation of these protocols will need a long work yet. In fact, the parameters to be investigated are many (e.g. combustion temperatures and times, gas fluxes) and their variability ranges are quite wide. The determination of the proper parameters requires the preparation and the AMS measurement of a large number of samples, since only one parameter at a time may be changed.

In this light, some implementations in the sample preparation line will be introduced in order to increase the cathode throughput, which is now one or at the most two cathodes per day. To this aim, a duplication of the graphitisation reactor is now foreseen. By just duplicating the graphitisation reactor, it would be possible to start the combustion of a new sample while the graphitisation of the previously burnt sample is

still going on in the first reactor, thus reducing the "dead time" between the preparation of two samples.

Moreover, a reduction of the dimensions of the graphitisation reactor itself is currently under study. In fact, the reduction of its volume should allow a better control of the graphitisation process in view of a further reduction of the sample size.

A further upgrade will be surely represented by the insertion of a thermal trap on the H_2 inlet, in order to get rid of any possible contamination. In fact, as discussed in Chapter 5, H_2 purity demonstrated to be a crucial issue for a proper sample production.

Finally, the CO_2 trap could also be reproduced: in this manner, the sample preparation line would be equipped with two collection-graphitisation systems working in parallel and it would be possible, in principle, to prepare cathodes from the CO_2 evolved from the same sample during different phases of the chosen thermal program.

As soon as all the procedures will be validated, we plan to start specific sampling campaigns focused on the carbonaceous aerosol source apportionment. Several environmental protection agencies have already asked us to measure the radiocarbon content of some samples they have already collected. Actually, as far as the TC is concerned, these measurements are already feasible and will surely be done in the very near future, when the results from the intercomparison exercise we took part in will be available.

Appendix

IBA applications in aerosol studies

Although the main project developed during this PhD work has been focused on the AMS radiocarbon measurements for carbonaceous aerosol source apportionment, during these three years I also continued some IBA activities I had approached during my degree project, which concerned the implementation of PIXE and PIGE analyses on atmospheric aerosol samples.

Methodological results on the combined use of PIXE and PIGE for an accurate geochemical characterization and quantitative analysis of the fine dust will be shown.

Moreover, a comparison of PIXE and XRF (X-ray Fluorescence), aimed to the optimisation of combined measurements, will be presented; such an optimisation may reduce the accelerator beam time necessary for our analysis with an improvement in the detection efficiency for the elements of interest.

§ A.1 Mineral dust

Besides carbonaceous aerosols, one of the most abundant aerosol species in the atmosphere is mineral dust, which accounts, on a global scale, for ~40% of the suspended particulate matter, the largest contribution being from arid and semi-arid regions of north and west Africa. Anthropogenic mineral dust originates mainly from agricultural activities and industrial practices (e.g., cement production, transport).

Dust particles have a size distribution changing during transport, as a result of dry and wet deposition, with the net result of a depletion of the coarse fraction during long-range transport. Mineral dust is made of various minerals whose proportions vary according to size but also to the mineralogy of the emission source region, to the

erosion conditions, and to the transport distance. Major components are, in order of average abundance, alumino-silicates (illite, kaolinite, smectite, montmorillonite, feldspar), quartz, calcium carbonates (calcite, dolomite), and iron oxides (hematite, goethite) [Pye87]. All these mineral phases have a specific importance in terms of dust impact on the Earth's radiation budget (see § 1.1), as they have spectrally different refractive indices in the visible and infrared spectra (relevant for the direct radiative effect) and/or different hygroscopicity and solubility properties (relevant for the indirect effects involving cloud microphysics).

The direct radiative effect for mineral dust, both from natural and anthropogenic sources, is evaluated to be in the range -0.56 to +0.1 W/m^2. The anthropogenic contribution to the dust load in atmosphere is nowadays estimated to be ranging from 0 to 20%, with a very large uncertainty due to the difficulties in distinguishing between natural and anthropogenic sources. On these bases, the anthropogenic direct radiative forcing is estimated to be (-0.1±0.2) W/m^2, at the 90% confidence level ([IPCC07], see also Figure 1.4).

Moreover, mineral dust appears to be linked to ocean fertility: in fact, soluble Fe can act as a micronutrient for phytoplankton, which, despite its tiny abundance (<1% of the Earth's biomass), carries out almost half of Earth's photosynthesis. This effect is currently object of interest because the enhancement of the photosynthesis due to phytoplankton could draw down atmospheric CO_2 and thus reduce the global warming [Mesk05].

§ A.2 Mineral dust analysis by PIXE-PIGE measurements

The mineralogical composition of mineral dust is often inferred from its elemental composition. With the exception of carbon and oxygen, Al, Si, Na, Mg, K, Ca, Fe are the most abundant and typical tracers of mineral dust [Pye87]. Because their relative proportions in every mineral differ, the inter-elemental ratios are used as a proxy of the relative abundance of one mineral with respect to another. Elemental ratios are also characteristic of different geographical areas and thus they may help in the identification of the dust source regions.

The PIXE (*Particle induced X-ray emission*) technique [Joha95] is unrivalled for the direct measurement of the mineral dust fraction in the aerosol, as it is highly sensitive to all the crustal elements but oxygen and carbon. In fact, PIXE is a multi-elemental

technique (i.e. it simultaneously detects a wide range of elements) and it is particularly sensitive to light elements, due to the high cross-sections for X-ray production of these elements. Moreover, as well as the other IBA techniques, PIXE is fast, non-destructive, and does not necessitate any sample preparation.

However, due to the self-absorption of the lower energy X-rays within the dust particles themselves, PIXE cannot detect low Z elements and also the quantitative analysis of the lighter detected elements (Na, Mg, Al, Si) can underestimate their concentration. Since particles contained in a sample have different composition and size, this underestimation cannot be calculated considering the average composition of the aerosol sample. In fact, this artefact depends on particle size, and can reach up to few tens of percent of the measured concentrations in PM_{10} particles. Estimating a correction factor as a function of particle size is therefore necessary when studying the mineral dust cycle and impact. Without a proper correction, self-attenuation induced artefacts can significantly alter the typical concentration ratios previously mentioned and prevent a firm identification of the region of origin of the analysed aerosol.

In order to evaluate this phenomenon and to improve the quantitative accuracy, PIGE (*Particle induced γ-ray emission*) analysis may be simultaneously carried out. PIGE exploits the γ-ray emission of nuclei excited by the interaction with an accelerated particle beam. Since γ-rays are more energetic than X-rays, they do not suffer significant attenuation when passing through particles with dimensions in the order of few microns.

In the case of mineral dust, PIGE is performed simultaneously with PIXE for the determination of aluminium, as Al is the most abundant light element in mineral dust showing a high proton induced γ-ray emission cross-section [Boni88]. PIGE measurements are carried out exploiting the 1013 keV γ-rays produced by the $^{27}Al(p,p_2\gamma)^{27}Al$ reaction. A 3.06 MeV in-vacuum beam energy has been selected in order to obtain a cross-section for the used reaction that, thanks to a ~100 keV wide plateau, remains constant despite the energy loss of the protons within the sample (see Figure A.1). In this way, the thin target approximation (negligible γ-ray attenuation and negligible cross section variation within the sample) is fulfilled and an accurate experimental Al concentration value can be measured without the need of any *a posteriori* approximated correction based on assumptions on the size and composition of the aerosol particles.

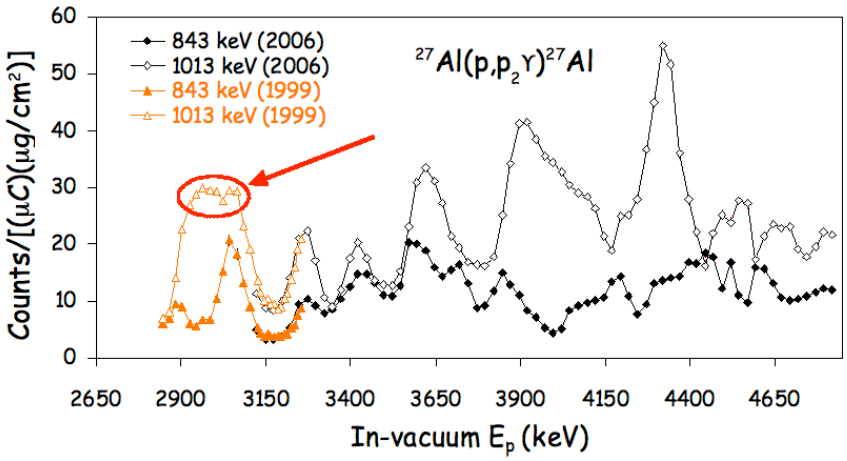

Figure A.1: Yield of aluminium (counts per unit of target thickness and integrated charge) as a function of the proton beam energy (in-vacuum energy). The selected plateau is highlightened. These measurements were performed at LABEC, using the external beam facility described in § A.3 [Calzxx].

During this PhD work, this approach has been successfully applied at LABEC for the analysis of mineral dust in remote areas. The variations of the aerosol properties during an air mass transport from North Africa have been investigated by the analysis of samples collected at the Global Atmospheric Watch (GAW) station of Mount Cimone (2165 m above mean sea level) [Cris09]. Particulate matter samples collected at ground level and by aircraft sampling over Western Africa have been analysed to study the desert dust composition [Form09]. Finally, this approach has been applied to the study of mineral dust in Antarctica for paleoclimatic investigations [Mari08]. For the sake of brevity, only the latter application will be described in details in the following paragraphs; more information on the other two issues can be found in the quoted references.

§ A.3 The PIXE-PIGE beam line for aerosol study

Among the operating beam lines shown in Figure 2.1, the +45° one is fully dedicated to environmental IBA analysis, and mainly to PIXE-PIGE measurements on aerosol samples.

For IBA measurements, the accelerated particles pass through the 115° AMS analysing magnet (not active in this case; see Figure 2.3) and reach the so-called switching-magnet, which bends the beam into the used beam line.

On the +45° beam line, the proton beam is extracted in air through a 7.5 μm thick Upilex window and the aerosol samples are positioned at a distance of about 1 cm from

the window, perpendicular to the beam (see Figure A.2). The volume of atmosphere between the bombarded sample and the X-ray detectors is saturated with helium, to reduce the absorption of the emitted radiation. The beam size is set by a collimator (usually to 1.0 × 2.0 mm^2) located in the last section of the in-vacuum beam line. Both the scanning of the aerosol filters and the change of the samples are automatically controlled by the acquisition system. A Faraday Cup positioned just behind the sample allows the measurement of the integrated beam current[1].

Since X-ray production cross sections range over 3 orders of magnitude, to obtain an efficient simultaneous detection of all the elements it is necessary to balance the counting rates produced by the low and medium-high Z elements. The adopted solution is the use of two detectors optimised for low and medium-high X-ray energies, respectively. The first one is a Silicon Drift Detector (SDD), the latter is a Si(Li) detector (145 eV and 175 eV FWHM energy resolution at the 5.9 keV Mn K_α line, respectively).

Finally, γ-rays for PIGE analysis are detected by a 60 mm × 23 mm Ge detector, with 28% efficiency and 1 keV FWHM energy resolution at 1.33 MeV, respectively.

More details on the PIXE-PIGE set-up may be found in [Calz06].

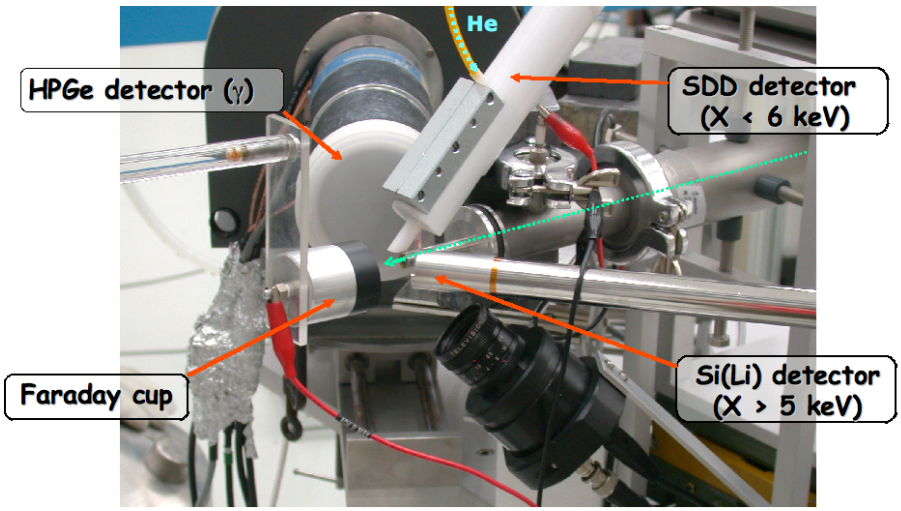

Figure A.2: External-beam set-up for Ion Beam Analysis on aerosol samples.

[1] Aerosol samples collected on filters are thin samples.

§ A.4 Ice core dust composition during glacial stages

The main purposes of paleoclimate research are extracting and interpreting the climate-related information attainable from many sources, e.g., tree-rings and polar ice cores. These studies enhance the knowledge of how the climate changes over interannual to millennial time scales and allow verifying how well climate models can simulate these variations. Therefore, paleoclimate research may help to better understand the present climatic age by studying the past ones.

As concerns Polar ice cores, they are extensive archives of records of the past atmospheric compositions; in fact, snow, accumulated layer by layer and gradually compressed into solid ice, contains traces of the gases and the aerosols present in the atmosphere at the deposition time. In particular, mineral dust in Antarctic ice cores is one of the most studied paleoclimatic and paleo-environmental proxies; with respect to other proxies, dust get indefinitely trapped in snow after deposition, without incurring in any post-depositional process. Moreover, in the inner Antarctic areas, local dust sources are negligible; therefore, ice-dust is only composed by particles reaching these areas after long-range transport from continental areas in Southern Hemisphere.

Many features of the insoluble dust trapped in the ice-cores are studied because of their potential to provide different kind of information: for example, dust concentrations and size distributions along the ice core may give information about atmospheric dustiness and transport processes, and also on the aridity of the continental sources.

The study of the geochemical composition of the trapped dust may give information on the location of the dust sources and, therefore, help in understanding the transport trajectories. To this aim, ice core dust composition has to be compared with the composition of the sediments of the potential source areas (PSA), which are selected on the basis of satellite observations and model simulations of dust production and atmospheric transport (sediments are preferentially collected in deflation areas).

In the framework of the EPICA (*European Project for Ice Coring in Antarctica*) project, two ice cores were drilled in two different regions of the East Antarctic Plateau, namely at Dome C and at Dronning Maud Land [EPIC04, EPIC06]. In this work, some ice-dust samples from the ice core drilled at Dome C were analysed. Such an ice core spans the last 800 kyr; anyway, the measured samples regard the main cold events of the last 220 kyr, except the last one (i.e. they cover the cold periods called MIS4 and MIS6, the two glacial stages before the last one, called *Last Glacial Maximum*, LGM).

Due to the tiny elemental concentrations (ng÷mg/kg of ice), ice samples were melted and the liquid was filtered through Nuclepore membranes paying special attention to avoid contaminations [Mari08].

Dust samples from different PSA regions were also analysed. Since dust, deflated from continental source areas, reaches the inner part of the ice sheets only after thousands of kilometres of long-range transport, it undergoes a strong dimensional selection in the atmosphere. Consequently, ice core dust is only composed by fine particles. Antarctic dust, for example, is composed by particles with diameter <5 μm and with a mode around 2 μm [Delm02]. Therefore, a reliable comparison between the geochemical composition of ice-core dust and PSA sediments can only be obtained by analysing particles of a comparable size range for both the sets of samples. To this aim, a granulometric selection of the PSA sediments was performed by selective sedimentation in ultra-pure water, following the Stokes law.

Moreover, blank filters and procedural blanks (i.e. filtration of ultra-pure water undergone to the whole preparation process) were also analysed.

Measurements were performed at the PIXE-PIGE external beam set-up described in § A.3, irradiating each sample for about 1000 s, with a proton beam current ranging from 5 to 30 nA, depending on the sample load.

Coming to the results, some impurities of Si and Br were found on the blank filters, while procedural blanks evidenced that sample preparation introduced small contaminations of S, Cl, Cr and Fe; however, blank values for the elements of interest in ice core dust analysis (Na, Mg, Al, Si, K, Ca, Ti, Mn, Fe, Sr) were always largely below the measured concentrations.

As far as the comparison of PIXE and PIGE results for the Al quantification is concerned, the average attenuation in Antarctic ice dust samples resulted ~10% (average attenuation coefficient, calculated as PIXE/PIGE ratio, equal to 0.91; see Figure A.3). This rather low value confirmed that X-ray self-absorption effects in Antarctic dust are moderate, due to the small dimensions of aerosol particles reaching the East Antarctic Plateau. The same value, within experimental uncertainties, was found for size selected PSA sediments: this result confirmed that the selection of a size range comparable to Antarctic dust was successfully achieved.

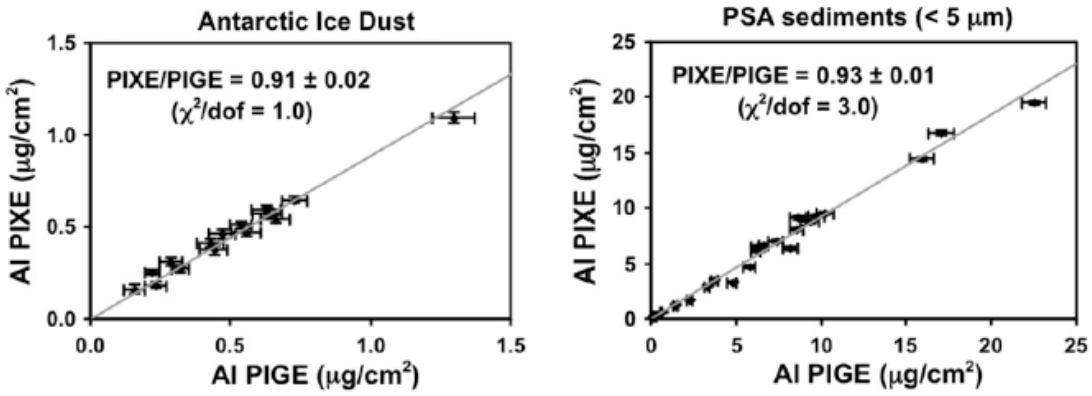

Figure A.3: Regression lines between Al concentration values measured by PIXE and PIGE in Antarctic ice dust and size selected PSA sediments.

In the realistic hypothesis that Antarctic dust and sediments are mainly composed by a mix of pure mineral particles (namely K-feldspar, Kaolinite, Illite and Quartz), the measured Al attenuation coefficients were used to evaluate an effective dimension of these mineral particles and hence to estimate the attenuation coefficients for the other light elements for each sample (see scheme in Figure A.4). Due to the very similar attenuation of Al X-rays in the different minerals that contain this element (namely K-feldspar, Kaolinite and Illite), particle dimensions turned out quite similar in spite of the different mineral composition used for calculations. For example, according to a simple attenuation model for single spherical particles [Holy81, Form09], the attenuation coefficient for the element *x*, $C_{att}(x)$, is given by the following relation:

$$C_{att}(x) = \frac{1 - e^{-\frac{2}{3}\cdot\mu\cdot\rho\cdot d}}{\frac{2}{3}\cdot\mu\cdot\rho\cdot d} \qquad (A.1)$$

where ρ and d are the density and the diameter of the particle and μ is the massive absorption coefficient. On the basis of this relation, an effective particle diameter of 0.90 μm, 0.99 μm and 1.00 μm can be found, respectively, for Illite, Kaolinite and K-feldspar, using a 0.91 attenuation coefficient (the average Al PIXE/PIGE ratio for ice dust).

Assuming a 1 μm diameter for quartz particles, the following attenuation coefficients can be estimated for the other elements: 0.79 for Na in K-feldspar; 0.87 for Mg in Illite;

0.90, 0.91, 0.92 and 0.94 for Si in Kaolinite, Illite, K-feldspar and Quartz respectively; 0.97 for K in both Illite and K-feldspar.

	Na	Mg	Al	Si	K
Kaolinite			0.91	0.90	
K-feldspar	0.79		0.91	0.92	0.97
Illite		0.87	0.91	0.91	0.97
Quartz				0.94	

Figure A.4: Scheme of the evaluation of the attenuation for the light elements on an ice dust sample, in the hypothesis that it is mainly composed by a mix of pure minerals, namely Kaolinite, Illite, K-feldspar and Quartz.

In the case of elements that are mainly present in only one mineral, like Na and Mg, the attenuation coefficients calculated for pure mineral particles may, in first approximation, be directly applied to real samples. The attenuation of potassium X-rays resulted the same and substantially negligible for both Illite and Kfeldspar. Quite similar values turned out also for Si, thus allowing the use of an average value over the different minerals. The quoted attenuation values are an example of realistic attenuation coefficients that can be found. However, in order to take into account changes in particle dimensions in the different collected samples, the calculations have been done using the Al PIXE/PIGE ratio measured in each sample.

The overall accuracy of the method, including sample preparation and IBA analysis was confirmed by the good agreement between the measured compositions and the certified ones for some bulk and size-selected (<5 µm) pure mineral standards, which were analysed in the same run. Standard materials were chosen among those constituting the main mineral components of dust.

Coming to the main results of this work, the measured compositions of ice dust and PSA sediments are reported in Figure A.5: as mineral dust is only composed of the oxides of the detected elements, the measured compositions are given expressing every oxide as percentage of the total mass. From this geochemical characterization, ice dust composition during the cold stages (MIS4 and MIS6) seems to be quite similar to the South-American one, while it relevantly differs from both the Australian and the South-

African one; this is even more evident when comparing specific oxide ratios (see Table A.1).

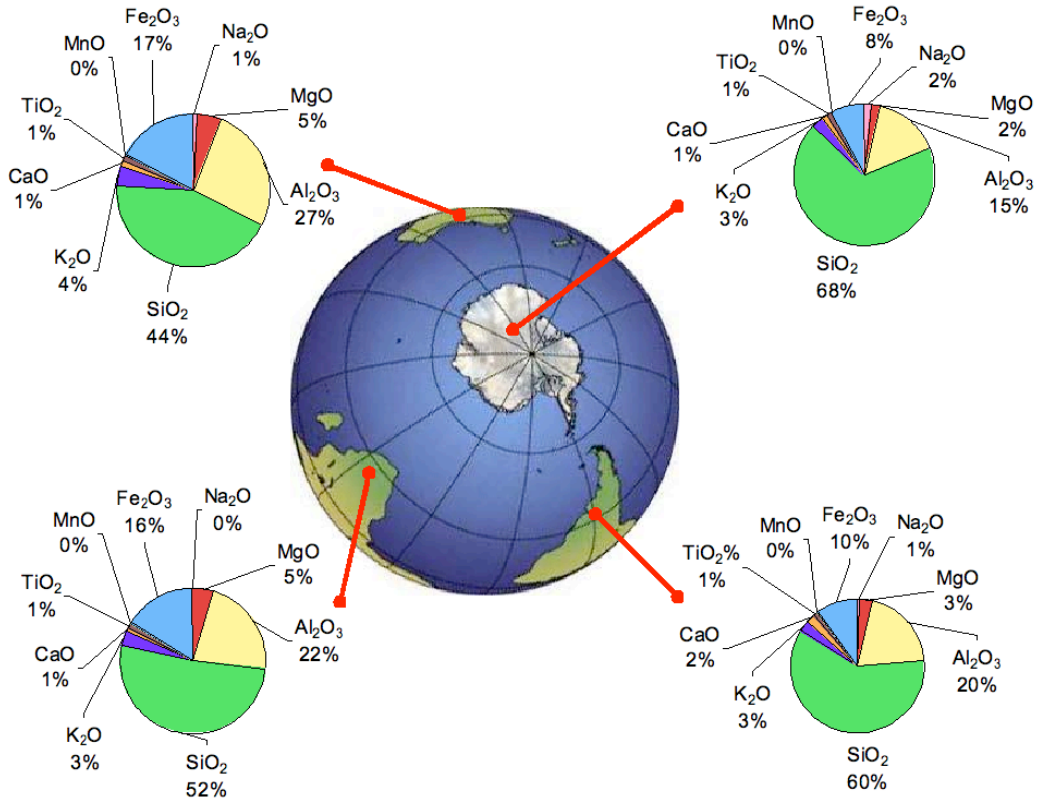

Figure A.5: Geochemical characterization of ice dust and PSA sediments.

	Al_2O_3/SiO_2	Fe_2O_3/SiO_2	Al_2O_3/Fe_2O_3
Antartica	0.22 (± 0.04)	0.12 (± 0.02)	2.0 (± 0.4)
South America	0.33 (± 0.04)	0.17 (± 0.02)	2.0 (± 0.3)
South Africa	0.43 (± 0.09)	0.31 (± 0.07)	1.4 (± 0.4)
Australia	0.61 (± 0.12)	0.39 (± 0.12)	1.5 (± 0.5)

Table A.1: Average ratios of some main oxides for the different groups of samples; the standard deviations of the ratios are also reported (in brackets) to quantify the variability of the ratios within each group of samples.

This work is still in progress. Further measurements are scheduled in the near future to increase the number of analysed samples (~20 ice-dust samples and ~30 PSA samples have been analysed so far) in order to obtain a more representative characterization. The increased number of samples will also allow the application of multivariate statistical analysis techniques to assess the contribution of the different PSAs to the Antarctic dust.

As previously mentioned, these measurements are carried out within the frame of a wider project, the EPICA project: although the work is still in progress, data obtained so far are still contributing to improve the EPICA data set.

In Figure A.6 the contribution of these measurements to the reconstruction of the dust mass concentration in the ice core drilled at Dome C is shown (a star denotes the data from this work). For the measured samples, which, as previously mentioned, cover the cold periods MIS4 and MIS6, the oxides sums calculated from the measured elemental compositions agree very well with the dust mass measured with other techniques. There is evidence that, during the cold periods (LGM, MIS4 and MIS6), dust concentrations are much higher than during hot periods.

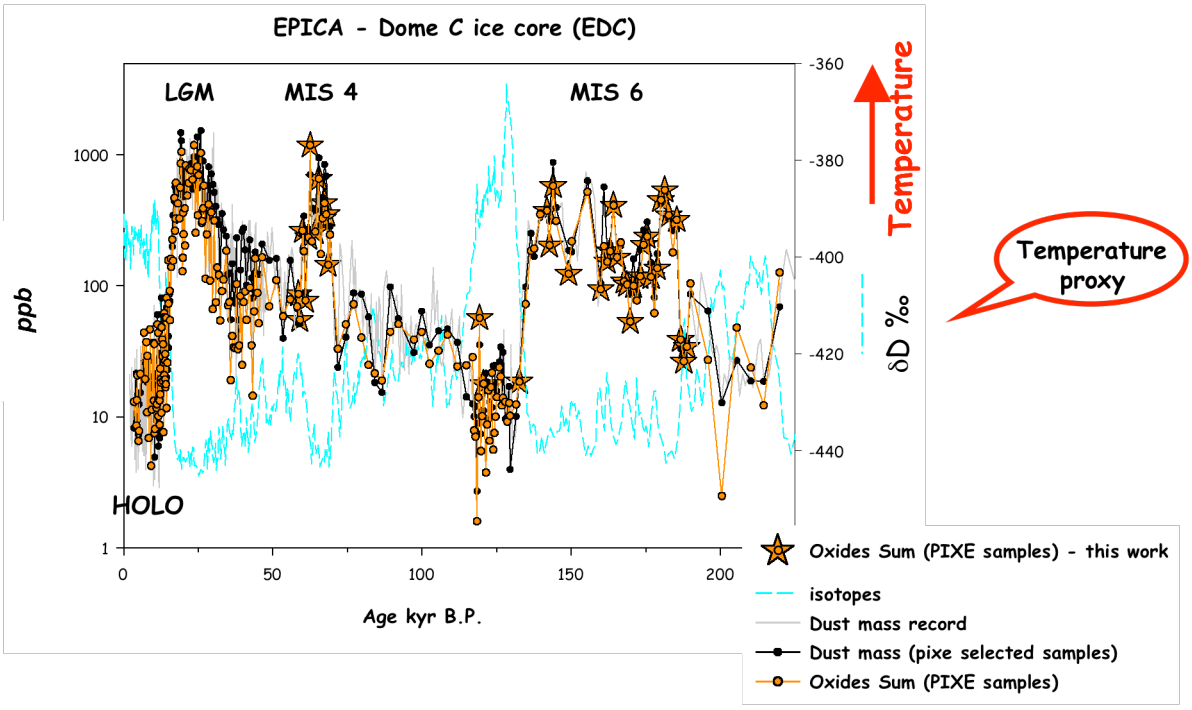

Figure A.6: Dust mass concentration in the ice core from Dome C. Samples analysed in this PhD work are indicated as star-dots. δD is the deuterium/ hydrogen ratio in ice and it is widely used as a temperature proxy [EPIC04].

In Figure A.7, the siliceous dust content is plotted versus the aluminium oxide content for the samples coming from both the two ice cores drilled in the framework of the EPICA project, at Dome C (EDC) and at Dronning Maud Land (EDML; see map in Figure A.7). Their composition is compared with the one of sediments collected in the PSA of Southern South America (SSA) and Australia (AUS) and from. Ice dust samples

span the glacial periods LGM, MIS4 and MIS6 and the present interglacial period (Holocene).

The similar geochemical signature during cold stages for the two drilling sites and the close similarity with the composition of Southern South American sediments, indicate a common dominant source for dust reaching the two Antarctic areas.

Conversely, geochemical data and model studies indicate that during interglacials an Australian source could have played an important role as dust supplier, at least for Dome C.

More details about the geochemical composition of EPICA ice-dust samples may be found in [Mari08b, Mari09].

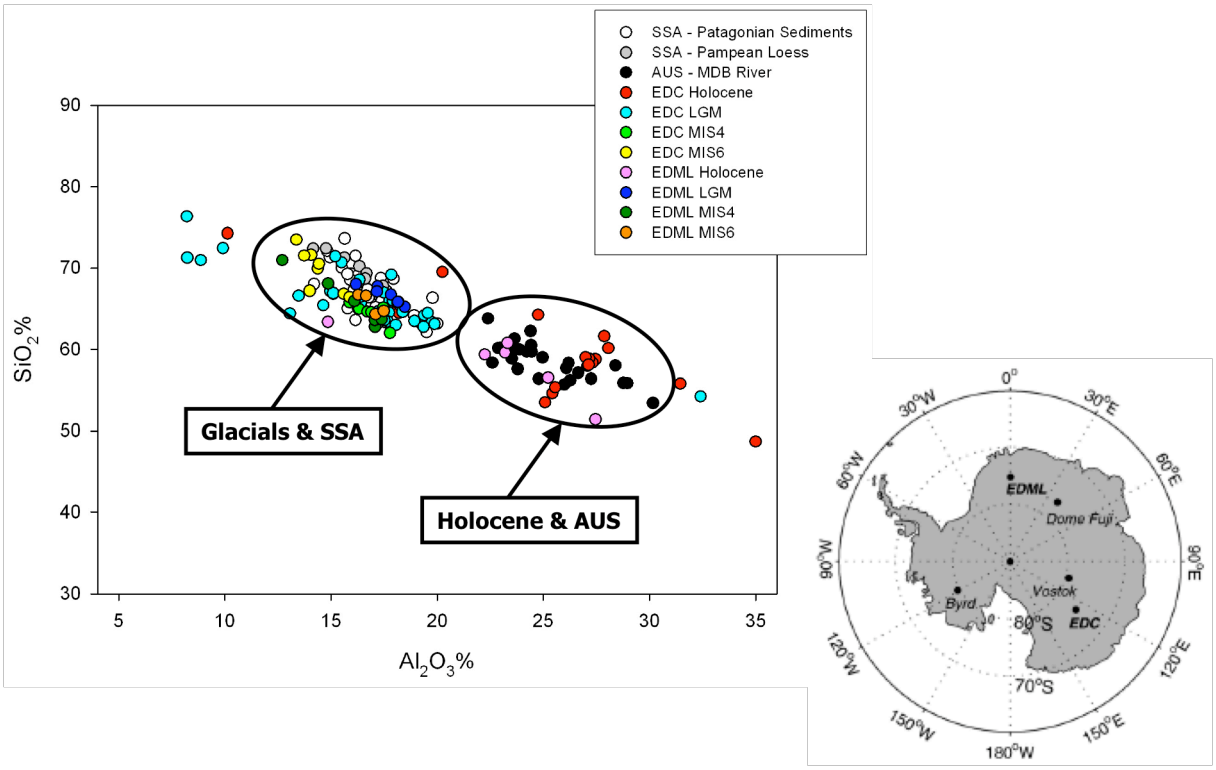

Figure A.7: Geochemical characterization of ice dust and PSA sediments. EDC MIS4 and EDC MIS6 samples have been analysed within this PhD work.

§ A.5 PIXE and XRF comparison

The EDXRF (*Energy Dispersive X-ray Fluorescence*) technique is based on the analysis of the X-rays emitted by the sample after excitation, which is produced by the interaction with an X-ray beam produced by an X-ray tube. As well as PIXE, EDXRF (hereinafter simply XRF) is a fast, quantitative, highly sensitive and multi-elemental analytical technique; it does not need any pre-treatment of the sample and it is non-

destructive, thus allowing the extension of the range of detectable elements by complementary techniques applied to the same sample.

All these features make PIXE and XRF very suitable techniques for the analysis of aerosol samples; in fact, due to the required resolution on both temporal and spatial scales, aerosol-sampling campaigns produce huge amounts of few μg particulate samples, which have to be fully characterised, therefore highly sensitive and fast analytical methods are required.

For many years, our group has been involved in very extensive aerosol monitoring and study programs aimed at the characterization of particulate matter in urban areas or industrial districts (e.g. PATOS projects, *PArticolato in TOScana*, *Particulate matter in Tuscany*), with the result of a relevant measurement load. As the accelerator is heavily used also for other IBA or AMS applications, the possibility of performing some measurements with a commercial, automated XRF spectrometer in place of PIXE measurements was taken into account. Moreover, as the XRF is routinely performed in the laboratories of Genoa and Milan, with which there is a close collaboration, the comparison between the results obtained by these two techniques, both in terms of absolute values and MDLs (Minimum Detection Limits), is worthwhile.

In the perspective of acquiring an XRF spectrometer in Florence too, the aim of the study was optimising the elemental analysis with the joint and complementary use of PIXE and XRF, minimising the analysis time at the accelerator and maximising the detection efficiency for a number of elements.

In order to identify the optimal technique to be used, in relation to filter type and to the goal of the specific campaign, a comparison between PIXE and XRF MDLs was made, for different elements and filter types. In fact, although for AMS application only quartz fibre filters were taken into account because of their unique property of being able to sustain high temperatures, aerosol may be collected on different types of filters, depending on the chemical-physical analysis that have to be done (see § 1.3). The most used supports are Teflon, polycarbonate, Kapton and cellulose mixed esters filters.

Fourteen daily samples of PM_{10} and $PM_{2.5}$, collected on different substrata, were taken into account (6 on Teflon, 3 on polycarbonate and 5 on cellulose mixed esters filters). These samples were collected by standard low-volume sequential samplers (see § 1.3) in an urban sampling site and they can be considered representative for urban aerosol samples. Samples were measured by XRF (in Milan and in Genoa) and by PIXE in Florence, under the typical conditions used for the routine analysis of aerosol samples.

PIXE measurements were performed at the external-beam set-up described in § A.3. Samples were bombarded with a 3.2 MeV extracted proton beam, with a 12 nA current (6 nA in case of Teflon filters), for about 10 minutes.

XRF measurements were carried out with an ED-2000 spectrometer by Oxford Instruments. A Coolidge tube (I_{max}= 1 mA, HV_{max}= 50 kV) with an Ag anode produces the excitation X-rays. Two measuring conditions were fixed to optimise the sensitivity for different groups of elements: runs with HV = 15 kV, I = 100 μA, no primary filter, livetime = 1000 s, to detect "low Z" elements (from Na to P), while the "medium-high Z" elements (from S to Pb) were measured setting HV = 30 kV, I = 500 μA, Ag primary filter (about 50 μm thick), livetime = 3000 s. The beam spot is elliptic with an area of about 1 cm^2; nevertheless, the automatic spinning on the sample axis allows the investigation of a much wider area. X-rays were detected by a Si(Li) with energy resolution lower than 145 eV FWHM at 5.9 keV.

For both PIXE and XRF measurements, elemental thickness (μg/cm^2) was obtained by comparing the filter yields with a sensitivity curve measured in the same geometry on a set of thin Micromatter standards, with a ±5% uncertainty on areal concentrations.

Amongst the detected elements, only those with concentrations above their MDLs in at least 8 samples, both in PIXE and XRF measurements, were selected; therefore, Al, Si, S, K, Ca, Fe, Cu and Zn were taken into account. Moreover, these elements are markers of aerosol sources, as mineral dust, sulfates, biomass burning and traffic. In both PIXE and XRF measurements, blank corrections were necessary to obtain accurate quantitative results. In the case of samples collected on cellulose mixed esters filters, we could not take into account Zn concentration data because of the high and inhomogeneous contamination of blanks.

XRF and PIXE measurements are in good agreement: differences between concentrations obtained by the two methods are always within 10%, except in two cases (being anyway not more than 15%, see Table A.2). These discrepancies can be due to different X-ray spectra fitting procedures[2], and to sample and blanks inhomogeneities, because of the different area covered by proton and excitation X-rays beams. Sample thickness spanned a wide range of aerosol deposit (~ 30 ÷ 500 μg/cm^2), so we can exclude any dependence from the deposited mass. In Figure A.8 linear regression plots for the 8 selected elements are shown; slopes and correlation coefficients are reportedin Table A.2.

[2] PIXE spectra and XRF spectra were fitted, respectively, with the GUPIX [Maxw95] and AXIL [vanE77] software packages.

	XRF (Genoa) versus PIXE		XRF (Milan) versus PIXE	
	Slope	r^2	Slope	r^2
Al	1.04 ± 0.02	0.96	0.89 ± 0.02	0.97
Si	1.03 ± 0.02	0.98	1.00 ± 0.02	0.98
S	1.04 ± 0.02	0.97	1.07 ± 0.02	0.97
K	1.00 ± 0.03	0.93	1.03 ± 0.03	0.97
Ca	1.02 ± 0.03	0.99	1.08 ± 0.03	0.99
Fe	1.07 ± 0.02	0.99	1.07 ± 0.02	1.00
Cu	0.99 ± 0.02	0.99	1.10 ± 0.02	1.00
Zn	1.12 ± 0.03	0.99	1.08 ± 0.03	1.00

Table A.2: Results of the XRF versus PIXE comparison on 14 aerosol samples, collected on Teflon, polycarbonate and cellulose mixed esters filters: slopes and correlation coefficients, obtained by a fitting procedure, are reported (linear regression plots are shown in Fig. A.8); intercepts were consistent with zero.

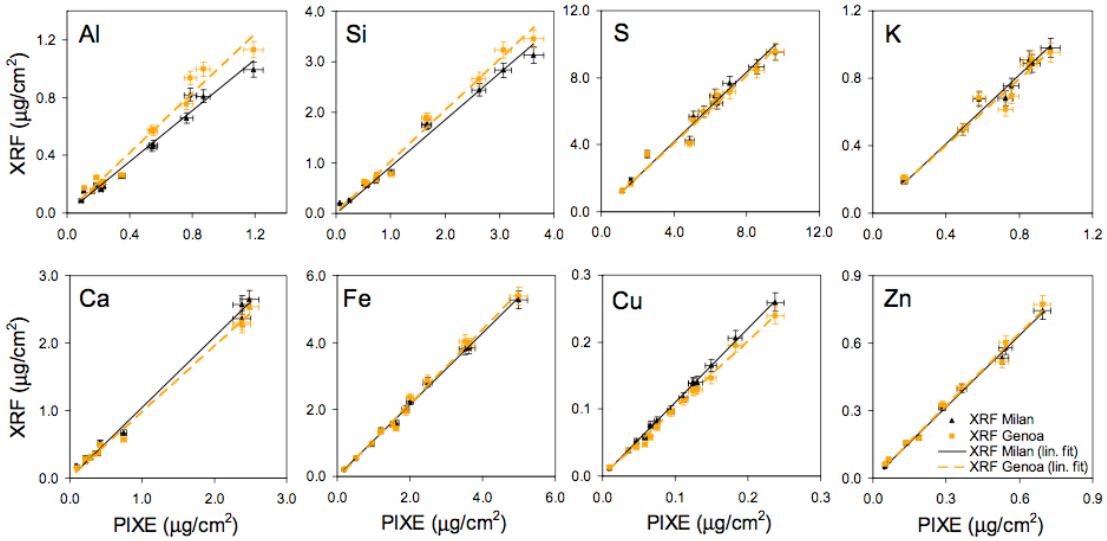

Figure A.8: Linear regression plots for the selected elements, namely Al, Si, S, K, Ca, Fe, Cu and Zn.

To evaluate the MDLs, the commonly accepted three-sigma criterion was used: an X-ray peak is considered detectable if its intensity exceeds a three-standard-deviation fluctuation of the underlying background [Joha95]. In PIXE spectra the background is originated by Compton interactions in the detector and by secondary Bremsstrahlung, which is dominant for energies up to about 5 keV (with a 3 MeV proton beam). In XRF spectra, the background is a continuum due to the Bremsstrahlung radiation of the exciting beam, and its shape and intensity are strongly related to the selected primary filter.

MDL values are shown in Figure A.9. Since MDLs for the XRF spectrometers of Genoa and Milan are in excellent agreement for all elements and filter types (as expected, being the two instruments identical), for the sake of clarity only data from oneof them are reported.

In relation to the purpose of each monitoring campaign, different filters types may be used; thus, the choice of the most suitable technique for analysing aerosol samples should take into account MDLs evaluation for different filter supports. Regarding samples on polycarbonate and cellulose mixed esters, MDL patterns have the same behaviour (for each technique), and MDLs for these two filter types are comparable[3].

As shown in Figure A.9, for polycarbonate and cellulose mixed esters filters the PIXE MDLs are always better or comparable with those of XRF, in spite of an XRF measuring time about 7 times longer, except for Al, Si and P; however Si and Al are normally found in elevated concentrations in atmospheric aerosol and higher MDLs do not give problems in the detection of these elements.

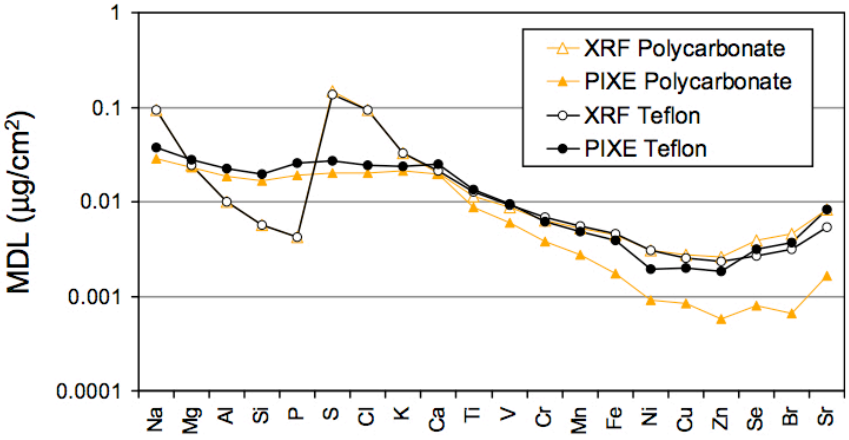

Figure A.9: PIXE and XRF MDLs, for different elements, for samples collected on polycarbonate and Teflon filters.

In the case of Teflon, for the "low-medium Z" elements the situation is similar to the one found for polycarbonate filters, while for Z > 20 PIXE MDLs increase and become similar to the XRF ones: in fact, the increase of the Compton background intensity in PIXE spectra (due to the γ-rays produced by F [Caci06], a Teflon major component) yields higher PIXE MDLs in the case of Teflon with respect to polycarbonate.

In order to optimise the measuring times at the accelerator, in the case of aerosol samples collected on Teflon filters it should be advisable to perform:

- One PIXE measurement lasting about 1 minute to get the "low-Z" elements concentrations (reducing considerably the beam time at the accelerator);

[3] Data on cellulose mixed esters filters are not reported for the sake of clarity, since the same comments concerning polycarbonate filters can be extended to these substrata.

- One XRF measurement (only the high voltage run) to get the concentrations of the "medium-high Z" elements, with measurement times of the order of 30-40 minutes, which is still quite a long measuring time, with respect to PIXE, but the analysis can be done in automatic mode (also during the night).

Bibliography

[Alde98] C. Alderliesten, K. van der Borg, A. F. M. de Jong, *Contamination and fractionation effects in AMS-measured $^{14}C/^{12}C$ and $^{13}C/^{12}C$ ratios of small samples,* Radiocarbon 40 (1998), 215

[Andr05] M. O. Andreae. C. D. Jones, P. M. Cox, *Strong present-day aerosol cooling implies a hot future,* Nature 435 (2005), 1187

[Bae04] M.-S. Bae, J. J. Schauer, J. T. DeMinter, J. R. Turner, D. Smith, R. A. Cary, *Validation of a semi-continuous instrument for elemental carbon and organic carbon using a thermo-optical method,* Atm. Env. 38 (2004), 2885

[Benn77] C. L. Bennett, R. P. Beukens, M. R. Clover, H. E. Gove, R. B. Liebert, A. E. Litherand, K. H. Purser, W. E. Sondheim, *Radiocarbon dating using electrostatic accelerators: negative ions provide the key*, Science 198 (1977), 508

[Boni88] C. Boni, E. Cereda, G. M. Braga Marcazzan, V. De Tomasi, *Prompt gamma emission excitation functions for PIGE analysis,* Nucl. Instr. & Meth. B 35 (1988), 80

[Bowm90] S. Bowman, *Radiocarbon Dating (Interpreting the Past Series)*, University of California Press and British Museum (1990)

[Brow97] T. A. Brown, J. R. Southon, *Corrections for contamination background in AMS ^{14}C measurements,* Nucl.Instr.&Meth. B 123 (1997), 208

[Cach89] H. Cachier, M.-P. Bremond, P. Buat Ménard, *Determination of atmospheric soot carbon with a simple thermal method,* Tellus 41B (1989), 379

[Caci06] A. Caciolli, M. Chiari, A. Climent-Font, M.T. Fernández-Jiménez, G. García-López, F. Lucarelli, S. Nava, A. Zucchiatti, *Measurements of γ-ray emission*

induced by protons on fluorine and lithium, Nucl. Instr. & Meth. B 249 (2006) 98

[Calz06] G. Calzolai, M. Chiari, I. Garcia Orellana, F. Lucarelli, A. Migliori, S. Nava, F. Taccetti, *The new external beam facility for environmental studies at the Tandetron Accelerator of LABEC*, Nucl.Instr.&Meth. B 249 (2006), 928

[Calzxx] G. Calzolai, M. Chiari, F. Lucarelli, S. Nava, S. Portarena, *Proton induced γ-ray emission yields for the analysis of light elements in aerosol samples in an external beam set-up*, Nucl. Instr. & Meth. B, accepted

[Char67] R. J. Charlson, N. C. Ahlquist, H. Horvath, *On the generality of correlation of atmospheric aerosol mass concentration and light scatter,* Atm. Env. 2 (1968), 455

[Chow93] J. C. Chow, J. G. Watson, L. C. Pritchett, W. R. Pierson, C. A. Frazier, R. G. Purcell, *The dri thermal/optical reflectance carbon analysis system: description, evaluation and applications in U.S. Air quality studies*, Atm. Env. 27A (1993), 1185

[Chow02] J. C. Chow, J. G. Watson, *$PM_{2.5}$ carbonate concentrations at regionally representative Interagency Monitoring of Protected Visual Environment sites,* J. Geophys. Res. 107 (2002), 8344

[Clay55] G. Clayton, J. Arnold, F. Patty, *Determination of sources of particulate atmospheric carbon,* Science 122 (1955), 751

[Crai54] H. Craig, *Carbon 13 in Plants and the Relationship between Carbon 13 and Carbon 14 Variations in Nature*, J. Geol. 62 (1954), 115

[Cris09] P. Cristofanelli, A. Marinoni, J. Arduini, U. Bonafé, F. Calzolari, T. Colombo, S. Decesari, R. Duchi, M. C. Facchini, F. Fierli, E. Finessi, M. Maione, M. Chiari, G. Calzolai, P. Messina, E. Orlandi, F. Roccato, P. Bonasoni, *Significant variations of trace gas composition and aerosol properties at Mt. Cimone during air mass transport from North Africa – contributions from wildfire emissions and mineral dust*, Atmos. Chem. Phys. 9 (2009), 4603

[Curr83] L. A. Currie, G. A. Klouda, R. E. Continetti, I. R. Kaplan, W. W. Wong, T. G. Dzubay, R. K. Stevens, *On the origin of carbonaceous particles in American*

cities: results of radiocarbon "dating" and chemical characterization, Radiocarbon 25 (1983), 603

[Curr89] L. A. Currie, T. W. Stafford, A. E. Sheffield, G. A. Klouda, S. A. Wise, R. A. Fletcher, D. J. Donahue, A. J. T. Jull, T. W. Linick, *Microchemical and molecular dating,* Radiocarbon 31 (1989), 448

[Curr00] L. A. Currie, *Evolution and multidisciplinary frontiers of ^{14}C aerosol science,* Radiocarbon 42 (2000), 115

[Curr02] L. A. Currie et al., *A Critical Evaluation of Interlaboratory Data on Total, Elemental, and Isotopic Carbon in the Carbonaceous Particle Reference Material, NIST SRM 1649a,* J. Res. Natl. Inst. Stand. Technol. 107 (2002), 279

[Delm02] B. Delmonte, J. R. Petit, V. Maggi, *Glacial to Holocene implications of the new 27,000 year dust record from the EPICA Dome C (East Antarctica) ice core*, Clim. Dynam. 18 (8) (2002), 647

[Dock93] D. W. Dockery, C. A. Pope, X. P. Xu, J. D. Spengler, J. H. Ware, M. E. Fay, B. G. Ferris, F. E. Speizer, *An association between air-pollution and mortality in 6 Unites States cities,* N. Engl. J. Med. 329 (1993), 1753

[Elle96] P. M. Eller, M. E. Cassinelli, *NIOSH Manual of Analytical Methods*, US Department of Health and Human Services, Cincinnati, Ohio

[EPA05] United States Environmental Protection Agency, *Review of the National Ambient Air Quality Standards for Particulate Matter: Policy Assessment of Scientific and Technical Information*, OAQPS Staff Paper, EPA-452/R-05-005 (June 2005)

[EPIC04] EPICA community members, *Eight glacial cycles from an Antarctic ice core,* Nature 429 (2004), 623

[EPIC06]] EPICA community members, *One-to-one coupling of glacial climate variability in Greenland and Antartica,* Nature 444 (2004), 195

[Fand99] M. S. H. Fandary, A. S. Aljima, J. A. Al-Kandary, *Liquid-Liquid Equilibria for the System Water + Ethanol + Ethyl tert-Butyl Ether*, J. Chem. Eng. Data 44 (1999), 1129

[Fedi04] M. E. Fedi, *Development of the radiocarbon AMS laboratory at the new Tandetron accelerator in Florence*, PhD thesis, University of Florence (2004)

[Fedi07] M. E. Fedi, A. Cartocci, M. Manetti, F. Taccetti, P.A. Mandò, *The ^{14}C AMS facility at LABEC, Florence*, Nucl.Instr.&Meth. B 259 (2007), 18

[Feis06] R.Feistel, W.Wagner, *A new equation of State for H_2O Ice Ih*, J. Phys. Chem. Ref. Data 35 (2006),1021

[Fern84] E. Fernandez-Fassnacht, F. Del Rio, *The vapour pressure of CO_2 from 194 to 243 K,* J. Chem. Thermodynamics 16 (1984), 469

[Form09] P. Formenti, S. Nava, P. Prati, S. Chevaillier, A. Klaver, S. Lafon, F. Mazzei, G. Calzolai, M. Chiari, *Self-attenuation artifacts and correction factors of light element measurements by X-Ray Analysis: implication for mineral dust composition studies,* J. Geophys. Res., accepted

[Gele04] A. Gelencsér, *Carbonaceous Aerosol,* Springer, Dordrecht, The Netherlands (2004)

[Gonf84] R. Gonfiantini, *Stable Isotope Reference Samples for Geochemical and Hydrological Investigations,* Report Adv. Group Meeting, Vienna, September 1983, Vienna, IAEA (1984)

[Hayw00] J. Haywood, O. Boucher, *Estimates of the direct and indirect radiative forcing due to the troposheric aerosols: a review*, Rev. Geophys. 38 (2000), 513

[Hell05] R. Hellborg, *Electrostatic Accelerators – Fundamentals and Applications*, Springer-Verlag, Berlin Heidelberg (2005)

[Hind99] W. C. Hinds*, Aerosol Technology – Properties, behavior, and measurement of airborne particles*, John Wiley & Sons (1999)

[Holy81] B. Holynska, A. Markowicz, *Experimental evaluation of the Rhodes-Hunter model for the particle size effect in X-ray fluorescence analysis of 'thin' samples*, X-ray Spectrom. 10 (1981), 61

[Horv93] H. Horvath, *Atmospheric light absorption – A review,* Atm. Env. 27A (1993), 293

[Hua01] Q. Hua, G. E. Jacobsen, U. Zoppi, E. M. Lawson, A. A. Williams, A. M. Smith, M. J. McGann, *Progress in radiocarbon target preparation at the ANTARES AMS centre,* Radiocarbon 43 (2001), 275

[Hua04] Q. Hua, U. Zoppi, A. A. Williams, A. M. Smith, *Small-mass AMS radiocarbon analysis at ANTARES,* Nucl.Instr.&Meth. B 223-224 (2004), 284

[Hua04b] Q. Hua, M. Barbetti, *Review of tropospheric bomb ^{14}C data for carbon cycle modeling and age calibration purposes,* Radiocarbon 46 (2004), 1273

[IMPRep] IMPROVE (*Interagency Monitoring of Protected Visual Environments*) Reports, available on-line at: http://vista.cira.colostate.edu/improve/Publications/improve_reports.htm

[IPCC07] P. Forster, V. Ramaswamy, P. Artaxo, T. Berntsen, R. Betts, D.W. Fahey, J. Haywood, J. Lean, D.C. Lowe, G. Myhre, J. Nganga, R. Prinn, G. Raga, M. Schulz and R. Van Dorland, 2007: Changes in Atmospheric Constituents and in Radiative Forcing. *In: Climate Change 2007: The Physical Science Basis. Contribution of Working Group I to the Fourth Assessment Report of the Intergovernmental Panel on Climate Change,* [Solomon, S., D. Qin, M. Manning, Z. Chen, M. Marquis, K.B. Averyt, M.Tignor and H.L. Miller (eds.)]. Cambridge University Press, Cambridge, United Kingdom and New York, NY, USA.

[Jaco00] M. C. Jacobson, H.-C. Hansson, K. J. Noone, R. J. Charlson, *Organic atmospheric aerosols: review and state of the science,* Rev. Geophys. 38 (2000), 267

[Jaco01] M. Z. Jacobson, *Strong radiative heating due to the mixing state of black carbon in atmospheric aerosols,* Nature 409 (2001), 695

[Jank08] N. Jankowski, C. Schmidl, I. L. Marr, H. Bauer, H. Puxbaum, *Comparison of methods for the quantification of carbonate carbon in atmospheric PM10 aerosol samples,* Atm. Env. 42 (2008), 8055

[Joha95] S.A.E. Johansson, J.L. Campbell, K.G. Malmqvist, *Particle- Induced X-ray Emission Spectrometry*, John Wiley & Sons (1995)

[Keit64] M. L. Keith, G. M. Anderson, R. Eichler, *Carbon and oxygen isotopic composition of mollusk shells from marine and fresh-water environments*, Geochim. Cosmochim. Acta 28 (1964), 1757

[Kenn07] I. M. Kennedy, *The health effects of combustion-generated aerosols,* Proc. Comb. Inst. 31 (2007), 2757

[Kieh97] J. T. Kiehl, K. E. Trenberth, *Earth's Annual Global Mean Energy Budget,* Bull. Am. Meteorol. Soc. 78 (1997), 197

[Kiis02] M. Kiisk, B. Erlandsson, M. Faarinen, R. Hellborg, K. Håkansson, P. Persson, G. Skog, K. Stenström, *The charge state distribution of a carbon beam measured at the Lund pelletron accelerator with the newly installed terminal pumping system in use,* Nucl. Instr. & Meth. A 481 (2002), 1

[Korf80] S. A. Korf, R. B. Mendell, *Variations in Radiocarbon Production in the Earth's atmosphere*, Radiocarbon 22 (1980), 159

[LeCl98] M. Le Clerq, J. Van Der Plicht, M. Gröning, *New ^{14}C reference materials with activities of 15 and 50 pMC,* Radiocarbon 40 (1998), 295

[Levi97] I. Levin, B. Kromer, *Twenty years of atmospheric $^{14}CO_2$ observations at Schauinsland station, Germany*, Radiocarbon 39 (1997), 205

[Levi08] I. Levin, S. Hammer, B. Kromer, F. Meinhardt, *Radiocarbon observations in atmospheric CO_2: Determining fossil fuel CO_2 over Europe using Jungfraujoch observations as background,* Sci. Total Environ. 391 (2008), 211

[Lewi04] C. W. Lewis, G. A. Klouda, W. D. Ellenson, *Radiocarbon measurement of the biogenic contribution to summertime PM-2.5 ambient aerosol in Nashville, TN,* Atm. Env. 38 (2004), 6053

[Libb49] W. F. Libby, E. C. Anderson, J. R. Arnold, *Age Determination by Radiocarbon Content: World-Wide Assay of Natural Radiocarbon*, Science 109 (1949), 227

[Liu09] J. Liu, D. L. Mauzerall, L. W. Horowitz, *Evaluating inter-continental transport of fine aerosols: (2) Global health impact,* Atm, Env. 43 (2009), 4339

[Lohm05] U. Lohmann, J. Feichter, *Global indirect aerosol effects: a review*, Atmos. Chem. Phys. 5 (2005), 715

[Lowe87] D.C. Lowe, W. J. Judd, *Graphite target preparation for radiocarbon dating by accelerator mass spectrometry,* Nucl.Instr.&Meth. B 28 (1987), 113

[Mand09] P. A. Mandò, *INFN-LABEC – Nuclear Techniques for Cultural Heritage and Environmental Applications*, Nucl. Phys. News 19 (2009), 5

[Mari08] F. Marino, G. Calzolai, S. Caporali, E. Castellano, M. Chiari, F. Lucarelli, V. Maggi, S. Nava, M. Sala, R. Udisti, *PIXE and PIGE techniques for the analysis of Antarctic ice dust and continental sediments*, Nucl. Instr. & Meth. B 266 (2008), 2396

[Mari08b] F. Marino, E. Castellano, D. Ceccato, P. De Deckker, B. Delmonte, G. Ghermandi, V. Maggi, J. R. Petit, M. Revel-Rolland, R. Udisti, *Defining the geochemical composition of the EPICA Dome C ice core dust during the last glacial-interglacial cycle,* Geochem, Geophys. Geosyst. 9 (2008), Q10018

[Mari09] F. Marino, E. Castellano, S. Nava, M. Chiari, U. Ruth, A. Wegner, F. Lucarelli, R. Udisti, B. Delmonte, V. Maggi, *Coherent composition of glacial dust on opposite sides of the East Antarctic Plateau inferred from the deep EPICA ice cores*, Geophys. Res. Lett. 36 (2009), L23703

[Marp76] V. A. Marple, K. Willeke, *Impactor design*, Atm. Env. 10 (1976), 891

[Maxw95] J. A. Maxwell, W. J. Teesdale, J. L. Campbell, *The Guelph PIXE software package II*, Nucl.Instr.&Meth. B 95 (1995), 407

[Mesk05] N. Meskhidze, W. L. Chameides,A. Nenes, *Dust and pollution: A recipe for enhanced ocean fertilization?*, J. Geophys. Res. 110 (2005), D03301

[Mook99] W. G. Mook, J. van der Plicht, *Reporting ^{14}C activities and concentrations*, Radiocarbon 41 (1999), 227

[Nade87] M.-J. Nadeau, W. E. Kieser, R. P. Beukens, A. E. Litherland, *Quantum mechanical effects on sputter source isotope fractionation,* Nucl.Instr.&Meth. B 29 (1987), 83

[Nade04] M.-J. Nadeau, A. E. Litherland, A. Rieck, P. M. Grootes, *Isotopic fractionation in recombinator based ^{14}C AMS measurements: how can we live with it?,* Nucl.Instr.&Meth. B 223-224 (2004), 346

[Pear98] A. Pearson, A. P. McNichol, R. J. Schneider, K. F. Von Reden, Y. Zheng, *Microscale AMS ^{14}C measurement at NOSAMS,* Radiocarbon 40 (1998), 61

[Pope02] C. A. Pope, R. T. Burnett, M. J. Thun, E.E. Callee, D. Krewski, K. Ito, G. D. Thurston, *Lung cancer, cardiopulmonary mortality, and long-term exposure to fine particulate pollution*, J. Am. Med. Ass. 287 (2002), 1132

[Pösc05] U. Pöschl, *Atmospheric Aerosols: Composition, Transformation, Climate and Health Effects,* Angew. Chem. Int. Ed. 44 (2005), 7520

[Pösc06] U. Pöschl, T. Fehrenbach, T. Franze, U. McKeon, A. Messerer, E. Mikhailov, R. Niessner, C. Schauer, A. Zerrath, *Carbonaceous Aerosol Components: Properties, Interactions, Climate and Health Effects,* Geophis. Res, Abs. 8 (2006), 07937

[Proc72] Proceedings of the Eighth International Conference on Radiocarbon Dating, Lower Hutt, New Zeland (1972), X

[Pye87] K. Pye, *Aeolian Dust and Dust Deposits*, Academic Press, New York (1987)

[Rama09] V. Ramanathan, Y. Feng, *Air pollution, greenhouse gases and climate change: Global and regional perspectives,* Atm. Env. 43 (2009), 37

[REN09] Renewable Energy Policy Network for the 21st Century, *Renewables – global status report 2009 Update*, available at

http://www.ren21.net/publications/default.asp

[Rom00] W. Rom, C. A. M. Brenninkmeijer, C. Bronk Ramsey, W. Kutschera, A. Priller, S. Puchegger, T. Röckmann, P. Steier, *Methodological aspects of atmospheric ^{14}CO measurements with AMS,* Nucl.Instr.&Meth. B 172 (2000), 530

[Sabb95] C. Sabbioni, *Contribution of atmospheric deposition to the formation of damage layers,* Sc. Tot. Env. 167 (19959, 49

[Sant07] G. M. Santos, J. R. Southon, S. Griffin, S. R. Beaupre, E. R. M. Druffel, *Ultra small-mass AMS ^{14}C sample preparation and analyses at KCCAMS/UCI Facility,* Nucl.Instr.&Meth. B 259 (2007), 293

[Sant07b] G. M. Santos, M. Mazon, J. R. Southon, S. Rifai, R. Moore, *Evaluation of iron and cobalt powders as catalysts for ^{14}C-AMS target preparation,* Nucl.Instr.&Meth. B 259 (2007), 308

[Slat02] J. F. Slater, L. A. Currie, J. E. Dibb, B. A. Benner Jr., *Distinguishing the relative contribution of fossil fuel and biomass combustion aerosols deposited at Summit, Greenland through isotopic and molecular characterization of insoluble carbon,* Atm. Env. 36 (2002), 4463

[Smit09] A. M. Smith, Q. Hua, A. Williams, V. Levchenko, B. Yang, *Developments in micro-sample ^{14}C AMS at the ANTARES AMS facility,* Nucl. Instr. & Meth. B (2009), doi:10.1016/j.nimb.2009.10.064

[Spur99] K. R. Spurny, *Analytical chemistry of aerosols,* CRC Press (1999)

[Stei06] P. Steier, R. Drosg, M. Fedi, W. Kutschera, M. Schock, D. Wagenbach, E. M. Wild, *Radiocarbon determination of particulate organic carbon in non-temperated, alpine glacier ice,* Radiocarbon 48 (2006), 69

[Stre71] A. G. Streng, *Miscibility and Compatibility of Some Liquid and Solidified Gases at Low Temperature*, J. Chem. Eng. Data 16 (1971), 357

[Stui77] M. Stuiver, H. A. Polach, *Discussion; reporting of ^{14}C data,* Radiocarbon 19 (1977), 355

[Stui83] M. Stuiver, *International agreements and the use of the new oxalic acid standard*, Radiocarbon 25 (1983), 793

[Sues55] H. E. Suess, *Radiocarbon concentration in modern wood,* Science 122 (1955), 415

[Sute90] M. Suter, *Accelerator mass spectrometry: State of the art in 1990,*Nucl. Instr. & Meth. B 52 (1990), 211

[Syna09] H.-A. Synal, L. Wacker, *AMS measurement technique after 30 years: Possibilities and limitations of low energy systems*, Nucl. Instr. and Meth. B (2009), doi:10.1016/j.nimb.2009.10.009

[Szid04] S. Szidat, T. M. Jenk, H. W. Gäggler, H.-A. Synal, I. Hajdas, G. Bonani, M. Saurer, *THEODORE, a two-step heating system for the EC/OC determination of radiocarbon (^{14}C) in the environment*, Nucl.Instr.&Meth. B 223-224 (2004), 829

[Szid04b] S. Szidat, T. M. Jenk, H. W. Gäggler, H.-A. Synal, R. Fisseha, U. Baltensperger, M. Kalberer, V. Samburova, L. Wacker, M. Saurer, M. Schwilowski, I. Hajdas, *Source apportionment of aerosols by ^{14}C measurements in different carbonaceous particle fractions,* Radiocarbon 46 (2004), 475

[Szid06] S. Szidat, T. M. Jenk, H.-A. Synal, M. Kalberer, L. Wacker, I. Hajdas, A. Kasper-Giebl, U. Baltensperger, *Contributions of fossil fuel, biomass-burning, and biogenic emissions to carbonaceous aerosols in Zurich as traced by ^{14}C,* J. Geophys. Res. 111 (2006), D07206

[Szid09] S. Szidat, M. Ruff, N. Perron, L. Wacker, H.-A. Synal, M. Hallquist, A. S. Shanningrahi, K. E. Yttri, C. Dye, D. Simpson, *Fossil and non-fossil sources of organic carbon (OC) and elemental carbon (EC) in Göteborg, Sweden*, Atmos. Chem. Phys. 9 (2009), 1521

[Szid09b] S. Szidat, *Sources of Asian Haze,* Science 323 (2009), 470

[tenB04] H. ten Brink, W. Maenhaut, R. Hitzenberger, T. Ganuk, G. Splinder, A. Even, X. Chi, H. Bauer, H. Puxbaum, J.-P. Putaud, J. Tursic, A. Berner, *INTERCOMP2000: the comparability of methods in use in Europe for measuring the carbon content of aerosol,* Atm. Env. 38 (2004), 6507

[Tuni98] C. Tuniz, J. R. Bird, D. Fink, G. F. Herzog, *Accelerator Mass Spectrometry – Ultrasensitive Analysis for Global Science,* CRC Press (1998)

[Turp90] B. J. Turpin, J. J. Huntzicker, K. M. Adams, *Intercomparison of photoacoustic and thermal-optical methods for the measurement of atmospheric elemental carbon,* Atm. Env. 24A, 1831

[Uchi09] M. Uchida, H. Kumata, Y. Koike, M. Tsuzuki, T. Uchida, K. Fujiwara, Y. Shibata, *Radiocarbon-based source apportionment of black carbon (BC) in PM_{10} aerosols from residential area of suburban Tokyo*, Nucl. Instr. & Meth. B (2009), doi:10.1016/j.nimb.2009.10.114

[UNEP09] United Nations Environment Programme, *Toward sustainable production and use of resources: Assessing Biofuels,* 2009

[Vand97] K. van der Borg, C. Alderliesten, A. F. M. de Jong, A. van den Brink, A. P. de Haas, H. J. H. Kersemakers, J. E. M. J. Raaymakers, *Precision and mass fractionation in ^{14}C analysis with AMS,* Nucl.Instr.&Meth. B 123 (1997), 97

[vanE77] P. van Espen, H. Nullens, F. Adams, *A computer analysis of X-ray fluorescence spectra*, Nucl.Instr.&Meth. 142 (1977), 243

[Voge84] J. S. Vogel, J. R. Southon, D. E. Nelson, T. A. Brown, *Performance of catalytically condensed carbon for use in accelerator mass spectrometry,* Nucl.Instr.&Meth. B 5 (1984), 289

[VonR98] K. von Reden, A. McNichol, A. Pearson, R. Schneider, *^{14}C AMS measurements of <100 μg samples with a high-current system,* Radiocarbon 40 (1998), 247

[Wats05] J. G. Watson, J. C. Chow, L.-W. A. Chen, *Summary of Organic and Elemental Carbon/Black Carbon Analysis Methods and Intercomparisons,* Aerosol Air Qual. Res. 5 (2005), 65

Acknowledgments

I think that acknowledgements have to be written in the language I speak with the people I want to thank, so... let's switch to Italian! E aggiungerei... finalmente!! Dopo tutto questo scrivere, rileggere e correggere sono rimasta un po' a corto di parole, ma, dopo lo sproloquio che chiudeva la mia tesi di laurea, questo potrebbe anche essere un bene! E chissà se ora mi ricorderò tutti... chi non è citato non se la prenda, che se mi conosce un po' sa che razza di testa c'ho!

I primi, dovuti, ringraziamenti sono per tutti quelli che mi hanno aiutato nello svolgere questo lavoro, in questi tre anni. Grazie a Silvia, Mariaelena, Massimo, Franco, e Francesco, che mi hanno seguito, insegnato e incoraggiato; grazie a Luca, Marco, Piero, Lorenzo, Silvia, Pamela, Alessandro, Novella, Mirko, Lucia, Antonio, Agnese, Paolo, insomma a tutti quelli che al LABEC lavorano o lavoravano, perché ognuno di loro ha in qualche modo contribuito a questo lavoro. Grazie ai collaboratori milanesi Vera, Francesco, Roberta e Gianluigi e ai genovesi Eleonora, Federico e Paolo. Grazie ai "chimici" e in particolare agli "antartici" Federica ed Emiliano. Grazie a tutti i ragazzi dell'officina, a Piero DC e a Marco per l'impagabile aiuto tra viti, argani e connessioni elettriche. Grazie a Fernanda per l'enorme lavoro di revisione linguistica!

Grazie alla mia splendida famiglia, a mamma, babbo ed Elena, che mi sono sempre vicini, e sul cui incondizionato appoggio so di poter sempre contare. Un ringraziamento speciale se lo merita Elena per i meravigliosi disegni con i'CAD! Grazie alla mia nonna, ai miei zii, cugini, biscuginette, e biszie, insomma a tutta la tribù, perché è sempre bello essere così tanti e così vicini.

Grazie a Valentina, che siccome dopo 25 anni non si sa più che inventarsi ha deciso di farmi anche da compagna-di-tesi-a-distanza.

Grazie a tutti i miei amici fisici, accompagnati a fisici o giù di lì, che a volte sento un po' come una seconda famiglia.

Grazie a tutti gli amici chimici, anche se il confine si sta perdendo vista la velocità con cui state importando sempre più fisici!

E poi grazie a tutti gli amici "non scientifici" (grazie al cielo ci sono anche loro!) e agli amici lontani ma sempre vicini (evviva il trio!).

Un ringraziamento speciale a Giordano, per tanti motivi, tra cui sicuramente quello di sopportarmi e starmi vicino anche quando le mie fragilità prendono il sopravvento.

Infine un pensiero va a coloro che, purtroppo, mi hanno lasciato in questi tre anni: grazie, davvero, per tutto quello che siete stati, vi porterò sempre nel mio cuore.